PATHOGENESIS OF CHRONIC KIDNEY DISEASE IN DOGS WITH X-LINKED HEREDITARY NEPHROPATHY

A Dissertation

by

SABRINA DENISE CLARK

Submitted to the Office of Graduate and Professional Studies of
Texas A&M University
in partial fulfillment of the requirements for the degree of

DOCTOR OF PHILOSOPHY

Chair of Committee,	Mary Nabity
Committee Members,	Robert Burghardt
	Rachel Cianciolo
	Gonzalo Rivera
Head of Department,	Ramesh Vemulapalli

May 2019

Major Subject: Veterinary
Pathobiology

ABSTRACT

Chronic kidney disease (CKD) is a common cause of morbidity and mortality in dogs that, by the time diagnosis occurs using traditional biomarkers, significant damage to the kidneys has occurred. Therefore, establishment of biomarkers for detecting kidney disease sooner and monitoring progression of disease is imperative for earlier therapeutic intervention. Glomerular cells engage in multidirectional signaling to maintain homeostasis. Alterations of these signaling pathways lead to disease development, including CKD. Additionally, a change in normal cellular pathways often causes aberrant expression of signaling molecules, which can be measured and used as biomarkers. The primary goal of this research was to evaluate kidney and urine samples from both affected dogs with CKD caused by X-linked hereditary nephropathy (XLHN) and unaffected, age-matched littermates at defined milestones of disease progression to identify variations in cellular molecules for use as potential biomarkers of CKD. Multiple experimental modalities including immunofluorescence, enzyme-linked immunosorbent assays, next-generation sequencing, quantitative real-time PCR, and *in situ* hybridization were employed.

First, we were able to establish that the early disease-initiating events demonstrated in Alport mice, namely, mesangial cell filopodia invasion into the GBM leading to aberrant deposition of laminin 211, are likely playing a role in disease initiation in XLHN dogs. We also identified alterations in endothelin-1 levels in both kidney tissue and urine of affected dogs. Furthermore, we found that let-7e, miR-21, miR-142, miR-378, miR-486, and miR-8890 are promising urinary biomarkers for either early detection of CKD and/or for use to monitor disease development. Last, we concluded that miR-21 expression increases in kidney tissue during disease progression, particularly in the renal tubules, and may result in the dysregulation of multiple cellular pathways, contributing to disease pathogenesis.

In conclusion, understanding the mechanisms of cellular crosstalk and how they relate to pathogenesis of CKD development and progression allows for the identification of detectable factors in the early stages of disease, which can lead to development of both better diagnostic makers and novel therapeutic targets. Given the complexity of CKD, a focused panel of biomarkers would be extremely rewarding. This would provide clinicians with crucial information for earlier diagnosis, evaluating prognosis, and establishing an individualized treatment plan for patients with CKD, thus improving the overall quality of life.

DEDICATION

This dissertation is dedicated to my son, Grayson, for being my greatest source of motivation and inspiration, especially when things seemed extraordinarily challenging. You are my reason and my most cherished blessing. I love you sandwich.

I also dedicate this dissertation to my mom, Monica, who has always encouraged me to keep going and supported my educational decisions so that I could be the "upgraded version of her". I hope this work makes you proud.

ACKNOWLEDGEMENTS

There are numerous people I would like to acknowledge that have made this endeavor possible. First and foremost, I would like acknowledge my mentor, Dr. Mary Nabity. Her continued support through all the ups and downs during this entire journey mean more to me than words could ever express, and I truly appreciate all she has done for me.

I would also like to give special heartfelt thanks to my beloved "lab family" whose support and encouragement, especially towards the end, really helped me to complete this process. Specifically, I would like to acknowledge the assistance of our technician, Mary Sanders, for not only her technical expertise from which I have learned so much, but more importantly, her friendship. Thank you for being there for me as a much needed and appreciated emotional sound board when times were tough, and I just needed to vent. I would also like to acknowledge my lab mate, Candice Chu, who not only provided a lot of the data analysis in this research but also provided a lot of emotional support during those challenging times. Additionally, I would like to acknowledge Kiera Pope for all her assistance both in the lab while I was running many of these experiments and as a friend on which I could always rely when I needed some help (especially with technical stuff) or just some encouragement. And a very special thank you to Carolina. You helped me learn so much in the little time that you joined the lab and I am so appreciative of that assistance.

I am grateful to each of the members of my Dissertation Committee, Drs. Burghardt, Cianciolo, and Rivera, who have provided me with both professional guidance and personal direction and have taught me a great deal about both scientific research and life in general.

I would like to express sincere gratitude to Dr. Dominic Cosgrove and his team at Boys Town National Research Hospital in Omaha, NE, for allowing me to spend time in the lab with them and to learn from such an exceptional group of people. It is truly an honor to be associated

with leaders in the field of Alport Syndrome. I would like to extend a very special thank you to Brianna Dufek, who put in countless hours troubleshooting the immunofluorescence techniques used in this study.

I would like to extend sincere gratitude to So-Young Park in the Genetics Lab of the GI Lab of TAMU, for her time and assistance in running all of the RT-qPCR plates. Without you, I really wouldn't have completed this work in time. Thank you so much.

And last but not least, I would like to thank my brother Damian, and my significant other, Carey Clark. I can't put into words the gratitude that I feel for your support. I know there were a lot of difficult moments during this process. Thank you for helping me take care of Grayson and putting up with me as I undulated through all the emotions that came along with completing this PhD.

And for all those that I am not able to specifically name. I want you to know that if I have turned to you at any point during this time, I recognize how amazing you are and that you have been instrumental in helping me in one way or another in the completion of this journey. Sincere thanks to all.

CONTRIBUTORS AND FUNDING SOURCES

This work was supported by a dissertation committee consisting of Professor Nabity and Professors Cianciolo and Rivera of the Department of Veterinary Pathobiology and Professor Burghardt of the Department of Veterinary Integrative Biosciences.

Portions of the immunofluorescence staining and confocal microscopy imaging in Chapter II and all of the staining and imaging in Chapter III were performed by Brianna Dufek at Boys Town National Research Hospital in Omaha, NE. Final figures for Chapter II were assembled by Dr. Dominic Cosgrove at Boys Town National Research Hospital in Omaha, NE. Analysis of the next-generation sequencing results in Chapter IV was performed by Dr. Candice Chu at Texas A&M University. Additionally, So-Young Parks in the Genetics Laboratory within the Texas A&M Gastrointestinal Laboratory assisted in running the RT-qPCR plates for miRNA evaluation. In Chapter V, RT-qPCR and statistical analysis of miRNA and mRNA expression was done by Dr. Wenping Song at Sanofi Genzyme in Cambridge, MA while statistical analysis of the clinical and histologic data was performed by Kiera Pope at Texas A&M University. The histologic analyses and scoring of pathological changes (excluding the evaluation of the *in situ* hybridization samples) described in Chapters II, III, and V was performed by Dr. Rachel Cianciolo at The Ohio State University. All other work for the dissertation was completed by the student, under the advisement of Professor Nabity of the Department of Veterinary Pathobiology.

This work was made possible in part by the Zoetis-Morris Animal Foundation Fellowship under Grant Number (Grant ID# D14CA-904). Its contents are solely the responsibility of the authors and do not necessarily represent the official views of Zoetis or the Morris Animal Foundation.

TABLE OF CONTENTS

Page

LIST OF FIGURES

Page

LIST OF TABLES

Page

CHAPTER I

INTRODUCTION

In 2002, the National Kidney Foundation–Kidney Disease Outcomes Quality Initiative (NKF-KDOQI) established guidelines for the evaluation, classification, and stratification of chronic kidney disease (CKD) in human medicine.[1] With recognition of CKD as a global health concern, the rationale for generation of these guidelines was to "provide a common language for communication among providers, patients and their families, investigators, and policy-makers" and to create "a framework for developing a public health approach to affect care and improve outcomes of chronic kidney disease".[1] Additionally, a major task of the group was to establish a set, universal definition for CKD. The guidelines defined CKD as an abnormality of kidney structure or function, regardless of cause or specific clinical presentation that is present for more than three months.[1]

Paralleling the developments of established guidelines for kidney disease in human medicine, at the 8th Annual Congress of the European Society of Veterinary Internal Medicine in Vienna, Austria, in 1998, the International Renal Interest Society (IRIS) was created to advance the scientific understanding of kidney disease in small animals.[2] The primary interest of the society was to strive and seek ways to enhance the field of veterinary nephrology. In 2000, the IRIS CKD Staging system was first devised, classifying CKD initially on a fasting blood creatinine concentration, and then sub-staging the disease based on the degree of proteinuria and blood pressure. This system provided veterinary practitioners with treatment recommendations linked to the staging system. Over the last 20 years, through continued advancements and interest in veterinary nephrology research, the staging system has evolved, leading to the development of

international recommendations and standards of practice excellence, thus improving the quality of care of animal patients with kidney disease.

As part of the IRIS initiative, in 2005, the World Small Animal Veterinary Association-Renal Standardization Study Group (WSAVA-RSSG) was created. Comprised of an international group of both veterinary nephrologists and pathologists, the group conducted a study to enable the establishment of guidelines for routine evaluation of renal biopsies.[3] In 2013, the group published the results of the study which confirmed that, as in human medicine, routine evaluation of the veterinary kidney biopsies should include the three modalities of light microscopy (LM) with a panel of histologic stains, transmission electron microscopy (TEM), and immunofluorescence (IF) microscopy, setting the stage for renal biopsy as the gold standard for diagnosis of kidney disease, specifically for glomerular disease.[3]

CKD in Dogs

CKD is a common cause of morbidity and mortality in dogs.[4] An unfortunate fact is that, for most patients, by the time strong evidence for loss of kidney function associated with CKD is detectable, approximately 60-75% of renal mass has already been irreversibly lost.5 CKD can be classified as either non-azotemic (serum creatinine (sCr) <1.4 mg/dl) or azotemic (sCr >1.4 mg/dL). Typically, non-azotemic patients are clinically normal and suspicion for a diagnosis is often discovered fortuitously during routine evaluation or while performing diagnostic testing for an unrelated disorder based on other renal abnormalities such as a decrease in urinary concentrating ability and/or evidence of proteinuria (specifically an elevated urine protein: urine creatinine ratio (UPC)). As determined by the IRIS Staging system, these patients are classified as Stage 1 CKD. Depending on the severity, azotemic patients may present with minimal to severe clinical signs such as

polyuria and polydipsia, inappetance, nausea, and/or vomiting along with systemic abnormalities such as hypertension. In these cases, per the IRIS guidelines, staging is based first on a fasting sCr concentration, assessed on at least two occasions in the stable patient with categories ranging from Stage 2-4 based on severity of elevation in sCr concentration. Once a stage has been established, the patient is then sub-staged based on the degree of proteinuria and systolic blood pressure, in order to facilitate appropriate treatment and monitoring of the patient. In questionable situations or very early or "at-risk" stages of CKD, measurement of symmetric dimethylarginine (SDMA) may prove useful for diagnosis and monitoring of disease as there are indications that SDMA may be a more sensitive biomarker of renal function. Once a diagnosis has been made, staging and sub-staging should be revised based on the patient's response (or lack thereof) to treatment with indication that the adjusted classification is based on treatment.

It is imperative to recognize that CKD is not a diagnosis in and of itself and that determination of a cause is crucial for providing both prognostic information and treatment recommendations.[6] In human medicine, the classification of CKD is based on the presence or absence of systemic disease along with the location of pathologic-anatomic findings as indicated by proteinuria, urinary sediment examination, imaging, and renal pathology.[6] Based on these two features, CKD can be classified into one of four general categories: 1) glomerular diseases, 2) tubulointerstitial diseases, 3) vascular diseases, or 4) cystic and congenital diseases.[6] Similarly, these categories can be discerned in veterinary medicine. However, kidney diseases are complex, and classification can be challenging as damage to a specific component of the kidney can result in secondary injury to other locations, particularly since many animals are not diagnosed until clinical signs are exhibited and pathologic damage is advanced.[4] When considering CKD in the dog, glomerular disease is

considered to be primary if the process that initiates renal injury originates in the glomerulus.[7] Many of the canine glomerular diseases are thought to develop secondary to systemic disease processes such as neoplasia, infectious, or non-infectious inflammatory causes.[8] A classification of a primary degenerative or inflammatory disease of the renal tubules and interstitium is typically made in the absence of glomerular changes and most commonly occurs due to either ischemic or toxic injury or inflammatory reactions.[9] Renovascular diseases comprise conditions that cause renal dysfunction and damage due to narrowing or blockage of renal blood vessels and can be diagnosed based on kidney lesions such as infarction, hyperemia, and hemorrhage.[9,10] By definition, congenital diseases are present at birth. While a majority of congenital kidney diseases are known to be genetic or inherited due to a familial or breed-associated pattern of disease occurrence, this may not always be the case.[11] Unlike humans, in which nephrogenesis is complete at birth, in dogs, nephrogenic growth and maturation continues until several weeks after birth.[12,13] Therefore, normal development of the kidney structures can be disrupted during gestation or the early neonatal period due to a variety of causes unrelated to genetics.[11] Therefore, not all hereditary disorders are congenital.

In dogs, glomerular disease has been indicated as a leading cause of CKD with an incidence ranging around 52%.[8,14] The average age of dogs identified as having glomerular disease is around 8 years with males and females being equally represented.[8] A renal biopsy is mandatory to classify the type of glomerular disease present in a particular patient. Through the WSAVA-RSSG, there is an ongoing effort to enhance the histologic classification of glomerular diseases in proteinuric dogs in order to improve the accuracy of diagnosis. In a recent study performed by the group, 144 parameters related to all compartments of the kidney were evaluated by several pathologists using LM, TEM, and

IF and scored based on a specifically defined system.[15] Hierarchical cluster analysis revealed that in dogs with glomerular disease, there are two large categories based on the presence or absence of immune complex deposition: the immune complex-mediated glomerulonephritis (ICGN) category and the non-ICGN category.[15] Further analysis partitioned the glomerular diseases into more specific clusters, encompassing the most commonly observed patterns of glomerular lesions. These more specific clusters were distinctly separate from the cluster composed of the control dogs. Dogs in the ICGN category had histologic patterns that were characteristic of either membranoproliferative glomerulonephritis (MPGN) or membranous glomerulonephritis (MGN), with further separation into additional clusters based on lesion severity. In the non-ICGN category, dogs were separated based on histologic patterns associated with either glomerular amyloidosis or focal segmental glomerulosclerosis (FSGS). Along with classification, this study further supported the necessity of advanced diagnostic modalities for the diagnosis of glomerular disease, revealing that evaluation of kidney tissue based on LM alone resulted in misclassification in 25% of cases. One of the most significant aspects of this study was that it allowed for the creation of a simplified and reproducible guide for use by veterinary pathologists, which will hopefully result in accurate classification of glomerular diseases in proteinuric dogs by pathologists that have not had extensive nephropathology training. With more accurate diagnostic information, more cases will be available for future studies in canine glomerular disorders, including investigation of molecular pathogenesis of disease.[15]

The Glomerular Cells

In order to begin to understand the pathogenesis of CKD due to glomerular disease, it is important to have a strong background in the participants involved. The kidney plays a

fundamental role in filtering blood, reabsorbing filtered electrolytes, solutes, and fluid, and excreting wastes, excessive electrolytes, and water through functional units called nephrons.[16] A nephron is comprised of two main parts: 1) the renal corpuscle that consists of the glomerular tuft (a network of capillaries) and Bowman's capsule and 2) the renal tubular system that includes the proximal tubule, loop of Henle, distal tubule, connecting tubule, and the collecting duct (although the collecting duct is not technically part of the nephron due to its origination from a different embryologic location). In the dog, it has been estimated that each kidney contains approximately 500,000 nephrons.[12,17] Interestingly, it has been shown that many of the ultrastructural features of the dog nephron more closely resemble those of the human nephron as compared to the laboratory rat or mouse.[18] For example, the proximal tubule brush border in the rat is complete (except for small skip areas), but in dog and human, the pars recta has larger areas devoid of microvilli. Another similarity is that in the dog, the transition from the ascending thin to the ascending thick segment of the loop of Henle is gradual, much like the transition seen in the human loop of Henle. Additionally, in the dog, the shape of the cells lining the thick ascending limb more closely resembles those in the human thick limb compared to rats.

The glomerulus is a spherical mass of specialized capillaries that is fed by the afferent arteriole and then drained through the efferent arteriole. Figure 1 shows the basic structure of the glomerulus.[19]

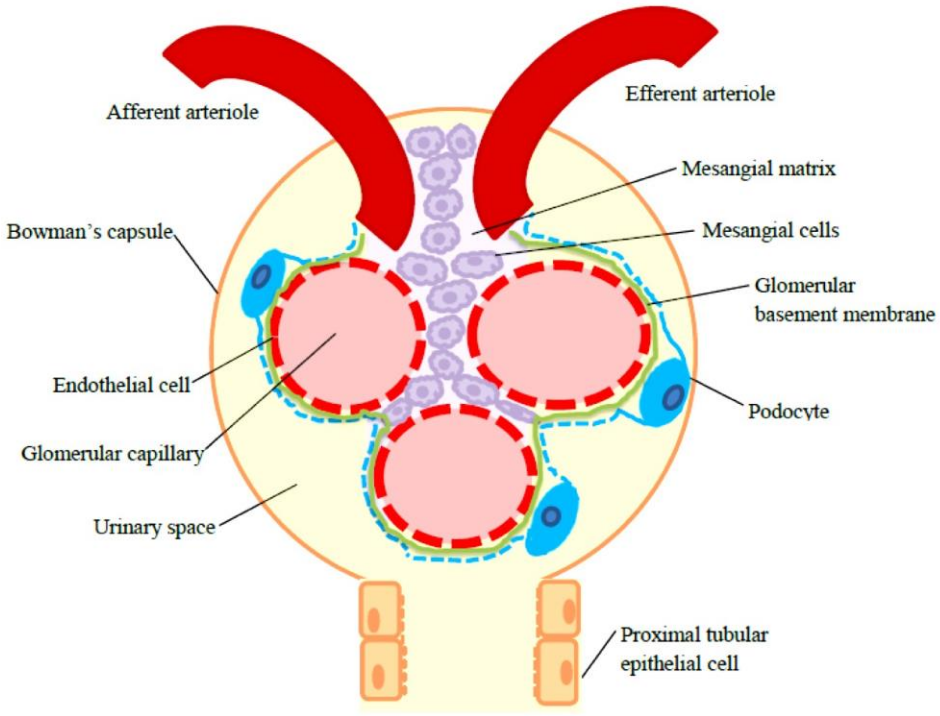

Figure 1 Schematic of the basic structure of the glomerulus. Artwork created by S. Clark.

The glomerulus itself is enclosed within Bowman's capsule, which is comprised of a basement membrane to which parietal epithelial cells (PEC) adhere, and it sits within the urinary (Bowman's) space. Mesangial cells and their matrix form a central structure that provides the scaffolding to support the glomerular microvasculature. One of the most important features of the glomerulus is the glomerular filtration barrier (Figure 2), which is composed of four layers: the endothelial surface layer (ESL, composed of the glycocalyx and endothelial cell coat), specialized fenestrated endothelial cells that line the inside of the capillary loops, the glomerular basement membrane (GBM), and the podocytes (also called the visceral epithelium).[20,21]

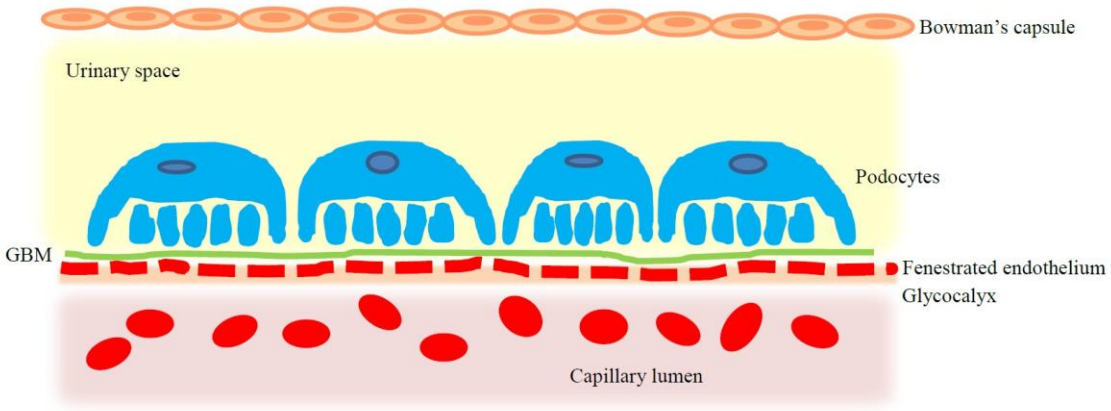

Figure 2 Schematic of the basic structure of the glomerular filtration barrier. Artwork created by S. Clark.

The glomerular filtration barrier functions to restrict passage of large molecules while remaining highly permeable to solutes and water. Through a connection of multiple integrin pathways, the endothelial cells, podocytes, and mesangial cells are able to engage in multidirectional crosstalk amongst each other. This allows all three cell types in the glomerulus to work in conjunction, forming a functional, interdependent unit in which changes in one cell type results in alterations in the others. The interaction of these cells plays an important role in both the normal physiology and the development of glomerular disease.[19,22] While they will be described individually, it is fundamental to recognize that it is by understanding the interaction of these cells with one another that the most valuable information on function in both normal and diseased states is obtained.

Podocytes

Probably one of the most well studied cells of the glomerulus is the podocyte. Podocytes are terminally differentiated, multifaceted cells that exhibit characteristics of both epithelial and mesenchymal cells.[23] They have a very complex cellular architecture consisting of a cell body from which long primary (or major) processes extend. Primary

processes divide into secondary and tertiary processes and end in individual foot processes (or pedicels) which form a network of interdigitations with adjacent foot processes that surround and enwrap the glomerular capillaries.[24-27] On the outside of the glomerulus, the area in between the foot processes at the cell-cell interface is known as the slit diaphragm and contains a meshwork of proteins that participate in filtration and signaling.[24,27,28] Described as having a characteristic zipper-like conformation, the slit diaphragm is a static sieve that connects the entire length of adjacent foot processes to provide a structural component to the filtration barrier and also serves as a specialized complex signaling hub.[27,28] The slit diaphragm contains elements of both adherens and tight junctions. Several essential molecules for slit diaphragm formation have been identified. Figure 3 shows the major molecular components of the slit diaphragm.

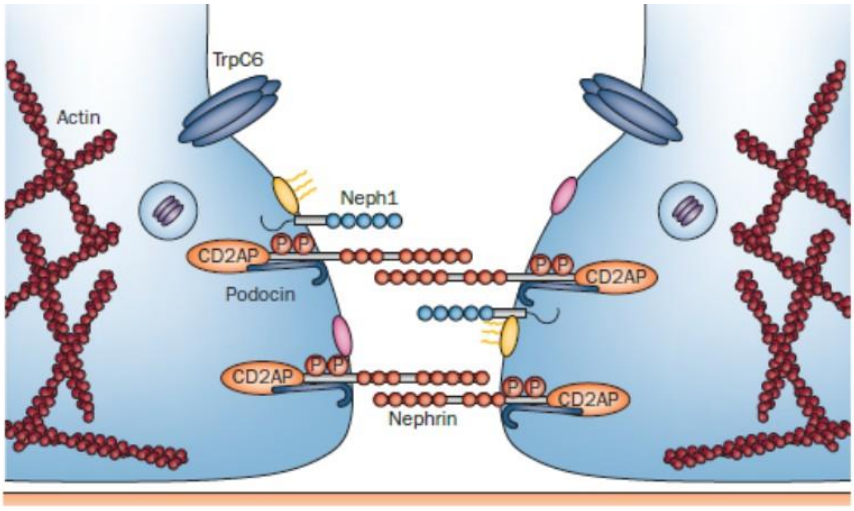

Figure 3 Molecular components of the podocyte slit diaphragm.[28] Reprinted with permission.

In mammals, nephrin plays a central role in the formation and mechanical properties of the slit diaphragm.[28] Studies in rodents and humans have shown that without

nephrin, the slit diaphragm will not form.[28] Nephrin is a type 1 transmembrane protein of the immunoglobulin family that bridges the 40 nm gap between the foot processes. Another important molecule group for the slit diaphragm composition is the NEPH1-3 protein family. These proteins share a similar homology with nephrin but are not long enough to cross the entire space of the slit junction and serve primarily as recruiters of scaffolding proteins. Podocin, a member of the stomatin family, is also unique to the slit diaphragm and is anchored to the membrane in the middle of the protein with both the N- and C-termini inside the foot process cytoplasm. Podocin plays an important role in recruitment of other proteins to the slit diaphragm complex in addition to facilitating the signaling properties of the nephrin-Neph 1 complex between the urinary space and podocyte cytoplasm.[27,28] Nephrin is attached to the cell membrane with the help of podocin and is supported by the Neph proteins. Another complex, TrpC6, is an ion channel that is crucial in adjusting the cationic ion flux in the region of the slit diaphragm. Numerous adaptor proteins such as Nck1/2, CD2-associated protein, MAGI-2, α-actinin-4 and Crk1/2 anchor nephrin (directly or indirectly) interact with the actin cytoskeleton to provide foot process stability and proper spacing and to relay signals to the actin cytoskeleton that may induce morphological changes to the cell.[27,28] The podocyte cytoskeleton is vital in maintaining the complex podocyte structure to ensure proper function.[23,25] When major alterations in the cytoskeleton occur, flattening of the actin filaments ensues, resulting in a morphologic change associated with podocyte injury known as podocyte foot process effacement.

Because podocytes are constantly exposed to biomechanical stress via trans-capillary filtration pressure, the normal functions of the podocytes rely heavily on both cell-matrix and cell-cell adhesions.[27,29] The cell body and primary and secondary

processes contain primarily vimentin-rich intermediate filaments, microfilaments, and microtubules, while the foot processes almost exclusively contain long actin fiber bundles.[23] Intermediate filaments are tension-bearing and help the cell maintain its overall shape and rigidity. While podocytes are rather stationary in the healthy glomerulus, cross-talk between microtubules and actin filaments is involved in cell movement and filopodia formation, especially as a response to injury.[23] But these proteins have a more vital role in adhering podocytes to a condensed sheet of extracellular matrix (ECM), known in the glomerulus as the GBM (discussed in more detail below), through interactions with transmembrane adhesion receptors.

A major family of proteins responsible for cell-ECM adhesions is the integrin family, which are αβ-heterodimers that link the ECM to the intracellular cytoskeleton, thus propagating signals from both within the cell to the surrounding extracellular environment and vice versa.[27] Additionally, the connection of the ECM to the cytoskeleton provides a strong physical reinforcement that is able to withstand considerable mechanical stress.[29] In the glomerulus, the components of the GBM, particularly type IV collagen and the laminin 521 network, act as ligands for the integrin receptors for initiating cell signaling and binding. The α3β1 heterodimer is the most highly expressed integrin on the podocyte cell surface and is also thought to be the most important link between the podocytes and the GBM. The tetraspanin CD151, which is also highly expressed on the podocyte cell surface, binds tightly to integrin α3β1providing additional structural integrity. Based on numerous experiments involving knockout mice, it has been determined that the integrin α3β1-CD151 complex increases the strength of podocyte adhesion to the GBM and is integral in order to withstand changes in biomechanical strain within the glomerulus.[27,29] The cytoplasmic tails of integrins do not have enzymatic activity, but rely on adaptor proteins

to conduct intracellular signaling. Integrins activate a number of protein kinases, including FAK, Src-family kinases, and integrin-kinked kinase (ILK) along with RhoGTPases.[30] The small GTPases, RhoA, Rac1 and Cdc42, are some of the most important proteins that regulated cytoskeletal dynamics.[23] Ultimately, activation of these pathways results in changes in gene expression. Because of this connection, changes in the GBM regulated by both the podocytes and endothelial cells (described below) are able to control a number of cellular processes including development, proliferation, metabolism, survival/apoptosis, and production.

Additional podocyte cell surface adhesion proteins, such as syndecan and dystroglycan, have also been shown to play significant roles in cell-matrix adhesion and signaling. Syndecan is a transmembrane heparan sulfate proteoglycan receptor that regulates integrin trafficking to the cell surface, controlling adhesion formation and disassembly.[27] Dystroglycan is located primarily at the base of foot processes and binds to laminins. However, absence of these proteins in knockout mice only cause mild changes and therefore, the criticalness of their involvement in podocyte adhesion has yet to be fully determined.[27,29] Integrins and the other cell-matrix proteins alone are not strong enough to withstand the mechanical forces to which podocytes are exposed. There are a number of linker proteins that connect integrins to the actin cytoskeleton, forming regions known as focal adhesions and providing additional strength for cell attachment.[27,29] Talin-1, a 270 kDa protein that has an N-terminal globular head and flexible rod domain, is required for the specialized actin morphology of the foot processes.[27] Binding of talin to the cytoplasmic tail of the β-integrins causes a conformational change in the extracellular domain of the integrins which then enhances the affinity of the integrins to the GBM.[27] Vinculin, a 123 kDa protein, is a key adaptor protein involved in integrin-mediated

adhesions and is recruited by talin. It is a force sensor that undergoes a conformational change when extended by mechanical stress. This change allows vinculin to interact with a number of proteins involved in the regulating the podocyte cytoskeleton dynamics including α-actinins, Arp 2/3, and actin.[27,29] Paxillin, is an important scaffolding protein in focal adhesions that is recruited by talin, and provides a docking site for a number of other adhesion proteins.[27]

Another focal adhesion protein, focal adhesion kinase (FAK), is a non-receptor tyrosine kinase, which is recruited by talin and paxillin and becomes phosphorylated upon podocyte injury.[27] The role of FAK in glomerular dysfunction is discussed in further detail in a later chapter. ILK is another important complex that influences the actin cytoskeleton in podocytes, interacting with a number of different proteins to regulate cytoskeletal dynamics including PINCH, parvin, kindling-2, and α-actinin-4.[27,29] ILK binds directly to the integrin β1 cytoplasmic tail and is crucial for signal transduction and mechanotransduction.[27,29] ILK is highly expressed in podocytes although its expression must be tightly regulated to maintain podocyte homeostasis as overexpression of ILK has actually been shown to decrease binding affinity of podocytes to the ECM.[29] Importance of these proteins in kidney development and function is illustrated by studies in mice with abnormalities (i.e. deletion, mutations, etc.) in any of these three proteins, where lethality or renal agenesis is observed.[27] Figure 4 illustrates the intricate connections between the podocytes themselves and between the GBM.

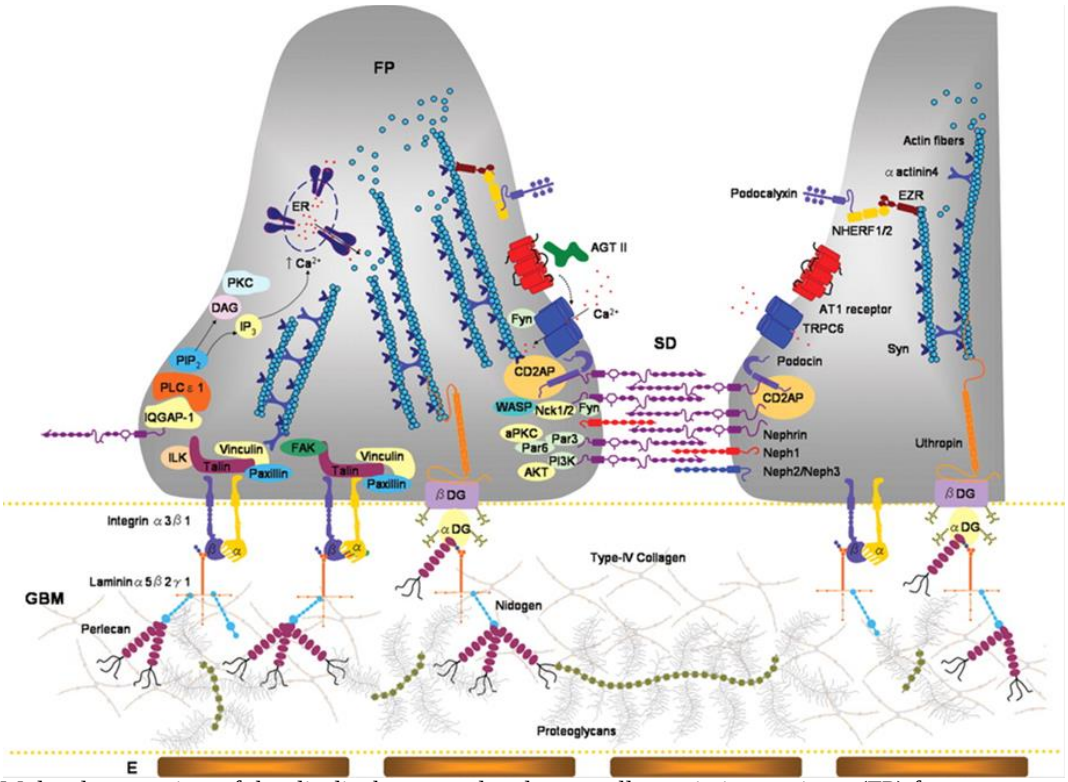

Figure 4 Molecular overview of the slit-diaphragm and podocyte cell–matrix interactions. (FP) foot-process, (SD) slit diaphragm, (GBM) glomerular basement membrane and (EF) fenestrated endothelium. At the SD, nephrin mediated signals that control actin cytoskeleton remodeling (NCK 1/2, WASp), cell polarity (Par3/6, aPKC) and survival (PI3K, AKT). TRPC6-podocin interactions modulate mechanosensation, whereas angiotensin II type 1 receptor (AT1) may increase TRPC6 mediated calcium influx upon stimuli by angiotensin II (AGT II). Activation of PLCε1 degrades phosphatidyl inositol-bisphosphate (PIP₂) into diacylglycerol (DAG) and inositol triphosphate (IP3), which leads to protein kinase C (PKC) activation and Ca²⁺ efflux from the endoplasmic reticulum (ER). Main component of the podocyte-matrix interaction structure include the integrin α3β1—laminin α5β2γ1 and dystroglycan—uthropin complexes which connect the GBM components (proteoglycans, nidogen, perlecan, agrin and type-IV collagen) to the cell actin cytoskeleton. Additional pathways controlling actin cytoskeleton remodeling include the podocalyxin, NHERF 1/2, ezrin (EZR) complex. Molecules and pathways included are only those relevant to GFB function as defects are related with a human or animal glomerular disease phenotype.[31] Reprinted with permission.

Endothelial Cells

The capillary loops of the glomeruli are lined by thin glomerular endothelial cells. These cells are considered as one of the components of the glomerular filtration barrier and are uniquely adapted for selective permeability and filtration.[19] The endothelial cell nucleus lies adjacent to the mesangium (described below) and within the cells, there is an extensive network of intermediate filaments and microtubules. The most defining characteristic of

glomerular endothelial cells are the fenestrations, which cover up to approximately 50% of the glomerular surface area and are surrounded by microfilaments.[19,32,33] Fenestrations are round transcellular "holes" about 60-80 nm in diameter concentrated in the peripheral cytoplasm away from the cell body and arranged in clusters also known as sieve plates that are separated by ridges of cytoplasm.[19,32] The formation of these fenestrations is thought to be controlled by expression of VEGF from the podocytes that act on VEGFR2 expressed by endothelial cells.[32,33] Ultrastructurally, each individual fenestration is surrounded by a network of actin microfilaments that are believed to regulate their shape and diameter.[32,33] Under normal conditions, formed elements of blood, including erythrocytes, leukocytes and platelets, are not able to gain access to the subendothelial space.

The glomerular endothelium is covered by a 200 nm thick carbohydrate-rich, gel-like mesh, called the endothelial cell surface layer (ESL), which has two components.[20] The first is the glycocalyx, which is composed primarily of membrane-bound proteoglycans. Second, is the endothelial cell coat (ECC), which is attached to the glycocalyx and is comprised of proteoglycans, glycosaminoglycans, glycoproteins, and plasma proteins synthesized by the endothelial cells. The negatively-charged glycosaminoglycan chains are covalently bonded to the cell surface and are thought to capture circulating plasma proteins to produce a thick mesh with anionic properties.[19,20,32] Within the fenestrae, the glycocalyx has been shown to have a higher ratio of heparan sulfates and hyaluronic acid to sialoproteins.[32] Overall, this net negative charge is believed to play a role in the charge selectivity of the filtration barrier, especially for larger molecules such as albumin.[34] Additionally, the glycocalyx plays important roles in capillary permeability, regulation of interactions between leukocytes and endothelial cells, and transduction of shear stress.[19]

Until recently, the contribution of glomerular endothelial cell injury in the pathogenesis of glomerular disease and renal fibrosis has been underestimated. In some kidney diseases, such as diabetic kidney disease, anti-neutrophil cytoplasmic antibody (ANCA)-associated GN, and lupus nephritis, endothelial cell injury is a prominent feature and can lead to altered microvascular permeability and microalbuminuria along with loss of fenestration causing reduction in glomerular filtration rate (GFR).[19,35] Nitric oxide (NO) is a potent vasodilator that can also inhibit inflammation, growth of vascular smooth muscle, and aggregation of platelets. Studies involving anti-GBM and remnant kidney models have demonstrated that deficiencies in endothelial nitric oxide synthetase (eNOS) can exacerbate renal injury and accelerate diabetic kidney injury, respectively.[36,37] Moreover, it was shown that eNOS-deficient mice with Adriamycin-induced nephropathy had endothelial cell injury and damage in conjunction with overt proteinuria, severe glomerulosclerosis, interstitial fibrosis, and inflammation that preceded podocyte damage by five days, indicating that endothelial cell dysfunction can initiate and propel development and progression of glomerulopathy.[38] In a later chapter of this dissertation, the role of endothelial-1(ET-1) released by glomerular endothelial cells in the initial pathogenic steps leading to end stage renal disease in Alport syndrome in both murine and canine models is discussed.

Mesangial Cells

The other glomerular cell that has attracted a lot of interest, especially as it relates to glomerular disease, is the mesangial cell. The exact origin of the mesangial cell precursor is still unknown, but mesangial cells have a variety of important functions, first of which involves playing a crucial role in the formation of the capillary tuft.[39] During glomerulogenesis, in the capillary loop stage, endothelial progenitor cells are recruited into

the vascular cleft through the expression of VEGF-A, produced by podocytes, to form the first capillary loop.[39] Under the control of PDGF-B, produced by endothelial cells, mesangial cells are recruited into the region turning the single vessel loop into multiple, parallel branches by a process known as intussusceptive splitting, thus forming the capillary tuft.[39] It has been shown that without the mesangial cells, glomerulogenesis would not proceed.[39]

At maturity, mesangial cells are described as specialized pericytes that, in conjunction with their matrix (referred to as the mesangium), form the central stalk of the glomerulus. Mesangial cells are large, irregularly shaped cells that have a dense nucleus with a number of cytoplasmic processes which run in an haphazard fashion throughout the extracellular mesangial matrix.[40] Although not as well studied, the mesangial matrix secreted by the mesangial cells is known to be of similar composition to the GBM (discussed below) but also contains a number of other glycoproteins, including fibronectin.[41] Recently, a study using an ECM enrichment strategy along with mass spectrometry-based proteomics identified several novel glomerular ECM proteins, including collagen VI and TINAGL1, both of which were localized to the mesangial matrix.[42] One of the most strongly and exclusively expressed integrins on the mesangial cells that is involved in both cell-matrix interactions and facilitation of phagocytosis is $\alpha 8$ integrin, which interacts with its ligand fibrillin-1 in the mesangial matrix.[43,44]

Mesangial cells possess an extensive array of microfilaments composed of actin, α-actinin, and myosin. Mesangial cell processes bridge the gap in the GBM at the base of the capillary loop, through bundles of microfilaments that interconnect the opposing parts. This arrangement is believed to prevent capillary wall distension that can occur with intracapillary hydraulic pressure.[45] Depending upon the region in which they are located,

mesangial cells can be described as being either extraglomerular or intraglomerular. Extraglomerular mesangial cells are located near the vascular pole of the renal corpuscle and are in direct connection with cells of the juxtaglomerular apparatus. Forming a continuum into the center of the glomerulus, the intraglomerular mesangial cells are located adjacent to the glomerular capillaries. In this region, mesangial cells are in direct contact with endothelial cells due to the absence of basement membrane. Here, cells are connected by interdigitations of their respective cell membranes and are capable of communicating via gap junctions.[22] Within both regions, two different types of mesangial cells have been described.[46] A majority of the mesangial cell population is comprised of vascular smooth muscle-like cells that contain smooth muscle actin and myosin. These cells are connected to the GBM and juxtaglomerular apparatus directly or through the ECM microfibrillar proteins and are able to contract, regulating blood flow of the capillaries, thereby influencing glomerular filtration.[46] The second population of mesangial cells that have been described consists of macrophage-monocyte-like cells that have the ability to phagocytize apoptotic cells as a normal cell function.[47] Within the glomerular tuft, the GBM deviates from its pericapillary course and extends out to cover the base of the capillary loop so that it is situated between mesangial cells and podocytes[48,49]; this region comprises the mesangial angle.

It is because of their centralized location and connection with the other cell types that mesangial cells are able to perform a variety of functions including: providing structural support for the capillary loops, generating and controlling the production and maintenance of the mesangial matrix, contributing to the regulation of glomerular filtration through the regulation of capillary flow and ultrafiltration surface, and serving as a source and target of growth factors.[22,46,50] Several surface receptors of the β-integrin family are

present on mesangial cells including α1β, α3β1, α8β1, and the fibronectin receptor, α5β1. These integrins mediate attachment of cells to the mesangial matrix and link the matrix to the cytoskeleton. These connections also allow mesangial cells to mediate an extensive crosstalk to both endothelial cells and podocytes to control and maintain glomerular function.[22] Additionally, mesangial cells contribute to the pathophysiology of a number of glomerular diseases. A common response to disease includes hypertrophy and proliferation, excessive matrix production, and formation of reactive oxygen species (ROS).[19,46] Induction of transcription growth factor1β1 (TGF-β1) has been shown to play a major role in the accumulation of matrix by mesangial cells through both increased synthesis and decreased degradation of matrix components in response to mechanical stress.[46,51] Nuclear Factor kappa B (NFκB), a transcription factor, is a major pathway involved in mesangial cell pathology where stimuli such as cytokines (e.g., IL-1, TNFα), immunoglobulins, and ROS lead to upregulation of MCP-1, ICAM, IL-6, and iNOS.[46] Activated mesangial cells also produce other pro-inflammatory molecules, including IL-1β, TNF-α, PDGF, and bFGF. These act in both a paracrine and autocrine fashion, recruiting leukocytes and sustaining inflammation.[50] PDGF is a potent mitogen that is responsible for a number of mesangial cell responses to injury including proliferation, increased ECM synthesis, and increased expression of TGF-β.[46,50] An increase in mesangial matrix can result in glomerulosclerosis, decreasing glomerular surface area and ultimately decreasing GFR. Ongoing mesangial cell activation can also result in ECM accumulation in the tubulointerstitial space, resulting in interstitial fibrosis and thus contributing to the development of pathologic changes associated with ESRD.[19]

Parietal Epithelial Cells

The urinary space is encapsulated by Bowman's capsule, a basement membrane to which a single layer of cells, known as parietal epithelial cells (PECs) adhere. This outer wall is continuous with the podocytes (or visceral epithelium) at the vascular pole. In humans, these cells are very similar in morphology to squamous epithelial cells. Several subpopulations of PECs have been described, based on either a descriptive or progenitor terminology, expressing a mixture of podocyte, progenitor, and tubular markers.[19,52] Because the role for PECs as progenitor cells is still controversial, a recent study suggests naming the subpopulation of PECs based on descriptive terminology as follows.[52] All PECs express unique proteins Pax-2 and caludin-1, which distinguish them from other types of glomerular cells.[52] These are healthy PECs that traditionally line Bowman's capsule. At the vascular pole, PECs come into direct contact with podocytes and these cells have an intermediate phenotype between traditional PECs and podocytes. In electron micrographs, these cells contain granules of albumin and immunoglobulins, yet their function is unknown; these cells are referred to as peripolar or transitional cells. Also close to the vascular pole are cells that are similar in phenotype to podocytes but are clearly a part of Bowman's capsule lining the inner aspect of Bowman's capsule; these cells are called parietal podocytes. PECs showing a different phenotype or marker expression profile as a result of a response to injury from disease are referred to as activated PECs (aPECs).

In order to gain a better understanding of the biology of PECs, cells can be studied *in vitro* as cultured cells or *in vivo* in animal models.[52] While use of cell culture for studying cellular processes is indispensable, when removed from their normal physiologic environment, almost all cells undergo considerable phenotypic changes. This has made it

particularly challenging for studying PECs, as in both rat and human cells, there is considerable overlap amongst glomerular cell protein markers, making identification of PECs challenging.[52] In translational medicine, *in vivo* studies using animal models are invaluable to investigate experimental disease and therapies. However, one of the major challenges with using animals models to study PECs is that many differences, including identification markers and response to injury, have been identified between humans and rodents.[52] Nevertheless, because many of the physiological mechanisms are the same, results obtained from rodents models can generally be extrapolated for humans, keeping in mind there are some differences.

To date, unlike all the other cells previously discussed, there are no "PEC-specific" glomerular diseases currently described in the literature.[52] However, there is evidence that PECs directly participate in glomerular disease pathogenesis in a number of ways.[52] As mentioned above, as a response to disease, PECs become activated (aPECs), which is characterized by increased cellular activity, such as increased migration, proliferation, and deposition of ECM.[52] CD44 is a specific marker used to identify aPECs from other cell types, and aPECs have been recognized in a number of histologic lesions within the kidney.[52] In many glomerular diseases, cellular crescents, defined as multilayered accumulations of additional cells within Bowman's capsule, are a common pathological lesion noted by LM.[52] When these crescents occlude the urinary outlet, the affected nephron degenerates.[52,53] While both macrophages and/or podocytes can cause crescent formation, there is increasing evidence that PECs might be the predominant cell type causing this pathologic lesion.[52] PECs have also been shown to play a role in pseudo-crescent formation, a lesion identified in collapsing focal segmental glomerulosclerosis (FSGS). Additionally, PECs contribute to sclerotic lesions by migrating to the glomerular

tuft and producing ECM matrix proteins.[52] It has been hypothesized by some that these cells represent a unifying feature of secondary glomerulosclerosis irrespective of etiology.[52] PECs have been shown to have the capability of differentiating into podocytes, playing a reparative role, although evidence of this is controversial.[52,54] Lastly, PECs have been shown to be impacted by filtered albumin. PECs are exposed to proteins filtered across the GBM under normal conditions, and this exposure increases in proteinuric conditions. In culture, PECs exposed to increased albumin in the urinary space show an increase in intracellular albumin, primarily through endocytosis, which leads to PEC apostosis.[55] PEC apoptosis has a number of deleterious consequences, including causing neighboring cells to proliferate, loss of potential reparative cells, and possibly leakage of albumin into the tubulointerstial space, inciting inflammation and fibrosis.[52,56] Although their primary role in kidney disease remains to be proven, PECs have shown to significantly contribute to glomerular disease pathogenesis and, as such, there is strong evidence that their involvement in these processes should be further explored for both disease pathogenesis and therapeutic purposes.

The Glomerular Basement Membrane

The extracellular matrix situated between the podocytes and endothelium in the glomerular capillary loops of the kidney is known as the GBM. It consists of three layers, a central dense layer called the lamina densa, and two thinner layers, the lamina rara externa (attached directly to podocyte foot processes) and the lamina rara interna. The GBM is composed of a thick meshwork of type IV collagen, laminin 521, nidogen, and the heparan sulfate proteoglycan agrin secreted by both the endothelial cells and podocytes.[57] The GBM deviates from its pericapillary course and extends out to cover the base of the capillary loop as described above.[48,49] The GBM is not only important in providing

strength and stability to the glomerular tuft, but it also forms a signaling platform for both podocytes and endothelial cells that controls various aspects of cell fate including shape, growth, differentiation, and survival. Additionally, the GBM modulates cell-cell signaling by forming a reservoir of sequestered growth factors and cytokines for controlled release.[58,59]

Collagen IV

Approximately 50% of the GBM is composed of type IV collagen. It is a trimeric protein, composed of three different alpha chains that wind around each other to form a triple helix. Unlike other collagens, type IV collagen has interruptions of the Gly-X-Y amino acid repeats, which is thought to contribute to the flexibility of the GBM.[57] There are six alpha chains that trimerize to form the protomers that make up collagen IV. These protomers self-polymerize at their NH_{2-} and $COOH_{-}$ terminal domains to form the crosslinks of the network.[57] During glomerulogenesis, the GBM is composed exclusively of α1α1α2 type IV collagen. As the capillaries begin to form, the podocytes secrete α3α4α5 trimers to create the major component of the mature GBM collagen IV network.[60]

The major collagen receptors in the kidney include integrin α1β1, α2β1, and α3β1.[61,62] Integrin α1β1 has been identified at modest levels in all cells of the glomerulus but appears particularly important in mesangial cells, which depend on α1β1 for attachment to collagen IV.[63,64] Integrin α2β1 has been associated with the binding of podocytes and mesangial cells to collagen in the GBM but to a lesser extent.[29,61] Podocytes use α3β1 as their major receptor for collagen attachment.[62,65]

Laminin

Laminins are secreted as αβγ heterotrimers that are stabilized by interchain disulfide bonds.[57] Laminin chains assemble with each other by the laminin coiled-coil (LCC)

domain. At one end of the coil is the laminin globular (LG) domain that contains the binding sites for cell surface receptors such as integrins. At the opposite end of the coil, the three chains form short arms referred to as the laminin N-terminal (LN) domains which are responsible for polymerization of the trimers which initiates the assembly of basement membranes.[66] Laminin does not bind directly to collagen in GBM formation but uses nidogen (described below). During glomerulogenesis, the laminins transition from 111 to 511 and ultimately to 521 in the mature GBM.[60]

The major link of neighboring cells to the GBM is the binding of integrin α3β1, present on the basal surface of podocytes and on mesangial and endothelial cells, to its receptor, the α chain of the LG domain of laminin 521.[49,62,67] Integrin $\alpha_3\beta_1$ function is supported by tetraspanin CD151, which is thought to increase the strength of podocyte adhesion.[27]

Nidogen (Entactin)

Nidogens are dumbbell-shaped glycoproteins that act as a bridge between laminin γ1 and type IV collagen.[57,68] There are two forms: nidogen-1 and nidogen-2. Studies have shown that nidogens provide extra stability to basement membranes but are not required for their formation or function.[69]

Agrin

The major heparin sulfate proteoglycan in the GBM is agrin.[70] The sulfated glycosaminoglycan side chains create a high net negative charge in the GBM. The N-terminal domain binds to the γ1 chain of laminin 521 while the C-terminal domain contains sites for binding of cell-surface receptors such as dystroglycans and integrins.[71] Originally thought to play a role in charge selectivity, numerous studies showed that agrin

does not play an important role in permselectivity[49,57] and no critical role for agrin has been identified.

Other integrins interacting with the GBM

Integrin αvβ3, which binds to fibronectin and vitronectin, has been identified in podocytes of rats and humans.[29,61] To our knowledge, expression has not been evaluated in canines. The integrin αvβ3 has been linked to a number of different processes including: focusing the proteolytic activity of furin and pro-MT1-MMP at the cell surface for GBM turnover, serving as a receptor for urokinase leading to podocyte effacement and proteinuria, and having increased activity due to elevations in biomechanical strain.[27,29,61] Endothelial and mesangial cells have been shown to express integrin α5β1 whose ligand is fibronectin.[62]

The Tubulointerstitium

While the primary focus up to this point has been on the components of the glomerulus, it is necessary to recognize the role that the tubulointerstitium plays in the progression of CKD. Therefore, discussion of the tubules is warranted, but a full description of the tubules and fine detail of their function is beyond the scope of this introduction.

As the name implies, the tubulointerstitium consists of the renal tubules and the intertubular, extraglomerular, extravascular space of the kidney.[72,73] The interstitium is bound on all sides by tubular and vascular basement membranes and filled with a variety of cells including dendritic cells, leukocytes, perivascular cells, and fibroblasts, along with ECM and interstitial fluid.[72] Microvessels, including arterioles, venules, capillaries, and lymphatics also run through the interstitium.[72] In normal kidney tissue, the interstitium is barely visible. Once thought to be passive tissue with a primary function of supporting the tubular epithelium, recent studies have shown that the renal interstitium has a physiologic endocrine function with cells serving as a source of both erythropoietin and renin in

addition to playing a role in fluid and electrolyte exchange and insulation between tubules.[72,74]

The renal tubule is a crucial part of the nephron as its role is to modify the ultrafiltrate from the glomerulus using selective reabsorption and excretion of filtered molecules. The tubule consists of the following sections: the proximal convoluted tubule, the proximal straight tubule, the loop of Henle (divided into the thin descending limb, thin ascending limb, and thick ascending limb), the distal convoluted tubule, and the collecting ducts. While a number of different solutes are regulated as a result of normal renal function, the most important transport functions of the tubules includes the control of water and the handling of sodium (Na^+) and potassium (K^+).[75] In most animals, including the dog, the net function of the nephron is to excrete urea, creatinine, K^+, hydrogen, ammonium, and phosphate, while conserving Na^+, chloride, bicarbonate, calcium, magnesium, glucose, proteins (amino acids), and water.[76]

The first part of the renal tubule is the proximal convoluted tubule (PCT), which is located in the cortex of the kidney, close to the renal corpuscle. Fluid that is filtered from the glomerular filtration barrier feeds into Bowman's space and enters into the proximal tubule. The PCT is formed by a single layer of cuboidal epithelial cells. One of the primary functions of the PCT is reabsorption of water and solutes. To facilitate this, the apical surface of the cells contains a brush border that increases surface area. A majority of water and solutes that enter the PCT are reabsorbed through active, facilitated, and passive transport.[76] Expression of Aquaporin-1, a water channel in the cell membrane, has been utilized to identify this region of the nephron by immunohistochemistry in many animals, including the dog.[77] Approximately 65-80% of filtered Na^+ is reabsorbed down a concentration gradient established by a Na^+-K^+-ATPase pump on the basolateral

membrane. A number of other ions including chloride (Cl^-), bicarbonate, phosphate, and calcium are also reabsorbed. Glucose, which freely passes through the filtration barrier, is reabsorbed in the PCT through a process known as secondary active transport using a Na^+-glucose cotransporter. Additionally, nearly all filtered proteins, including vitamins, hormones, and enzymes, along with amino acids are reabsorbed in the proximal tubules.[78] Amino acids are reabsorbed by specific carriers while small proteins are hydrolyzed at the brush border into amino acids and reabsorbed. Larger proteins (including albumin) enter tubular cells by receptor-mediated endocytosis and then are degraded into amino acids by lysosomes and returned to the blood.[78,79] Megalin and cubilin are multi-ligand endocytic receptors that are expressed on the apical membranes of the proximal tubule cells and have been identified as essential receptors in this process.[78] Megalin contains a single transmembrane domain with the cytoplasmic tail that regulates receptor trafficking and clathrin-mediated endocytosis.[78] Cubulin is an extracellular protein that depends on other membrane proteins, like megalin or amnionless, for localization and endocytosis.[78] Upon uptake, ligands are released from the endocytic vesicles and transferred to other compartments, including lysosomes, for further processing, while megalin and cubulin are recycled back to the apical surface through dense apical tubules.[78] Due to the highly efficient tubular uptake of proteins, particularly albumin, albumin is considered not to be present in the urine of healthy individuals, except for in dogs, where low concentrations may be present.[76,80] Megalin and cubulin are likely involved in the development of protein overload-induced CKD, but further investigation is needed to clarify their role.[78,80]

After the filtrate leaves the PT it enters the loop of Henle. This is a u-shaped tube containing different segments that perform different functions.[81] Nephrons can be classified as either short-looped or long-looped. Long-looped nephrons originate from the

juxtamedullary region and have three segments: the thin descending limb, the thin ascending limb, and the thick ascending limb (TAL).[81] Short loop nephrons, which originate from the superficial and mid-cortical regions, lack a thin ascending limb.[81,82] While there are distinct morphological differences in the cells that construct these structures, in general, tubes are lined by simple cuboidal epithelium without a brush border.[82] In the descending limb, the cells are impermeable to Na^+ so that tubular fluid is concentrated while the volume is reduced by the passive reabsorption of water. Aquaporin-1 expression has also been described as an identifying marker of the descending thin limb on immunohistochemistry in many animals, including the dog.[77] In the ascending limb, solutes, primarily Na^+, K^+ and Cl^-, passively leave the tubular fluid using a Na^+-K^+-$2Cl^-$ carrier. This region is impermeable to water; therefore, tubular fluid becomes more dilute.[81] Cells of the TAL express the membrane bound protein uromodulin (also known as Tamm-Horsfall glycoprotein), which has been used as an identifying marker in kidney tissue, including the dog.[77,81] More recent reports demonstrate that in the mouse and human kidney, uromodulin is also expressed in the early portion of the distal convoluted tubule (DCT).[83] Uromodulin is the most abundant protein in healthy mammalian urine and is exclusively expressed in the kidney.[83] Uromodulin has been shown to play a role in regulation of sodium and chloride and thus blood pressure, protecting against urinary tract and kidney stone development, and immunomodulation.[83,84] Additionally, uromodulin has an influence on urinary concentrating ability in the TAL by creating a hydrophobic, gel-like structure that may act as a seal to contribute to the impermeability of water.[84] Uromodulin serves as the matrix component of hyaline casts.[84] Because uromodulin is a kidney-specific protein produced by tubular cells, urinary uromodulin has been explored as a biomarker for tubular dysfunction as decreased production has been reported to

correspond with advanced kidney disease.[84,85] Towards the end of the segment, the TAL comes into close contact with the glomerulus from which it originated at the vascular pole, forming the junction that constitutes the macula densa.[81] The macula densa consists of approximately 20 cells per nephron, and it acts as a renal sensor element to detect changes in distal tubular fluid composition. It transmits signals to the glomerular vascular elements to control GFR and blood flow in a process termed tubuloglomerular feedback described in more detail below.[86]

The next segment of the nephron immediately downstream from the macula densa is the distal convoluted tubule (DCT). Cells in the DCT have a unique morphology in that their nuclei are apically located due to numerous basolateral invaginations within the cell, and their cytoplasm is tightly packed with mitochondria indicating they are highly metabolically active.[87] The DCT plays a crucial role in NaCl reabsorption, K^+ secretion, and calcium and magnesium handling.[87] It is also unique in that it has the capability to respond to hormonal stimuli.[87] Cells of the macula densa are able to detect variations in NaCl, which is highly dependent on urine flow rate.[86] Elevations in urine flow rate result in increases in luminal NaCl concentrations. This is detected by the macula densa that initiates a tubuloglomerular feedback response, leading to vasoconstriction of afferent arterioles thus reducing glomerular hydrostatic pressure and returning the GFR to normal.[86] Additionally, in response to volume depletion or hyperkalemia in the DCT the macula densa sends signals to increase renin release from the juxtaglomerular cells, activating the renin–angiotensin–aldosterone system (RAAS), which in turn regulates blood pressure and volume.[87] Calcium reabsorption in the DCT is partially regulated by a calcium binding protein known as Calbindin-D28k that is expressed primarily by DCT

cells.[88] This protein has been used in the dog for identification of the DCT using immunohistochemistry with both nuclear and cytoplasmic staining expected.[77]

The last segment of the renal tubule system is the collecting duct (CD). The CD runs through the cortex into the medulla and opens into the renal papilla. The epithelium in this region varies from cuboidal to columnar (near the papilla). There are two major populations of epithelial cells in the CD: principal cells and intercalated cells.[89,90] The principal cells are regulated by a wide variety of stimuli including hormonal, autocrine, and paracrine factors, osmotic conditions, and physical factors. These cells are crucial for the maintenance of salt and water transport reflected by its defining transporters: the epithelial sodium channel and the aquaporin 2 water channel.[89] These functions are regulated by the hormones aldosterone and vasopressin, respectively. Aldosterone, described above, causes increased sodium reabsorption and potassium secretion. Vasopressin is released in response to changes in osmolality primarily determined by Na concentration detected by baroreceptors in the aortic arch and hypothalamic chemoreceptors.[89] Vasopressin enhances water reabsorption through stimulation and accumulation of aquaporin 2 water channels in the luminal plasma membrane.[89] When vasopressin binds to its type 2 receptor on the basolateral membrane of the cell, a cAMP signaling cascade is activated, ultimately leading to the translocation of aquaporin 2 from intracellular vesicles to the apical membrane. Through an osmotic gradient, water is then able to pass through the channels into the cell and exits into the interstitium via aquaporin 3 and 4 channels. Aquaporin 2 can be used as a marker on immunohistochemistry for the identification of the CD in many species, including the dog.[77] The second major cell population in the CD, and also the most abundant, is the intercalated cell.[90] These cells are traditionally associated with the regulation of acid-base homeostasis but also participate in

K^+ and ammonia transport.[90] Additionally, these cells have been shown to play a role in the innate immune system through the expression of Toll-like receptors (TLRs), which help mitigate the development of urinary tract infections and pyelonephritis.[90] The most common uropathogen, *Escherichia coli*, is recognized by TLR4, which is expressed in intercalated cells.[90] Intercalated cells also secrete a bacteriostatic protein known as neutrophil gelatinase associated lipocalin (NGAL).[90] Expression of NGAL is intensely upregulated in various causes of acute kidney injury and, as such, can be used as a biomarker for this process.[91]

Exploring the Pathogenesis of CKD

CKD is ultimately a progressive disorder. Traditionally, the diagnosis of CKD relies heavily on biomarkers that provide an estimation of kidney function, particularly GFR, including sCr concentration, blood urea nitrogen (BUN), and urinalysis. Due to compensatory mechanisms that are able to maintain GFR within normal limits, CKD can remain clinically silent for an extended period of time and once detected, a substantial amount of kidney damage has already occurred. Therefore, the identification of biomarkers that would allow for the detection of disease at the initial stages is crucial. While CKD can develop from a number of etiologies, irrespective of the cause, histologic hallmarks of CKD include interstitial fibrosis and inflammation, peritubular capillary loss resulting in tissue hypoxia, and tubular atrophy.[92,93] Given these similarities, it is plausible that the mechanisms leading to progression of CKD share commonalities regardless of initiating event. Therefore, evaluating the pathogenesis of one etiology leading to CKD could be beneficial in all cases, shedding light on the developmental process. This in turn can lead to a more comprehensive understanding of disease development which then could assist in the discovery of biomarkers allowing for earlier detection of disease. Additionally, this

may also open the door to the identification of potential therapeutic targets that could help ameliorate disease progression. These advancements would allow veterinarians to provide dogs with appropriate treatments sooner due to earlier diagnosis, which ultimately would lead to an improved quality of life.

A model of CKD: Alport syndrome and X-linked hereditary nephropathy

In humans, Alport syndrome (AS) is a hereditary disease caused by a mutation in any one of the three type IV collagen genes, *COL4A3*, *COL4A4*, or *COL4A5*. Normally, the three collagen chains come together to form heterotrimers (called protomers) by precise interactions of the carboxyl-terminal globular NC1domains. However, loss of any one of these chains prevents protomer formation and further assembly into the basement membrane superstructure resulting in complete absence of the of the α3(IV)/α4(IV)/α5(IV) network of the GBM.[94] Only the thinner, less supportive structure of the α1 (IV)/α2 (IV) GBM remains.

There are essentially two principal genetic variations of AS. The most common form, resulting in approximately 80-85% of cases, is X-linked AS (XLAS) which is associated with mutations in the *COL4A5* gene located on the X chromosome. To date, more than 1100 unique variants have been identified in the *COL4A5* gene of humans resulting in XLAS.[95,96] It has been noted that there is an association between severity of mutation and severity of disease.[94] Missense mutations that result in glycine substitutions are generally less severe than those mutations that result in chain termination such as deletions, insertions, rearrangements, and nonsense mutations.[94,95] Approximately 15% of AS cases are autosomal recessive (ARAS) and result from a mutation in both copies of either the *COL4A3* or *COL4A4* genes. Cases of an autosomal dominant form of AS (ADAS), resulting from a heterozygous mutation in either *COL4A3* or *COL4A4* genes,

have been reported.[97,98] This form of the disease is much milder compared to the other two. Originally thought to be rare (and its existence is even questioned by some), data using next generation sequencing analysis suggests that the frequency of ADAS may actually be underestimated.[99] Unlike the other forms of AS, in ADAS, all three chains of collagen IV are still present in the affected GBM; it has been suggested that the structure of the α3 or α4 chain is altered thereby disrupting the normal GBM function which leads to the disease.[100,101]

Animal models are crucial to understanding normal kidney physiology and pathophysiology of kidney diseases and evaluating the efficacy of therapeutic interventions in CKD. In dogs, there is an equivocal disease of XLAS known as X-linked hereditary nephropathy (XLHN). In 1997, a colony of dogs with the disorder was established by Dr. George Lees at Texas A&M University and has been maintained since.[102] Affected males have a naturally occurring 10 base pair deletion in the gene encoding the α5 chain of type IV collagen. Just as in human counterparts, disease in affected males quickly progresses during adolescence, and end-stage renal failure typically occurs before one year of age. Development and progression of XLHN in these dogs has been described.[102] Representative images of pathologic changes observed on LM are featured in Appendix A-1. In advanced stages of disease, histopathologic changes are typical of CKD due to glomerular disease including global glomerulosclerosis, tubular dilation, interstitial fibrosis, and inflammation.[103-105] This large animal model provides an efficient, controlled model of CKD progression due to primary glomerular disease, and data generated from these dogs could potentially be applied to all causes of CKD development.

Cellular crosstalk between glomerular cells

As described above, both glomerular and tubular cells use a number of signaling pathways to regulate their activity in order to communicate and maintain homeostasis in a normal physiologic state. It is the modification of these normal pathways that typically lead to the development of disease, including CKD.[106] Glomerular cells function as an integrated unit through the secretion of growth factors and signaling peptides that act as effector molecules by engaging in target receptors and inducing signal transduction.[107] The ECM also plays an important role in storing secreted ligands, generating concentration gradients, and presenting ligands to cell receptors.[107] Many of these signaling ligands serve in both an autocrine and paracrine fashion (Figure 5).

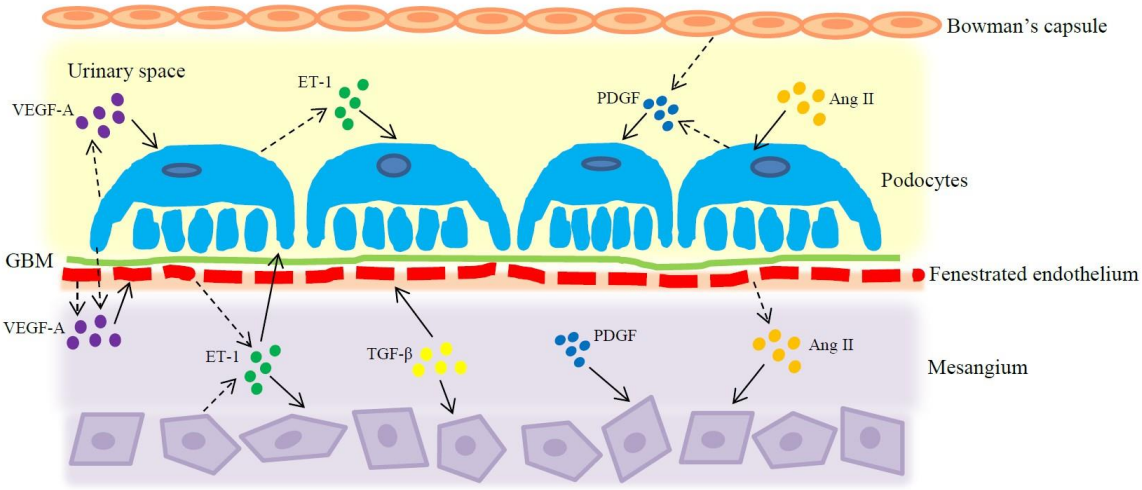

Figure 5 Schematic representation of the action of secreted signaling ligands involved in cellular crosstalk between cells in the glomerulus. Ang II-angiotensin II; ET-1-endothelin-1; PDGF-platelet derived growth factor; TGF-β-transforming growth factor-β; VEGF-A-vascular endothelial cell growth factor A; Artwork created by S. Clark.

Many studies have confirmed the importance of vascular endothelial growth factor A (VEGF-A), secreted from podocytes, in the maintenance of glomerular filtration, and increased levels have been associated with many glomerular diseases.[107] After severe or recurrent injury, renal tubular cells undergo changes in structure and cell cycle that result

in altered expression and production of cytokines that promote crosstalk with inflammatory cells, endothelial cells, and fibroblasts resulting in fibrosis.[93] It is well-documented that both TGF-β and platelet-derived growth factor (PDGF) signaling are important in the induction of fibrosis in CKD. In one study exploring gene expression in renal pathogenesis of dogs with XLHN, it was shown that TGF-β, connective tissue growth factor, and PDGFα were overexpressed early in the disease when compared to expression in controls.[108] Changes in normal cellular pathways often lead to aberrant expression of signaling molecules, which are either up-regulated or down-regulated.[106] It is by exploring the mechanisms of the cellular crosstalk and capitalizing on these alterations that will expand our understanding of CKD pathogenesis and open the door to discovering earlier biomarkers of disease in addition to more effective therapies. Activation of cell signaling pathways, either by cell-matrix or cell-cell interactions, can also result in changes in gene expression. Therefore, exploring key elements of gene regulation is also an important avenue to consider.

microRNAs (miRNAs) and CKD

MicroRNAs (miRNAs) are a class of small non-coding RNAs that bind to complementary target sequences in messenger RNA serving as posttranscriptional regulators of gene expression and thus protein production.[109,110] Their sequences are highly conserved across species.[111] The processing of miRNA is tightly regulated, and miRNAs are involved in a number of biological pathways and cellular processes including cell proliferation, apoptosis, cellular development and cell signaling.[110] The processing of miRNAs is commonly explained by the canonical biogenesis pathway, a linear process originally thought to be universal to all miRNAs.[112-115] However, as our understanding of miRNA processing has improved, it has been determined that the biogenesis of miRNAs can be a

complex process with various strategies applied that either interfere with or facilitate each step, including recruitment of transcription factors, RNA-binding proteins, and various modifying enzymes.[112,115] For a general overview, the next section will refer to the canonical biogenesis pathway to describe the regulation of miRNA processing and mention important variations where applicable.

The biogenesis of a miRNA begins with transcription of the miRNA gene from chromosomal DNA by RNA polymerase II into the primary miRNA (*pri-miRNA*). A majority of miRNA sequences are encoded by introns of non-coding or coding transcripts, but they may also be located within exonic regions.[115] This transcript, which is typically over 1 kb long, forms a stem-loop structure in which the mature miRNA is embedded, along with a single stranded 5' guanosine cap and a 3' poly-adenylated tail. The precise promoter locations for miRNAs have not yet been mapped for most genes, but transcription of pri-miRNAs can be regulated through a number of processes including transcription factors (p53, MYC), methylation of promoter sequences, or histone modifications.[115] Studies have revealed that editing of the pri-miRNA itself can also occur by Adenosine deaminases acting on RNAs (ADARs), which catalyze adenosine to inosine in double stranded RNAs.[116] Because inosine preferentially base pairs with cytidine, this generates a conversion equivalent to an adenosine to guanosine change, thus altering the structural properties of the pri-miRNA.[112,116] This ultimately affects miRNA biogenesis by either causing degradation of the miRNA or by altering the set of messenger RNAs that they regulate.[116]

Following transcription, the pri-miRNA is cleaved by a nuclear microprocessor complex comprised of two proteins: Drosha (an RNase III enzyme) and DGCR8 (or Pasha). This results in a 70-120 nucleotide long, double-stranded, hair-pin like structure

called precursor miRNA (*pre-miRNA*). Drosha cleaves the hairpin at approximately 11 base pairs away from the basal junction between single-stranded and double-stranded RNA and approximately 22 base pairs away from the apical junction linked to the terminal loop.[115] The basal junction is crucial in determining the cleavage site.[115] Other elements have also been shown to be involved in pri-miRNA processing. Drosha has been shown to form larger complexes that contain additional helicases and proteins that can act as specificity factors for processing specific pri-miRNAs through the binding of specific motifs.[112,115] Additionally, the microprocessor itself can be regulated by either enhancement of Drosha processing through SMAD binding or inhibition of Drosha by LIN28.[112,113,115] The processing of pri-miRNA to pre-miRNA by the Microprocessor is not necessarily required; if an intron-derived miRNA is comparable to the size of a pre-miRNA, it can bypass the microprocessor step. These miRNAs are referred to as mitrons.[112,114]

Following Drosha processing, the pre-miRNA is actively exported into the cytoplasm by Exportin-5 complexed with Ran-GTPase where maturation is completed. It is the defined length of the double-stranded stem along with the 3' overhang of the pre-miRNA that is important for binding to Exportin-5 and ensuring the export of an appropriately processed pre-miRNA.[112,115] Exportin is ubiquitously expressed, and while regulation of this protein has been less investigated, studies have shown that it can be induced upon DNA damage or repressed in some tumors.[115] In the cytoplasm, the pre-miRNA is cleaved by Dicer, an RNase III-type endonuclease, near the terminal loop. In general, Dicer binds to pre-miRNA and cleaves in one of two ways: 1) with a preference for a two-nucleotide-long 3' overhang at which it cleaves at sites located at fixed distances (known as the 3'-counting rule) or 2) at the 5' phosphorylated end where it cleaves 22

nucleotides away (the 5'-counting rule).[115] The 5' end binding occurs when the end is thermodynamically unstable but not when the end is strongly paired (i.e. GC pairing).[115] Dicer interacts with its cofactor, TAR RNA-binding protein (TRBP) which modulates the proficiency and tunes the length of the mature miRNA.[115] The binding of TRBP causes a conformational change that activates Dicer cleaving the hairpin and forming the miRNA duplex (referred to as miRNA/miRNA*) to its mature length of approximately18-23 nucleotides long. After cleavage, the Dicer-TRBP complex dissociates from the miRNA duplex where it is subsequently loaded onto an Argonaute family protein (AGO) to form the pre-RNA-induced silencing complex (pre-RISC). RNA duplexes are preferentially loaded onto particular types of AGO proteins, AGO 1-4, depending on their intrinsic structural properties, and this is an active process that requires ATP.[115] The guide strand is determined during the loading step, mainly based on stability of the two ends of the RNA duplex; the strand with an unstable terminus at the 5' side is typically selected.[112,115] However, strand selection is not completely restricted. AGO proteins may select guide strands with a U at the nucleotide position.[115] Additionally, alternative strand selection, described as arm switching, has also been observed.[115] The passenger strand is quickly removed, either by unwinding of the strands or cleavage of the passenger strand. It is then degraded, leaving the guide strand bound to AGO and thus forming the mature RISC.[115] The guide strand directs the complex to the target mRNA through complementary binding to the 3'-untranslated region (UTR) or open reading frame (ORF). The target mRNA is then silenced either through repression of translation, cleavage, or deadenylation. It is thought the more complementarity in the miRNA-mRNA pairs result in degradation while the lesser complementarity pairs lead to inhibition of translation.[114] Structures called P-bodies have been identified that contain miRNAs bound to their target mRNA where they

are believed to be stored for degradation.[114] Additionally, miRNAs can be packed into exosomes or microvesicles, loaded into high-density lipoproteins (HDL), or bound by AGO2 protein outside of vesicles (**Figure** 6) where they are able to be delivered to other cells, generating a form of intercellular communication or crosstalk.[111]

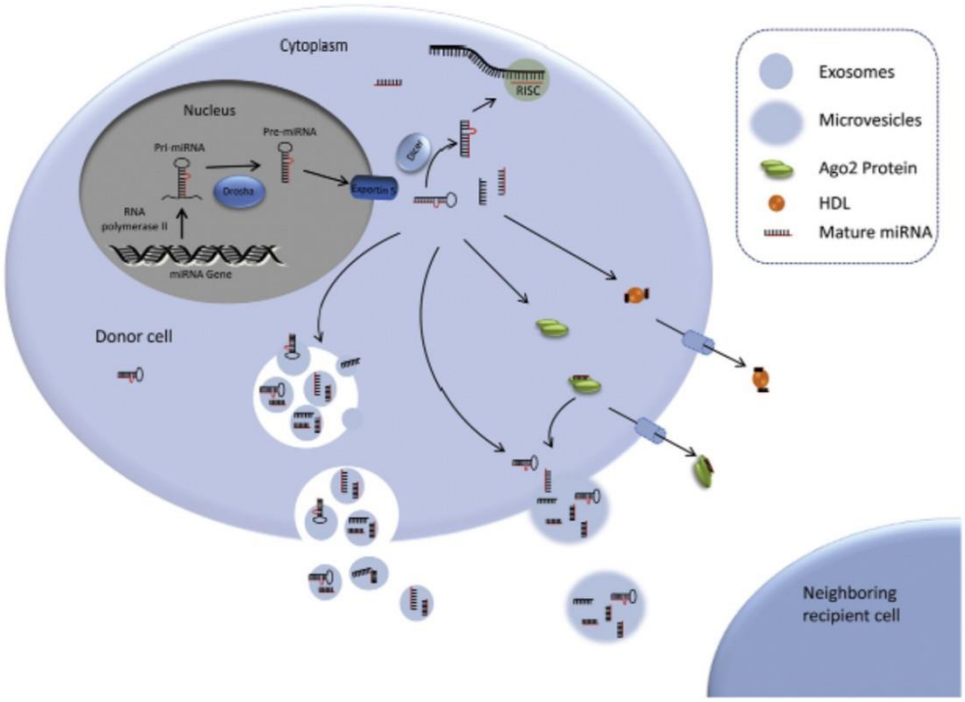

Figure 6 miRNA biogenesis and the release of miRNAs into the extracellular environment.[110] Reprinted with permission.

Numerous studies have shown that miRNAs are extremely stable in extracellular fluid, including serum, body fluids, and urine.[111] Changes in normal cellular pathways often lead to aberrant expression of signaling molecules and thus gene expression, including differential expression of miRNAs. The aberrant expression of miRNAs has been implicated in disease pathogeneses allowing for the generation of specific miRNA expression profiles for certain diseases, including CKD.[114,117] Because of their disease specificity, extracellular stability, and relative ease of quantification, mature circulating

miRNAs have been elucidated for use as biomarkers.[118-120] For example, a key finding of CKD is the presence of tubulointerstitial fibrosis on histopathological evaluation.[121] The TGF-β/Smad pathway is a key promoter of CKD progression and fibrosis development. Several miRNAs have been identified as target genes regulated by TGF-β and have been shown to modulate renal fibrosis including miR-21, Let7b/c, miR-30, miR-215, miR-377, miR-216, miR-217, miR-93, and miR-25. [121-124]

In addition to aberrant expression of individual miRNAs, the overall level of total miRNAs in circulation or different panels of miRNAs have been evaluated. One study showed that compared to normal patients, patients with Stage 4 CKD (and ESRD) had lower total miRNA levels in plasma.[125] They also determine that all five of the miRNAs evaluated, miR-16, miR-21, miR-155, miR-210, and miR-638, showed a significant inverse correlation between abundance and kidney function (eGFR). In another study, patients with UUO-induced renal fibrosis had notable increased expression of miR-21, miR-142-3p, miR-142-5p, miR-214, and miR-223 while miR-101a, miR-193, and miR-218 were significantly downregulated.[123]

Multidirectional crosstalk among renal cells is controlled by a number of signaling pathways and is a crucial component of both normal physiology and in the pathogenesis of chronic kidney disease. These modalities of communication and interactions between cells range from signaling molecules to short, non-coding RNA messengers. As such, the overall goal of the research presented in this dissertation is to gain further insight into the pathogenesis of CKD development and progression by exploring mechanisms of cellular crosstalk using dogs with XLHN as a large animal model. This will allow for numerous advancements including: 1) the possibility of developing minimally invasive diagnostic tools that can be used for earlier detection and better monitoring of progression of CKD

and 2) identification of potential therapeutic targets in the hope of improving the overall quality of life in dogs with CKD. Additionally, given the commonalities of XLHN to AS, many of these features may translate to improved diagnostics and therapeutic efficiencies in human medicine as well.

CHAPTER II

INVESTIGATION OF THE EARLY MOLECULAR CHANGES OF DISEASE IN DOGS WITH XLHN*

Background and Significance

The glomerular basement membrane (GBM) is a distinct, thin layer of extracellular matrix (ECM) situated between podocytes and endothelium and composed of a meshwork of type IV collagen, laminin 521, nidogen, and the heparan sulfate proteoglycan, agrin. The GBM plays an integral role in glomerular filtration through both size and charge-selectivity.[49,57] Additionally, the GBM deviates from its pericapillary course and extends out to cover the base of the capillary loop between the mesangial cells and the podocytes.[48]

Approximately 50% of the GBM is composed of type IV collagen, which is essential in maintaining both stability and function.[126] Type IV collagen alpha chains form heterotrimers, which self-assemble forming a tissue-specific cross-linked network.[57,126] During nephrogenesis, the GBM is composed exclusively of α1α1α2 type IV collagen. As the glomerulus matures, the sub-epithelial α1α1α2 network is replaced by α3α4α5 type IV collagen secreted by the podocytes, a composition that predominates in the mature GBM.[60,127] The α3α4α5 type IV collagen network is more heavily cross-linked and protease-resistant than α1α1α2, and is therefore better suited for maintaining GBM integrity from increasing hydrostatic pressure associated with maturation to which glomeruli are exposed.[49,128-130] Laminin is the most prevalent non-collagenous protein of the GBM. These cross-shaped heterotrimers consists of an α, β, and γ chain with sixteen

* Reprinted from Clark SD et al. (2016) X-Linked Alport Dogs Demonstrate Mesangial Filopodial Invasion of the Capillary Tuft at an Early Event of Glomerular Damage. *PLOS ONE* 11(12): e0168343.doi: 10.1371/journal.pone.0168343.[177]

different isoforms being identified.[131] The mature GBM is comprised of laminin 521 (α5β2γ1).

Alport syndrome (AS) is a hereditary disease that has been characterized in mice, dogs, and humans.[97,102,132-135] It is caused by mutations in the α3, α4, or α5 type IV collagen genes, leading to delayed-onset progressive glomerulopathy. The disease has similar renal clinical manifestations in all species, including hematuria and/or proteinuria and eventually end-stage renal disease. Two main forms of AS exist. XLAS is due to a mutation in the COL4A5 gene and accounts for approximately 80% of cases. Autosomal AS (dominant or recessive) results from a mutation in either COL4A3 or COL4A4 and accounts for the remainder of the cases.[97] Because of the way collagen is assembled, a mutation in any one of the α chain genes prevents formation of the α3α4α5 type IV collagen protomer resulting in absence of the sub-epithelial α3α4α5 type IV collagen network and a GBM comprised only of α1α1α2 type IV collagen. With fewer interchain crosslinks, this change in composition compromises the long-term integrity of the GBM.[49,136,137] On renal biopsy, the lack of α3α4α5 results in thinning and thickening of the GBM often referred to as a "basket weave" appearance in electron micrographs that is virtually pathognomonic for the disease and serves as one of the components of a definitively diagnosing the disease.[97,128,136,138]

In normal glomeruli, laminin 211 (α2β1γ1) is located within the mesangium but not the GBM. The laminin of the GBM consists only of laminin 521. Evaluation of glomeruli obtained from mice, dogs, and humans in the early stages of AS show a distinctive feature of aberrant laminin deposits within the GBM, including patchy, non-linear deposits of laminin 211, regardless of the mode of inheritance.[139] However, the source of this abnormal deposition was unknown.[139,140] Using integrin α1-deficient mice crossed with AS

mice to create a double knockout, the abnormal deposits of laminin 211 were associated with the degradation of the GBM early in the disease process.[140] In autosomal recessive 129/Sv Alport mice, GBM laminin 211 was shown to originate from mesangial cell filopodia that progressively invaded capillary loops.[141] Additionally, biomechanical strain in the capillary wall due to the thinner GBM and fewer cross-links of α1α1α2 type IV collagen is associated with induction of mesangial cell process invasion, contributing to initiation and progression of disease.[141] Furthermore, focal adhesion kinase (FAK) activation occurs specifically in regions where abnormal laminin is present, causing increased expression of interleukin-6 (IL-6) and matrix metalloproteinases (MMPs), particularly MMP-9, MMP-10, and MMP-12, all of which contribute to disease progression by propagating GBM destruction.[142-145] Recent work performed in Alport mice revealed that the biomechanical strain placed on the abnormal GBM causes induction of endothelin-1 (ET-1) by endothelial cells in the glomeruli. This in turn activates endothelin A receptors (ET_AR) on mesangial cells, leading to mesangial filopodial invasion, and ultimately to the inflammatory response as described above.[130] Evaluation of urine from AS mice compared to wild type showed elevated levels of ET-1 in the urine prior to the development of proteinuria.[130] As such, it has been suggested that ET-1 levels in urine may be used as an early biomarker for Alport renal disease.

Advancement in understanding the molecular mechanism of AS progression has been established primarily using murine models. While mice have rapid progression of disease and are less expensive compared to large animal models, they also possess a number of limitations.[103] They lack genetic heterogeneity, have different immune and metabolic responses compared to people, and knockout mouse models do not always emulate human disease.[146,147] Large animal models provide a strong link from mice to

humans, particularly for testing of therapeutic efficacy. Thus characterization of these models is imperative.

Specific Objective and Hypothesis

The specific objectives of this aim are to: 1) identify the early structural/functional changes associated with the pathogenesis in canine to demonstrate that these mechanisms are similar to those that are observed in AS mice. This helps to support the hypothesis that the pathogenesis in humans is also likely comparable to that observed in these animal models; and 2) validate that the dog is a suitable large animal model for evaluation of AS progression and novel therapeutic trials.

We hypothesize that the early events of disease initiation, which involves extension of mesangial filopodia into the GBM followed by laminin 211 depositions, will mirror, in canine tissue of dogs affected with XLHN, that which has been observed in tissue from Alport mice and humans. This will support the notion that the dog is a suitable large animal model for human AS.

Experimental Design and Methods

Sample Collection

Samples were obtained from a colony of male dogs with X-Linked Hereditary Nephropathy (XLHN) and all protocols used were approved by the Texas A&M University Institutional Animal Care and Use Committee. Starting at 7 weeks of age, blood and mid- stream voided urine were collected on a weekly basis. Physiologic data, including serum creatinine (sCr), urine protein: urine creatinine ratio (UPC), symmetric dimethylarginine (SDMA), and iohexol clearance were used as previously described [30] to detect advancement of disease defined by set milestones (MS). Additionally, ultrasound-guided needle biopsies of the kidneys were obtained from all dogs at these time points. Milestones

were defined as: MS 1-presence of microalbuminuria for two consecutive weeks, MS 2-UPC ≥ 2 for two consecutive weeks, MS 3-sCr ≥ 1.2 mg/dL, MS 4-sCr ≥ 2.4, and MS 5-sCr ≥ 5 mg/dL. Testing for microalbuminuria was performed only until MS 1 was reached using a semi-quantitative test (E.R.D. HealthScreen Canine Urine Test strips, Heska, Loveland, Colorado). WT dogs were paired with an AS littermate for milestone evaluation to serve as a control. SDMA is a methylated arginine that is released in the blood during protein degradation and excreted by the kidneys. In dogs, it serves as a useful marker for evaluation of decreasing renal function.[148]

For kidney biopsy collection, dogs were anesthetized using a premedication combination of 0.011 mg/kg glycopyrrolate (Fort Dodge, Overland Park, KS) and 0.30 mg/kg butorphanol (Zoetis, Florham Park, New Jersey) injected subcutaneously. Dogs were intubated following administration of 4-6 mg/kg propofol (Abbott, Worchester, Massachusetts) intravenously, and anesthesia was maintained using isoflurane (Zoetis Florham Park, New Jersey). Once the dog was fully anesthetized, biopsies were obtained using a 16-18 gauge Bard Monopty® Disposable Core biopsy instrument. Biopsies were performed on alternating kidneys as each MS was reached. Samples were divided and placed into formalin, glutaraldehyde or Optimal Cutting Temperature (OCT) compound (Tissue-Tek OCT Compound, Sakura Finetek USA, Torrance, CA). Samples in OCT were flash frozen in liquid nitrogen vapor and stored at -80^{o}C until evaluation. When AS dogs reached MS 5 or had clinically significant disease, they were humanely euthanized following biopsy collection.

Light and Electron Microscopy Evaluation

For light microscopy, formalin-fixed, paraffin-embedded biopsies were sectioned at 3 µm and stained with H&E, Masson's trichrome, and Periodic acid-Schiff. Sections were scored

as previously described.[149] An average glomerulosclerosis score was determined for each milestone in both the WT and AS dogs using the following features: segmental sclerosis, global sclerosis, and synechia. Similarly, an average tubulointerstitial damage score was determined using the following features: tubular dilation, loss of brush border, tubular atrophy, tubular epithelial cell degeneration/regeneration, tubular single cell necrosis, interstitial fibrosis, and chronic interstitial inflammation (nephritis).

For transmission electron microscopy (TEM), tissues were fixed in chilled 3% glutaraldehyde and post-fixed in 1% osmium tetroxide. Dehydration was performed using a series of alcohols followed by infiltration in an acetone/epoxy plastic for embedding. Semi-thin sections were cut with an ultramicrotome (EM UC6, Leica Microsystems, Buffalo Grove, IL) and stained with a mixture of Azure II and methylene blue. When the optimal area for evaluation was identified, ultrathin sections were cut (65-85 nm) and mounted on copper grids. The sections were post-stained with uranyl acetate and lead citrate. Grids were imaged on a JEOL JEM-1400 TEM (JEOL USA, Inc., Peabody MA) and photographed with an Olympus SIS Veleta 2K camera (Olympus Soft Imaging Solutions GmbH, Munster, Germany).

Immunofluorescence Antibodies

The following antibodies were used: rabbit anti-mouse fibronectin (Sigma, St. Louis, MO, USA, Cat# F3648), goat anti-mouse integrin α8 (R&D Systems, Minneapolis, MN, USA, Cat# AF4076), mouse anti-bovine laminin β2 C4 (Developmental Studies Hybridoma Bank, University of Iowa, Iowa City, IA, USA), rabbit anti-mouse collagen IVα5 (Cosgrove) and rabbit anti-human laminin α2 (gift from Dr. Peter Yurchenco, Robert Wood Johnson Medical School, Piscataway, NJ, USA). Alexa-fluor conjugated secondary antibodies (Invitrogen, Carlsbad, CA, USA) included: donkey anti-rabbit 594 for anti-

fibronectin and anti-collagen IVα5, and donkey anti-goat 568 for anti-integrin α8 and donkey anti-rabbit 488 for anti-laminin α2 or donkey anti-mouse 488 for anti-laminin β2 C4 (for dual staining). Negative controls were performed using the host serum in combination with the specific antibodies described above.

Immunofluorescence and Confocal Microscopy

Immunofluorescence was performed at Boys Town National Research Hospital. Frozen OCT-embedded kidney biopsy samples were sectioned at 6 µm and acetone fixed. Sections were incubated overnight at 4ºC in a primary antibody solution comprised of 0.3% PBST (Triton X-100), 5% fetal bovine serum, and the following antibody dilutions: 1:500 (fibronectin and collagen IVα5), 1:200 (integrin α8 and laminin α2) or 1:50 (laminin β2 C4). Slides were rinsed with 1X PBS and incubated at room temperature for 1 hour with the appropriate secondary antibody solution consisting of the secondary antibody along with 0.3% PBST (Triton X-100), and 5% fetal bovine serum to make a 1:500 antibody dilution. Slides were rinsed again with 1X PBS and mounted using Vectashield mounting medium, which contained DAPI to counterstain the nuclei (Vector, Burlingame, CA). Confocal images were captured using a Leica TCS SP8 MP microscope interfaced with a LSM510 META confocal imaging system, using either a 10 x 0.3 N.A. dry, 40x1.3 N.A. oil, or 63x1.4 N.A. oil objective (Carl Zeiss, Oberkochen, Germany). Final figures were assembled by Dr. Dominic Cosgrove using Adobe Photoshop and Illustrator software (Adobe Systems, San Jose, CA).

Statistical Analysis

Using JMP Pro 11.0, a Shapiro-Wilks Goodness of Fit test was performed on the residuals of sCr, SDMA, UPC, and iohexol clearance values along with glomerulosclerosis and tubulointerstitial fibrosis scores to determine normality. A Mann-Whitney U test was

performed to determine statistical significance of clinicopathological data and light microscopy scores between WT and AS dogs at each milestone defined by a p-value of <0.05.

Results

Clinical Course of Dogs

The first clinical indication of disease in AS dogs was the onset of microalbuminuria between 10-18 weeks of age (versus hematuria as the first detectable abnormality typically identified in humans). This progressively worsened to overt proteinuria between 14-29 weeks of age, followed by rapid advancement to renal failure. Between 26-52 weeks of age, AS dogs were euthanized following biopsy collections at end point. Figure 7 summarizes the average values of clinicopathologic parameters at defined milestones for AS dogs compared with WT, age-matched littermates. Estimates of GFR (sCr, SDMA, and iohexol clearance), which are commonly used to detect renal insufficiency, were not significantly altered until MS 3. Proteinuria based on UPC was significantly increased at MS 2 (Figure 7), and presence of microalbuminuria was the defining feature of MS 1. Therefore, proteinuria is more sensitive than GFR for identification of early events in disease development in dogs.

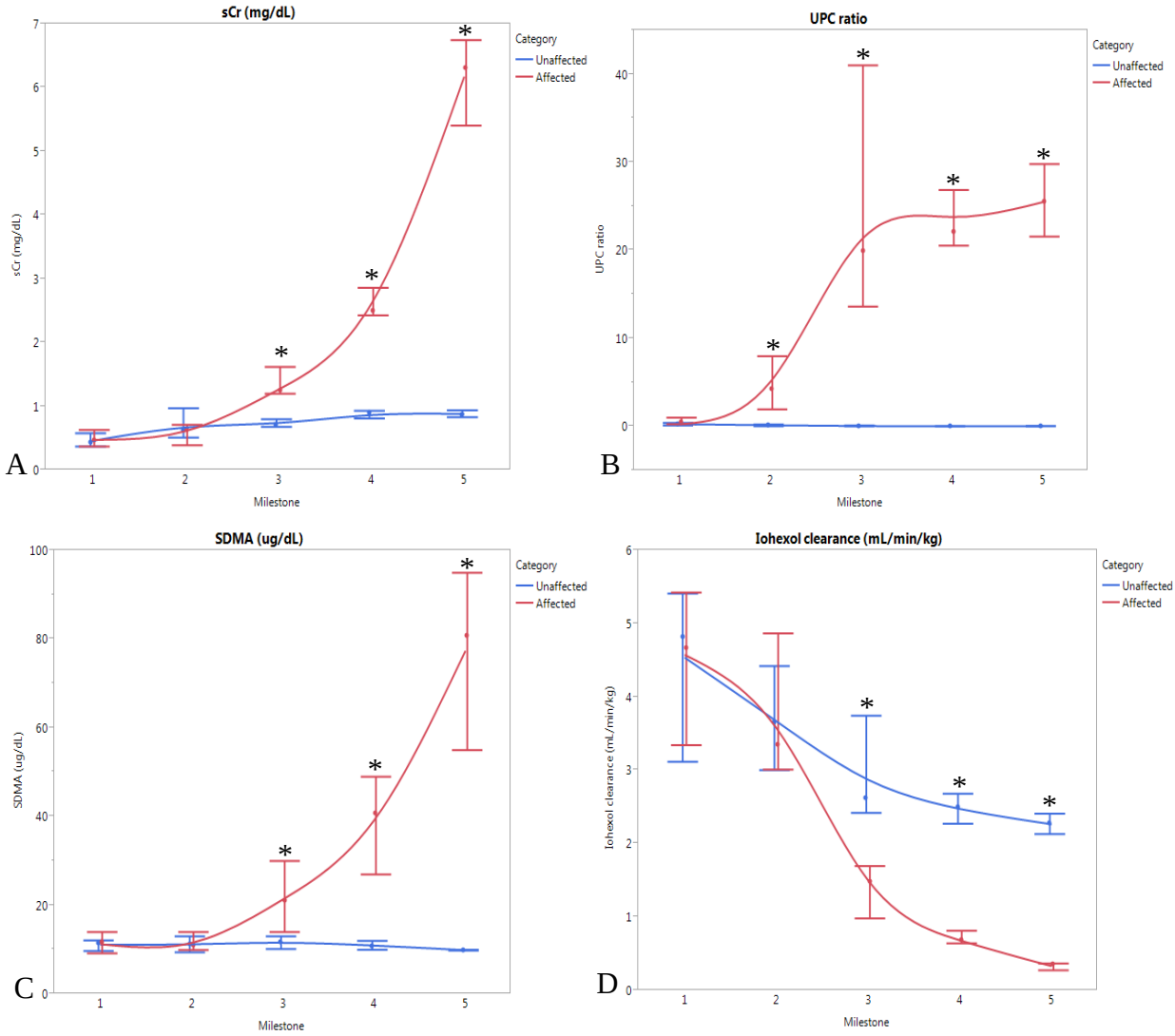

Figure 7 Clinical parameters (average, range) at each milestone in affected (n = 8, blue) vs. unaffected dogs (n = 4, red). (A) Serum creatinine (sCr); (B) Symmetric dimethylarginine (SDMA); (C) Urine protein: urine creatinine (UPC); (D) Iohexol clearance; *p<0.05. Reprinted from [177].

Pathologic Evaluation

Light microscopy also proved insensitive to identifying pathologic changes early in disease. Glomerulosclerosis and tubulointerstial fibrosis were not significantly increased until MS 3 and MS 4, respectively, corresponding with significant changes in the clinical estimates of GFR (Figure 8).

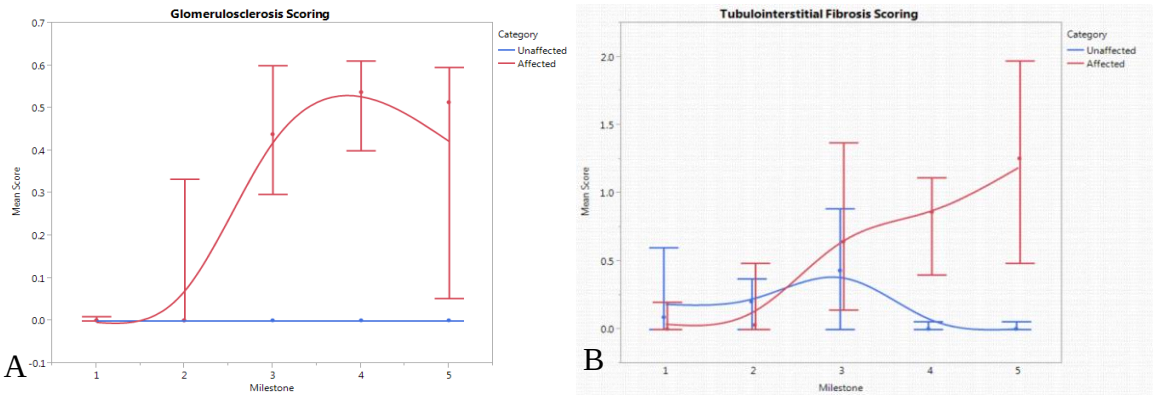

Figure 8 Pathologic parameters (average, range) at each milestone in affected (n = 8, red) vs. unaffected (n = 4, blue) dogs. (A) Glomerulosclerosis score; (B) Tubulointerstitial damage score; *p<0.05. Reprinted from [177].

However, by TEM of tissue from two AS dogs, mild, focal, segmental multilamination of the GBM was observed at MS1 (not shown). Additionally at MS 1, immunofluorescence showed increased staining for fibronectin both within the glomeruli and throughout the interstitium of AS dogs compared to WT dogs (Figure 9A-B), indicating initiation of fibrosis as early as the onset of microalbuminuria. Staining for fibronectin intensified with progression of disease at each MS (not shown).

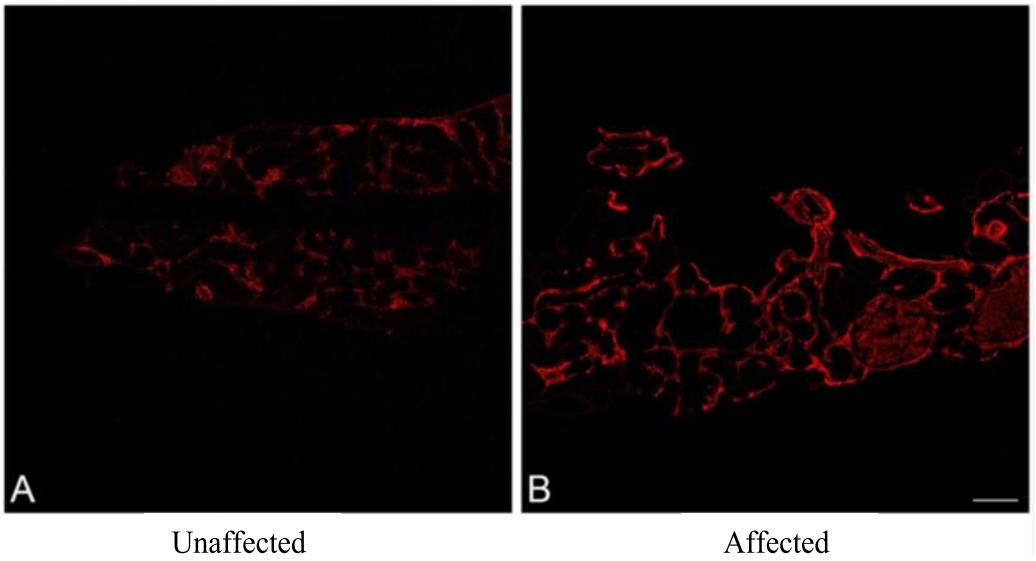

Figure 9 Immunofluorescence staining for fibronectin in kidney from an unaffected and affected dog at milestone 1. Staining for fibronectin reveals fibrosis in AS dogs (B) as early as milestone 1 on confocal microscopy when compared to WT littermates (A) at the same milestone, 10x0.3 n.a. dry. (Line scale 25 μm). Reprinted from [177].

At MS 2, TEM demonstrated small foci of cellular interpositioning (cytoplasmic extensions) along the capillary loops in the two AS dogs evaluated, which is consistent with invasion of mesangial cell processes (Figure 12C). This finding corresponded with an increased UPC in the AS dogs.

Detection of Mesangial Cell Invasion

The laminin β2 chain of laminin 521 is located in the GBM of mice, dogs, and humans[139] and thus can be used as a marker for the GBM in both WT and AS kidney tissue. In the normal glomerulus, laminin 211, identified by the laminin α2 chain, is found primarily within the mesangium and there is no expression of laminin 211 within the GBM of non-diseased kidney.[139] Figure 10A demonstrates the distinctness of laminin β2 as a GBM marker in normal canine kidney tissue and shows the more diffuse distribution of laminin α2 staining within the mesangium (Figure 10B-C). In contrast, in the AS dog, there is

segmental expression of abnormal deposits of laminin α2 in the GBM (Figure 10D-F), particularly where the GBM is thickened.

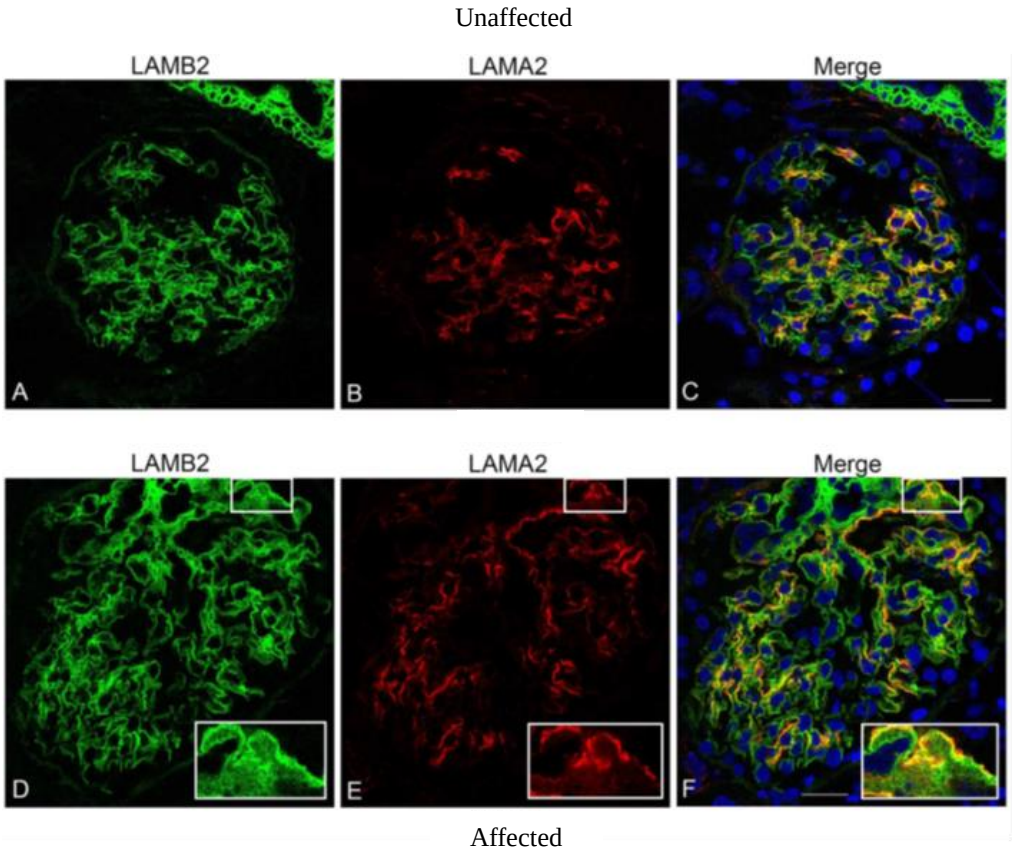

Figure 10 Identification of laminin 211 in the GBM of an affected but not an unaffected dog.
Dual immunofluorescence immunostaining of kidney from am unaffected dog (A-C) and an affected dog at milestone 2 (D-F); 63x1.4 n.a. oil. Laminin 521 of the GBM was labeled with anti-laminin β2 (LAMB2), and laminin 211 produced by mesangial cells, was labeled with anti-laminin α2 (LAMA2), demonstrating co-localization of laminin 211 with the GBM of several capillary loops in the affected dog. (Line scale 25 µm). Reprinted from [177].

The α8 integrin has been shown to be strongly and exclusively expressed on the surface of mesangial cells of mice, rats, and humans.[150] As demonstrated in tissue from a WT dog, Figure 11A-C, integrin α8 can be used as a mesangial cell surface marker in canine tissue as compared with the GBM marker α5 type IV collagen. Using dual immunofluorescence labeling with laminin α2 and integrin α8 in Alport mice, the source of

GBM laminin 211 was shown to originate from mesangial cell processes that invade into capillary loops.[141] This same dual immunostaining was performed on canine kidney tissue. Figure 11D-I shows intense co-localization of laminin α2 and integrin α8 outlining the capillary loop in an AS dog at MS 2, supporting that laminin α2 deposition is correlated with mesangial cells.

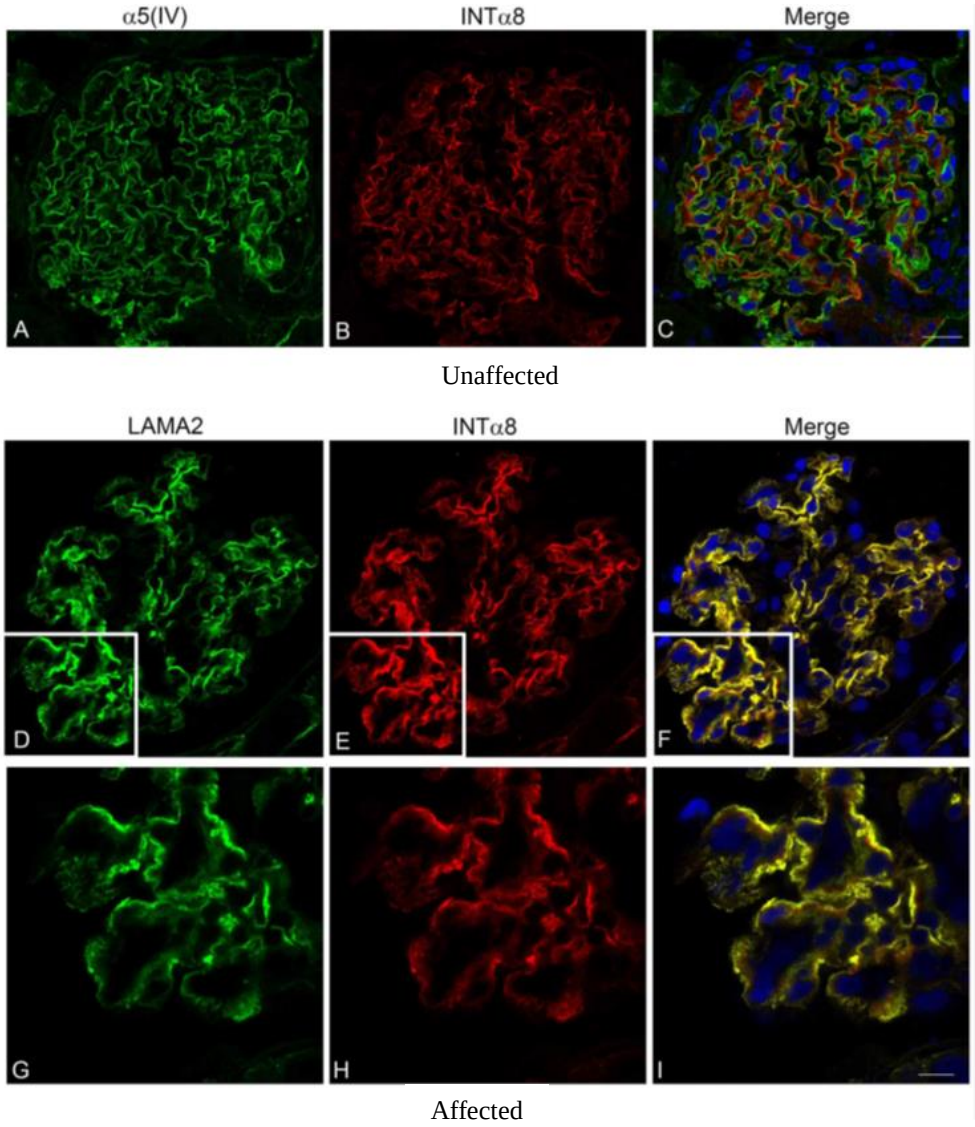

Figure 11 Integrin α8 co-localizes with laminin 211 in the GBM of affected but not unaffected dogs. A-C: Dual immunofluorescence immunostaining of kidney from an unaffected dog; 63x 1.4 n.a. oil. The GBM was localized with anti-collagen α5 (α5 (IV)) and the mesangium was localized with anti-integrin α8 (INTα8). D-I: Dual immunofluorescence immunostaining of kidney tissue from an affected dog at milestone 2. Laminin 211, produced by mesangial cells, was labeled with anti-laminin α2 (LAMA2) and mesangial cells were localized with anti-integrin α8 (INTα8), demonstrating co-localization of laminin 211 with mesangial cell extension in capillary loops. Images D-F were taken with 40x1.3 n.a. oil; images G-I were taken with 63x1.4 n.a. oil with 2X zoom. (Line scale 25 μm). Reprinted from [177].

Additionally, dual immunofluorescence staining was performed on kidney tissue from both a WT and AS dog using laminin β2 to stain the GBM with integrin α8 to stain the mesangium. Mesangial extension was clearly absent from the GBM in the WT dog while extension of mesangial cells within the GBM was observed in the AS dog (Figure 12A-B). This corresponded with the TEM findings of mild cellular interpositioning (cytoplasmic extensions) along the capillary loops, which is consistent with invasion of mesangial cell processes (Figure 12C). Collectively, these data support that, as determined in the mouse, the unique deposition of laminin 211 within the GBM is likely a result of mesangial cell invasion of capillary loops in dogs with AS.

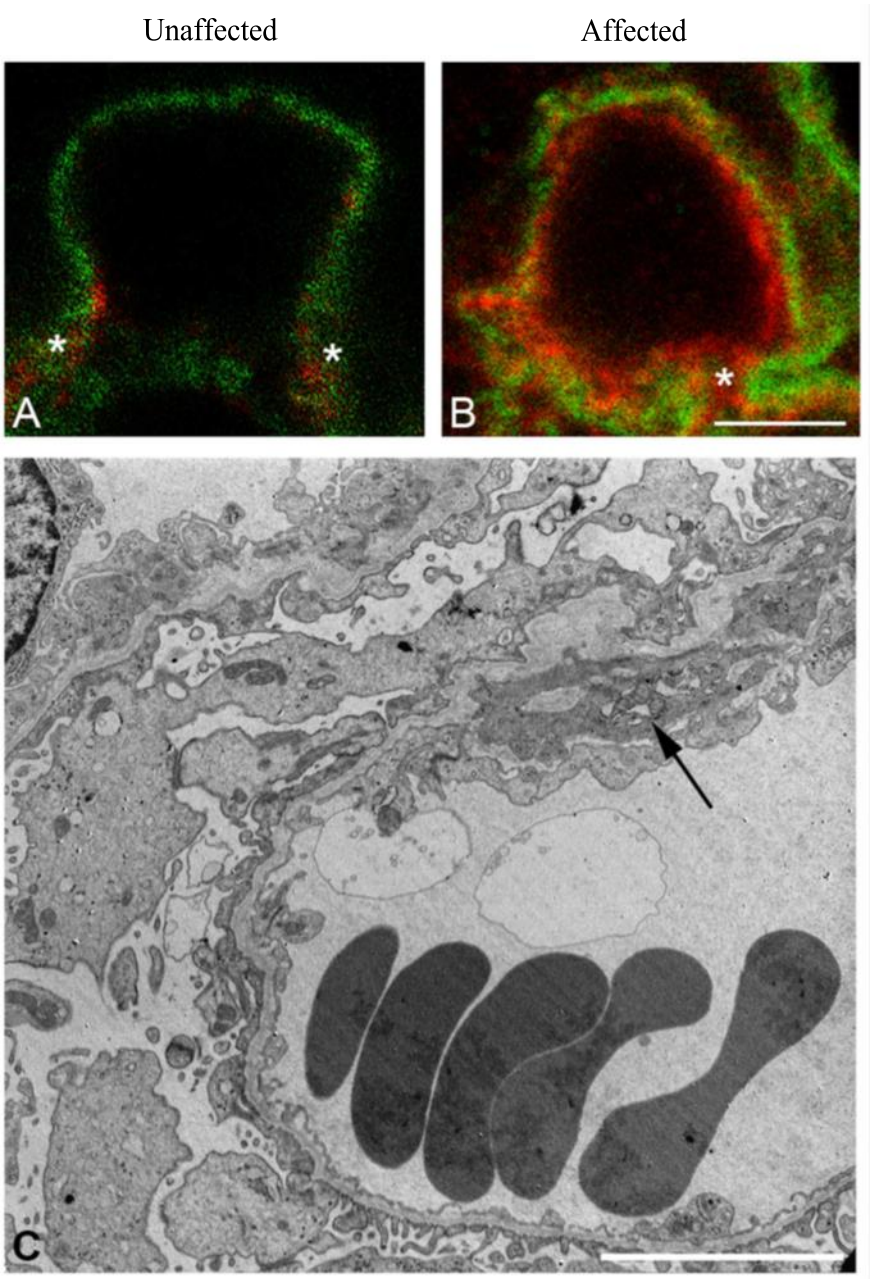

Figure 12 Mesangial cell process extension into the GBM of affected but not unaffected dogs. A-B: Dual immunofluorescence immunostaining of kidney from an unaffected dog and an affected dog, 63x1.4 n.a. oil with 3X zoom. Anti-laminin β2 and anti-integrin α8 antibodies were used to stain the GBM and mesangial cells, respectively. Staining reveals distinct delineation of mesangium absent from the GBM of the normal dog (A) but extension of mesangium within the GBM of the AS dog (B). C: Transmission electron microscopy (10 µm) of kidney tissue from an AS dog at milestone 2. Cytoplasmic extensions, also described as cellular interpositioning, are observed at the base of the capillary loops, consistent with invasion of mesangial cell processes (arrow) corresponding with extension of the mesangium (B). TEM image provided by Dr. Rachel Cianciolo. Reprinted from [177].

Discussion

Mutations in α3, α4, or α5 type IV collagen genes result in absence of the normal type IV collagen composition of the GBM, permitting α1α1α2 type IV collagen to predominate. The thinner and less cross-linked composition of α1α1α2 type IV collagen likely allows for increased biomechanical strain in the capillary tuft due to increasing blood pressure as evidenced by acceleration of glomerular damage in salt-induced hypertensive mice.[151] This added stress on the capillary loop induces mesangial cell process invasion and contributes to initiation of disease.[141,151,152] The abnormal deposition of laminin 211 in the GBM is a feature that has been described as unique to AS.[139] As noted previously in mice and as seen in this study in dogs, the accumulation of 211 seems especially prominent in regions of the GBM that appear thickened on IF staining.[141] Using ferritin injections, these thickened areas have been shown to correlate with regions of loosely assembled or degraded extracellular matrix of the Alport GBM where permeability defects are present, and it is the deposition of aberrant laminins that contributes to these defects.[153] Using integrin α8 as a mesangial cell marker[150], we were able to show that, as reported in the mouse[141], there is extension of mesangial cell processes into the capillary loop of AS dogs and that the aberrant laminin 211 deposition in the GBM corresponds with these invading mesangial cell processes.

To further support the relationship between mesangial cell process invasion and deposition of laminin 211 in the GBM, mice with a deletion of CD151 have also been evaluated.[141] These mice have abnormalities of the adhesive interface between the podocyte foot processes and the GBM and display progressive morphological changes in the GBM similar to that in AS. Evaluation of glomeruli from these mice also demonstrates mesangial cell process invasion and GBM laminin 211 deposition supporting that,

regardless of the cause of structural change, increased biomechanical strain on the capillary tuft stimulates mesangial cells to react. It is notable in this regard that CD151 null mice show accelerated progression of glomerular disease under conditions of hypertension, similar to mice.[154] Additionally, evaluation of capillary tufts in glomeruli of integrin α1-null Alport mice (integrin α1 is important for mesangial cell expansion) have reduced mesangial process invasion and thus reduction of laminin 211, further supporting that laminin 211 originates from mesangial cells.[140] Lastly, immunogold-labeled integrin α8 is present in blebs noted in the subendothelial region of capillary loops in AS mice but not WT mice.[142] In AS, mesangial cell invasion ultimately leads to an inflammatory response, likely in part driven by laminin 211-mediated FAK activation in podocytes, which is responsible for disease progression, including the development of glomerulosclerosis and tubulointerstitial fibrosis. While mesangial cell filopodia invasion is thought to be mediated by a Rac1/CDC42 activation mechanism in mice[141], further evaluation to explore this mechanism in the dog is needed.

In addition to demonstrating mesangial cell process invasion as an initiating event in dogs with AS, this study also allowed for comparison of clinical and structural changes throughout the course of disease through serial evaluations of individual dogs. XLAS is a hereditary progressive glomerular disease that typically results in rapidly progressive renal failure in affected males. Many affected individuals either do not have, or are not aware of, a family history of the disease and are not diagnosed until GFR declines, when clinical signs of disease become evident. In this study, comparison of serial biopsies with concurrent clinical data during the course of disease showed that significant pathologic changes to the kidney occur well before clinical markers of decreased GFR are altered. For instance, in AS dogs, sCr and SDMA did not show statistically significant changes until

around milestone 3, while identification of fibronectin using IF evaluation of kidney tissue suggests instigation of fibrosis as early as milestone 1. On average, dogs in this study were around 28 weeks of age at MS 3 and all of the AS dogs evaluated in this study succumbed to disease before one year of age. Thus, approximately half of their lifespan was complete before disease was detectable by estimators of GFR. In contrast, microalbuminuria was highly sensitive to detection of structural changes evident with only electron microscopy and immunofluorescence staining. Institution of routine testing for microalbuminuria in human patients with hematuria and a family history of AS or renal failure without obvious cause may help ensure early clinical detection of AS.[155] From a clinical standpoint, early detection of proteinuria is paramount to early institution of therapy (e.g., ACE inhibition) that slows disease progression and helps extend life expectancy.[155,156]

Currently, there are few accepted treatments for AS patients, none of which are directed at processes specific to initiation of disease. Understanding the pathogenesis of disease development helps determine the best targets for early intervention. In mice, FAK activation in podocytes occurs specifically where laminin 211 is being deposited, propagating disease progression.[142] It is conceivable that therapeutics that either inhibit FAK[142] or abate laminin 211 deposition could be developed for treatment of Alport syndrome. While mice have proven to be a useful model for understanding the molecular mechanisms of AS and are helpful in identifying therapeutic targets at earlier stages of disease, large animal models need to be established for drug trials. In particular, the dog provides a transition platform between the pre-clinical testing of novel therapeutic drugs in mice and their use in humans. This is important from both a therapeutic efficacy and safety standpoint, as dogs have been shown to better mimic human disease in many conditions.[147,157] While AS itself only accounts for approximately 3% of end stage renal

disease in children, the prevalence of chronic kidney disease (CKD) in the United States has risen dramatically.[158] Therefore, establishing a large animal model for CKD may be of broad importance for testing therapeutics. Given the rapidly progressive nature of AS in mice and dogs, AS serves as a good model for CKD development in general.

In summary, these findings collectively support, in a large animal model, the induction of mesangial cell filopodial invasion of the glomerular capillary tuft leading to the irregular deposition of mesangial laminin 211 in the GBM as an early initiating event in Alport glomerular pathology. Because of the similarities observed among canine and human disease progression, these findings also provide support that the dog is a suitable large animal model for evaluation of AS disease progression and novel therapeutic trials.

CHAPTER III

EVALUATION OF ENDOTHELIN-1 (ET-1) LEVELS IN TISSUE AND URINE OF DOGS WITH XLHN

Background and Significance

Endothelin (ET) is a potent vasoconstrictor that is produced by a variety of tissues, including the kidney.[159,160] Since its discovery, it has also been determined that ETs are involved in regulation of a variety of physiological and pathologic processes, such as modulation of cell proliferation and apoptosis, induction of inflammation, inotropic effects in the heart, activation of epithelial-to-mesenchymal transition (EMT), resistance to chemotherapy, and neovascularization in neoplasia.[161-163] There are three subtypes of endothelin, denoted as ET-1, ET-2, and ET-3, each regulated by three separate genes *EDN1*, *EDN2*, and *EDN3*, respectively.[164,165] ET-1 is the predominant isoform produced.[161,162] The synthesis of ET involves the production of an approximately 212 amino acid preprohormone, referred to as pre-pro-ET, which is then proteolytically cleaved by specific furin-like proteases to an approximately 40 amino acid long protein denoted as Big-ET.[162] In general, Big-ET is considered biologically inactive, although it can escape conversion and be released into the blood, where it has the ability to bind to endothelin receptors, albeit with a much lower affinity than active ET-1.[162,166] Endothelin converting enzyme (ECE), found on the surface of endothelial cells, cleaves Big-ET into the biologically active form, ET-1, and a C-terminal fragment. ET-1 is released into the bloodstream, and its half-life is extremely short (less than two minutes).[165] In human endothelial cells, circulating levels of ET-1 are controlled by a dual secretory pathway consisting of: 1) the constitutive pathway, in which low levels of ET-1 are continuously

released, and 2) a regulated pathway, which causes release of ET-1 from Weibel-Palade bodies inside endothelial cells in response to external stimuli. These pathophysiological stimuli, which can include hypoxia, shear stress, thrombin, cytokines, other hormones, and TGF-β, increase ET-1 levels by upregulating the transcription of the *EDN1* gene.[161,167] The amino acid sequence of active ET-1 is shown in Figure 13. Its sequence is identical in humans, pigs, dogs, and rats.[165]

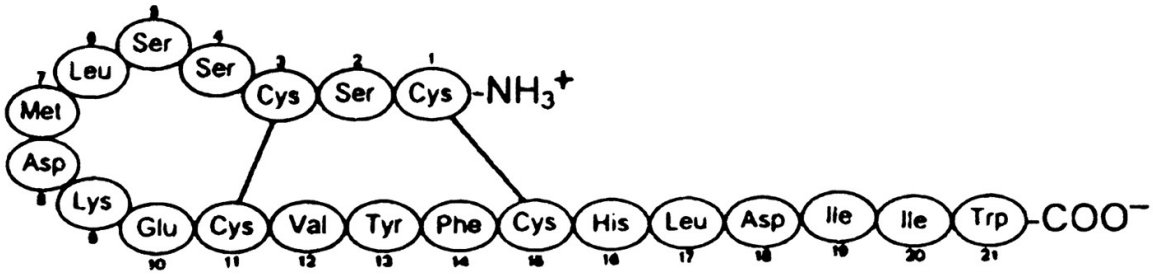

Figure 13 Schematic drawing of active Endothelin-1. The amino acid sequence of active ET-1 is identical in humans, pigs, dogs, rats, mice and fish.

The biological effects of ETs are mediated by two types of seven transmembrane G protein-coupled receptors: endothelin receptor type A (ET_AR) and endothelin receptor type B (ET_BR).[162] The sequences of these receptors display a high degree of conservation across species, with the main differences identified in the N terminus and not within the transmembrane domains that contribute to binding.[167] For ET_AR, the amino acids involved in ligand binding are located in the extracellular loops in the first, second, third, and sixth transmembrane regions. For ET_BR, they are located in the first, second, third, and seventh transmembrane regions.[167] The ET_AR binds ET-1 and ET-2 with greater affinity compared to ET-3 (ET-1=ET-2>ET-3) while the ET_BR binds all three isoforms similarly (ET-1=ET-2=ET-3).[167,168] ET-1 has a similar affinity for both receptor types.[169] While binding of

ET_AR and ET_BR may result in synergistic or opposing effects, depending on the cell and tissue type, ET_AR tends to have a more predominant role in physiologic and pathologic processes, such as contributing to fibrosis and inflammation. ET_BR is more involved in regulation of ET-1 levels by controlling clearance of circulating ET-1 through internalization and lysosomal degradation.[162,167,170] Tissue levels of ET-1 are much higher than circulating concentrations. In the kidney tissue of mice, ET-1 levels have been shown to be 1000 times higher than plasma concentrations.[171] This large difference between tissue and circulating concentrations means that locally produced ET-1 is likely more biologically important than circulating ET-1, reinforcing that ET-1 acts primarily as an autocrine and paracrine hormone. Studies have shown that very little circulating ET-1 is cleared into the urine, therefore, urinary excretion can be used as an indicator of intrarenal production.[172] While the half-life of active ET-1 itself is extremely short, the effects it exerts tend to be long-lasting, particularly due to its slow (usually described as irreversible) dissociation from the receptor.[162,165]

Recent work performed in Alport mice showed that the biomechanical strain placed on the structurally abnormal GBM induces expression of ET-1 by glomerular endothelial cells.[130] ET-1 binds to endothelin A receptors (ET_AR) on mesangial cells, which, in turn, activates Rac1-CDC42 Rho GTPases, leading to mesangial filopodial invasion and laminin 211 deposition. This ultimately stimulates the inflammatory response, including activation of MMPs and pro-inflammatory cytokines, resulting in proteolytic degradation of the GBM.[130] Additionally, this same study showed that before the development of proteinuria, AS mice have elevated levels of ET-1 in their urine compared to wild-type mice, suggesting that urinary ET-1 may be a useful early biomarker of AS.[130] ET-1 has been extensively studied in a number of processes involving kidney pathology including: a) its

role in the proinflammatory and profibrotic effects leading to kidney disease, b) its involvement in the development of numerous other causes of CKD, c) its role in progression of acute kidney injury (AKI) to CKD, and d) its usefulness as a marker of disease.[173-176]

Specific Objectives and Hypothesis

In AS mice, it is biomechanical strain on endothelial cells in the glomeruli that causes release of ET-1 from these cells, which then binds ET_AR on mesangial cells, initiating the pathological cascade that ultimately leads to GBM damage and disease.[130] Given its role in initiation of disease development, it follows that ET-1 levels, particularly in the urine, should be elevated prior to early signs of disease development, particularly proteinuria. Relative levels of ET-1 are elevated in pre-proteinuric AS mice compared to wild type mice of the same age.[130] We have previously shown that the early mechanisms of disease development in AS dogs is similar to that of AS mice.[177] Based on these findings, we surmise that ET-1 should play a similar role in initiation of AS disease in dogs as in mice. Likewise, urinary ET-1 levels in AS dogs should also be elevated during the pre-proteinuric stage.

The first objective of this project was to confirm that canine glomerular endothelial cells express ET-1 and that canine mesangial cells express ET_AR to support that the initiators of disease identified in mice are also present in the dog. The second objective was to measure ET-1 in the urine of dogs with XLHN (AS) to determine if it is also elevated as identified in the AS mouse model and to determine if urinary ET-1 can be useful as a biomarker for detection of XLHN in dogs prior to proteinuria. Based on the findings from the AS mouse model, we hypothesized that canine glomerular endothelial cells express ET-1 and canine mesangial cells express ET_AR. We also hypothesized that ET-1 levels

increased in the urine of dogs with XLHN, as compared to their unaffected counterparts, particularly prior to development of proteinuria.

Experimental Design and Methods

Sample Collection

For assay validation, mid-stream, voided urine obtained from one healthy dog was used as the sample matrix for spiking and recovery. For ET-1 evaluation, banked urine from four unaffected dogs and eight affected dogs was used. As previously described, blood and mid-stream, voided urine samples were collected for determination of physiologic data, including serum creatinine (sCr) and urine protein: creatinine ratio (UPC) (Vitros 250, Johnson & Johnson Co, Rochester, NY). Glomerular filtration rate (GFR) was performed as previously described for each dog using either renal scintigraphy[149] or iohexol clearance[178] throughout disease progression. To monitor disease progression, milestones (MS) were set and defined by the following criteria: MS 1-presence of microalbuminuria for two consecutive weeks, MS 2-UPC ≥2 for two consecutive weeks, MS 3-sCr ≥1.2 mg/dL, MS 4-sCr ≥2.4, and MS 5-sCr ≥5 mg/dL or clinical signs of uremia for 2 or more consecutive days (i.e. anorexia, dehydration, vomiting). Testing for microalbuminuria was performed only until MS 1 was reached using a semi-quantitative test (E.R.D. HealthScreen Canine Urine Test strips, Heska, Loveland, Colorado). Samples were stored at -80°C until evaluation.

Ultrasound-guided needle biopsies from alternating kidneys were obtained from all dogs at each defined MS during disease progression as previously described.[149,177,178] Unaffected dogs were paired with an affected littermate for biopsy collection and evaluation to serve as a control. In short, dogs were anesthetized using a premedication combination of 0.011 mg/kg glycopyrrolate (Fort Dodge, Overland Park, KS) and 0.30

mg/kg butorphanol (Zoetis, Florham Park, New Jersey) injected subcutaneously. Dogs were intubated following administration of 4-6 mg/kg propofol (Abbott, Worchester, Massachusetts) intravenously, and anesthesia was maintained using isoflurane (Zoetis Florham Park, New Jersey). Once the dog was fully anesthetized, biopsies were obtained using a 16-18 gauge Bard Monopty® Disposable Core biopsy instrument. Biopsies were performed on alternating kidneys as each MS was reached. Samples were divided and placed into formalin, glutaraldehyde, RNALater (Thermo Fisher Scientific, Waltham, MA) or Optimal Cutting Temperature (OCT) compound (Tissue-Tek OCT Compound, Sakura Finetek USA, Torrance, CA). Samples in OCT were flash frozen in liquid nitrogen vapor and stored at -80^{o}C until evaluation. When affected dogs reached advanced disease as defined by serum creatinine $\geq$ 5 mg/dL or had clinically significant disease (as described above), they were humanely euthanized under anesthesia following biopsy collection.

Immunofluorescence Antibodies

The following antibodies were used: goat anti-mouse integrin α8 (R&D Systems, Minneapolis, MN, USA, Cat# AF4076), sheep anti-mouse Endothelin A Receptor (Novus Biologicals, Littleton, CO, USA, Cat# NB600-836), goat anti-mouse α-actinin-4 (N-17) (Santa Cruz Biotechnology, Santa Cruz, CA, USA, Cat# sc-49333) and rabbit anti-mouse Endothelin-1 (Biomatik, Wilmington, DE, USA, Cat# CAU27820). Alexa-fluor conjugated secondary antibodies (Invitrogen, Carlsbad, CA, USA) included: donkey anti-sheep 488 for anti-endothelin A receptor, donkey anti-goat 568 for anti-integrin α8 and anti-α-actinin- 4 or donkey anti-rabbit 488 for anti-endothelin-1.

Immunofluorescence and Fluorescence Microscopy

Immunofluorescence was performed by Brianna Dufek at Boys Town National Research Hospital. Frozen OCT-embedded kidney biopsy samples were sectioned at 6 µm and

acetone fixed. Sections were incubated overnight at 4ºC in a primary antibody solution comprised of 0.3% PBST (Triton X-100), 5% fetal bovine serum, and the following antibody dilutions: 1:200 (Endothelin A Receptor), 1:150 (integrin α8), 1:100 (Endothelin-1) or 1:50 (α-actinin-4). Slides were rinsed with 1X PBS and incubated at room temperature for 1 hour with the appropriate secondary antibody solution consisting of the secondary antibody along with 0.3% PBST (Triton X-100), and 5% fetal bovine serum to make a 1:500 antibody dilution. Slides were rinsed again with 1X PBS and mounted using Vectashield mounting medium, which contained DAPI to counterstain the nuclei (Vector, Burlingame, CA). Images were captured using a Zeiss Axio Imager A1 microscope with a 63x/1.4 N.A. oil objective (Carl Zeiss, Oberkochen, Germany). Final figures were assembled using Adobe Photoshop CC 2018 software (Adobe Systems, San Jose, CA).

ELISAs for measurement of ET-1 levels in urine of dogs

Two different commercial enzyme-linked immunosorbent assay (ELISA) kits for measurement of ET-1 were evaluated: 1) Dog Canine Endothelin PicoKine™ ELISA Kit (BosterBio, Pleasanton, CA, USA, Cat# EK0945-CN), marketed specifically for measuring ET-1 levels in canine serum but not urine and 2) Endothelin ELISA (1-21) kit (ALPCO, Salem, NH, Cat #04-BI20052) which is not marketed for use in dogs, but is indicated for use with both serum and urine samples. Both kits are sandwich ELISAs. For kit 1, the wells were pre-coated with a biotinylated monoclonal antibody from mouse specific for ET-1. The detection antibody was a goat-derived polyclonal antibody. A synthetic form of ET-1 (Sigma-Aldrich, St. Louis, MO, USA, Cat #E7764-10UG) was used for spiking. For kit 2, the wells were pre-coated with polyclonal anti-ET-1 antibody, and the detection antibody was a monoclonal mouse anti-human ET. Kit 2 included a stock solution of synthetic ET-1 (1-21) that was used for spiking. Each kit was completed as per the

manufacturer's recommendations. Prior to use on test samples, analytical validation to assess the accuracy of each kit for measurement of ET-1 in urine for further use was performed including, spike-and-recovery and linearity-of-dilution. To do this, a known concentration of synthetic ET-1 (10 fmol/L=25 pg/µL) was added (spiked) to urine collected from a normal dog and then serially diluted at 1:2. The response was measured (recovered) in the assay and compared to the standard curve, which consisted of the same synthetic ET-1 serially diluted at 1:2 but reconstituted in distilled water. Spike recovery was calculated as % recovery = concentration (spiked sample)-concentration (neat sample)/ concentration (expect) X 100%. Linearity was calculated as % recovery at the dilution = observed concentration at the dilution/expected concentration. All samples were measured in duplicate and the average was used for further calculations. To compare values between dogs and milestones, urine ET-1 (uET-1) values were normalized to urine creatinine (uCr) concentration, generating a uET-1:uCr ratio, to account for variances that might be due to differing urine concentrations. To do this, uET-1 concentrations were converted from fmol/L to pg/mL while uCr was converted from mg/dL to pg/mL and the ratio calculated. For ease of comparison, all the ratios were multiplied by 10^8.

Statistical Analysis

Using XLSTAT, a Shapiro-Wilks Goodness of Fit test was performed on the residuals of urine ET-1: urine creatinine ratios. Since the data was non-parametric, a Mann-Whitney U test was performed to determine statistical significance between the unaffected and affected dogs at each milestone defined by a p-value of <0.05. Additionally, a Grubbs' test was performed on the ratios calculated to evaluate for the presence of outliers.

Results

Detection of ET-1 and ET_AR in canine kidney tissue

Based on the literature, virtually all cells in the kidney produce and bind ET-1 in varying degrees.[179] While it has been demonstrated that, overall, the highest production of ET-1 is in the inner medulla, glomeruli have been identified as a major site of ET-1 production within the renal cortex.[179,180] To confirm expression of ET-1 in canine glomeruli, tissue obtained from both an unaffected dog and a dog affected with XLHN at MS1 (microalbuminuria) were immunostained with an antibody specific for ET-1 (Figures 14A and 14D). In Alport mice, the cellular source of ET-1 was determined to be endothelial cells, based on co-localization of ET-1 with the endothelial cell marker CD31.[130] However, after multiple attempts of troubleshooting several protocols and antibodies, the endothelial marker, CD31, was unsuccessful for use on the canine kidney tissue. Therefore, α-actinin-4, an antibody commonly used for podocyte identification, was selected (Figures 14B and 14E) to identify podocytes instead. In the healthy glomerulus, ET-1 is constitutively expressed[181] and podocytes are known to produce and secrete ET-1[182], so it is not unexpected to observe some degree of co-localization of ET-1 with α-actinin-4 as seen in Figures 14C and 14F. Relative fluorescence of ET-1 was greater in kidney tissue from the unaffected dog, and ET-1 is prominently co-localized within the podocytes, although there is still a significant amount of ET-1 (green) that is not co-localized with α-actinin-4 in the merged image. In the affected dog, co-localization of ET-1 within podocytes appeared less prominent as compared to the unaffected dog at the same MS MS1). This may be an indication that early in the disease process, as compared to tissue in a normal physiologic state, ET-1 is from an additional cellular source such as endothelial cells, which are considered the principal source of ET-1 in the glomerulus.[183]

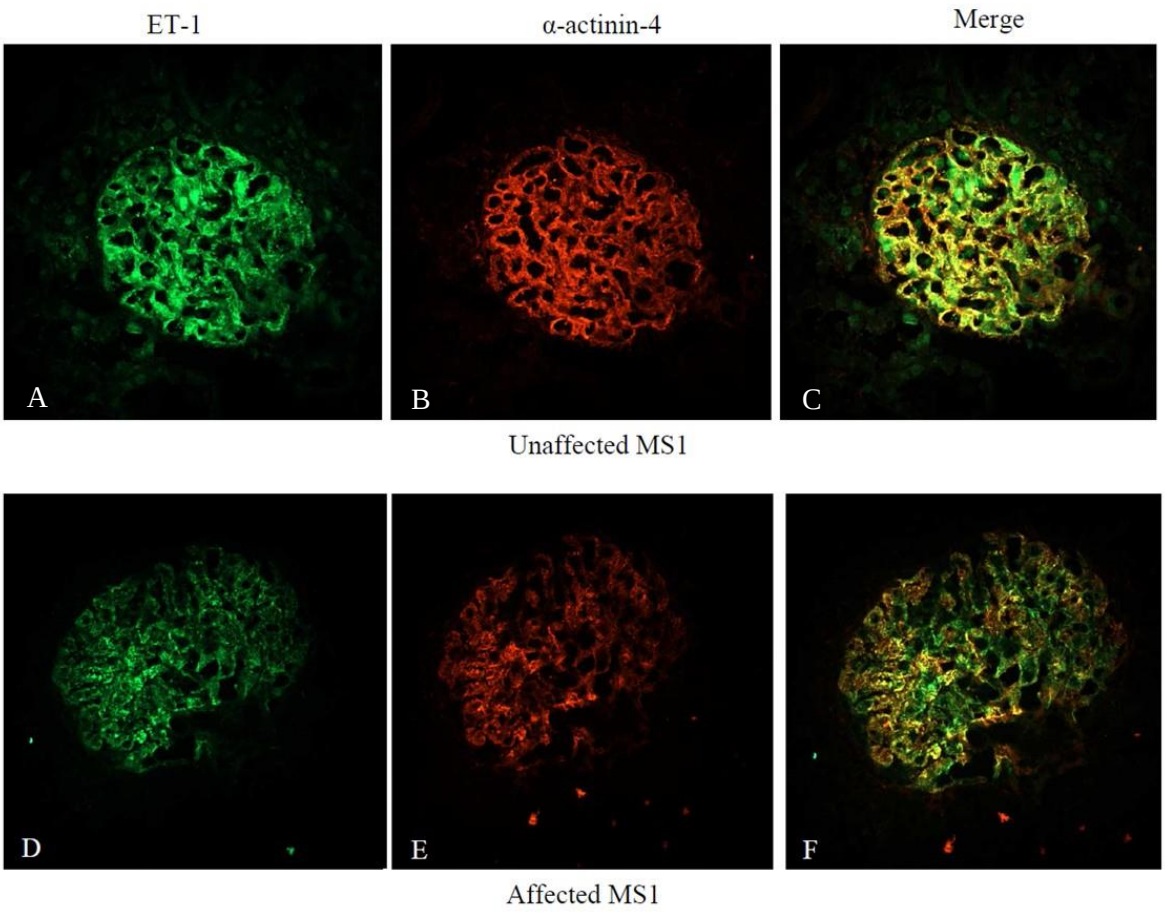

Figure 14 Immunostaining for ET-1 and α-actinin-4 in canine kidney tissue in an unaffected vs. an affected dog at MS1. Confocal images provided by Brianna Dufek.

Kidney tissue from a second affected dog, also obtained at MS1, was immunostained for ET-1 and α-actinin-4, and a similar pattern of less prominent co-localization staining within the podocytes, as compared with the unaffected dog, was observed (Figure 15). This further supports that in the early diseased state, ET-1 expression may be produced from other cellular sources, such as endothelial cells.

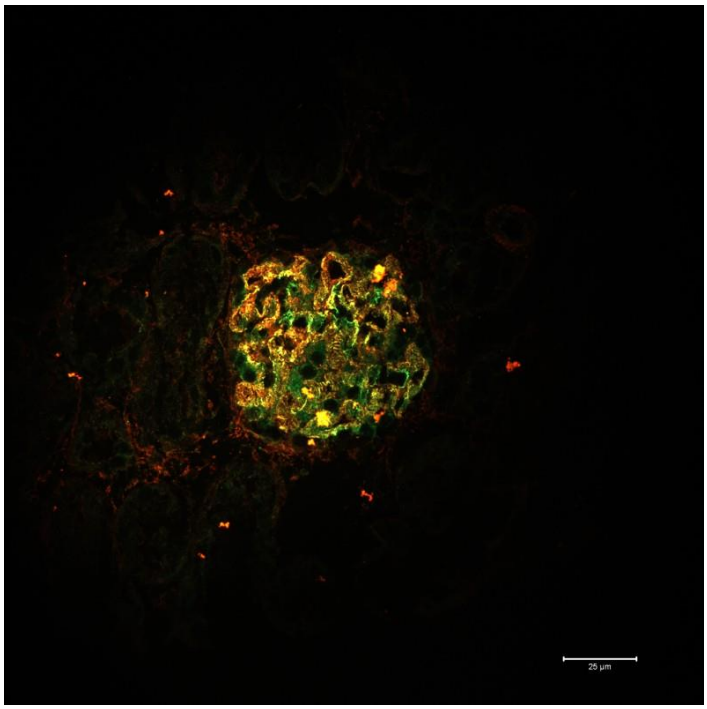

Figure 15 Immunostaining for ET-1 and α-actinin-4 in canine kidney tissue from a second affected dog at MS1. Confocal image provided by Brianna Dufek.

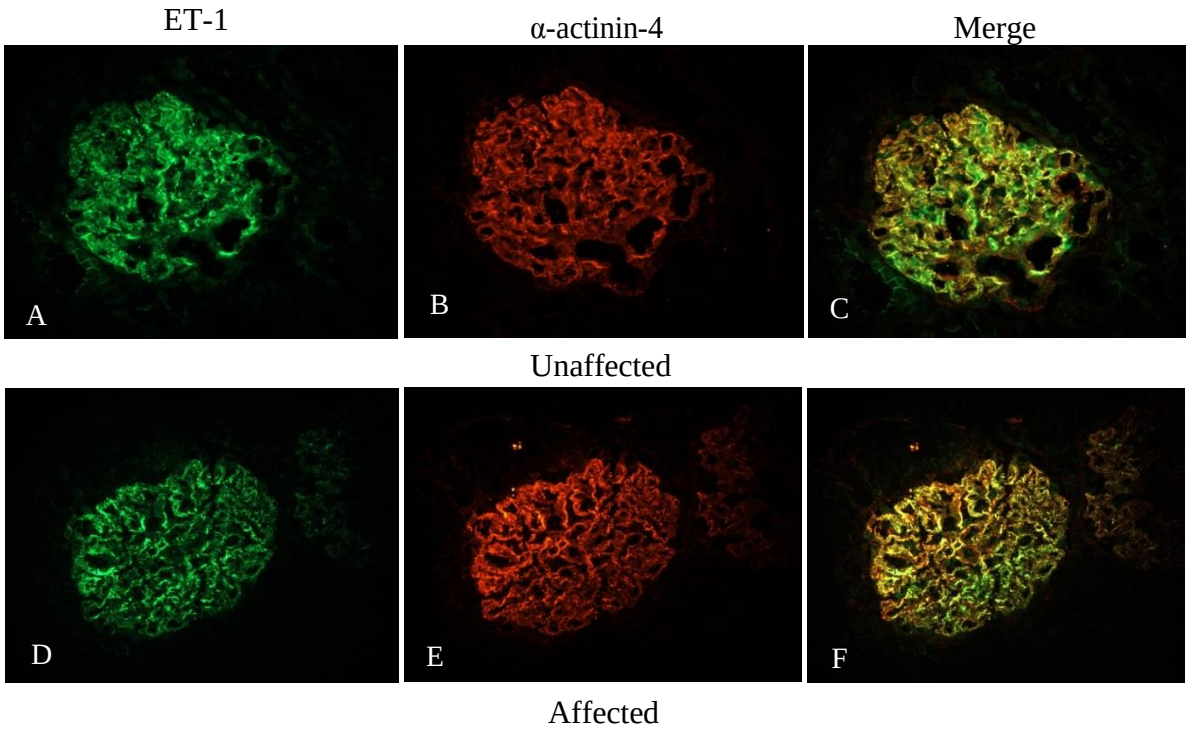

Figure 16 Immunostaining for ET-1 and α-actinin-4 demonstrating co-localization in canine kidney tissue of an unaffected dog (A-C) compared to an affected dog (D-F) at MS2. Confocal images provided by Brianna Dufek.

When immunostaining of ET-1 and α-actinin-4 were compared between the unaffected dog and an affected dogs at MS2 (Figure 16), which corresponds with overt proteinuria in the affected dogs, there appeared to be more co-localization of ET-1 within podocytes in the affected dog compared with the unaffected dog. Additionally, there appears to be an increase in co-localization of ET-1 and α-actinin-4 at MS2 when compared to MS1. At MS5, identification of glomeruli for evaluation in affected dogs was challenging, as few glomeruli were present among the tubulointerstitial fibrosis and most demonstrated severe glomerulosclerosis.

The α8 integrin has been shown to be strongly and exclusively expressed on the cell membrane of mesangial cells of mice, rats, and humans.[150] Additionally, we have demonstrated its use as a mesangial cell marker in canine kidney tissue.[177] Expression of ET_AR on mesangial cells has been previously identified in mice and rats.[130,184] We

examined the relative expression of ET_AR in kidney tissue from an unaffected and affected dog. Figure 17A-F shows that expression of glomerular ET_AR co-localizes with integrin α8, which is consistent with the presence of ET_AR on mesangial cells.

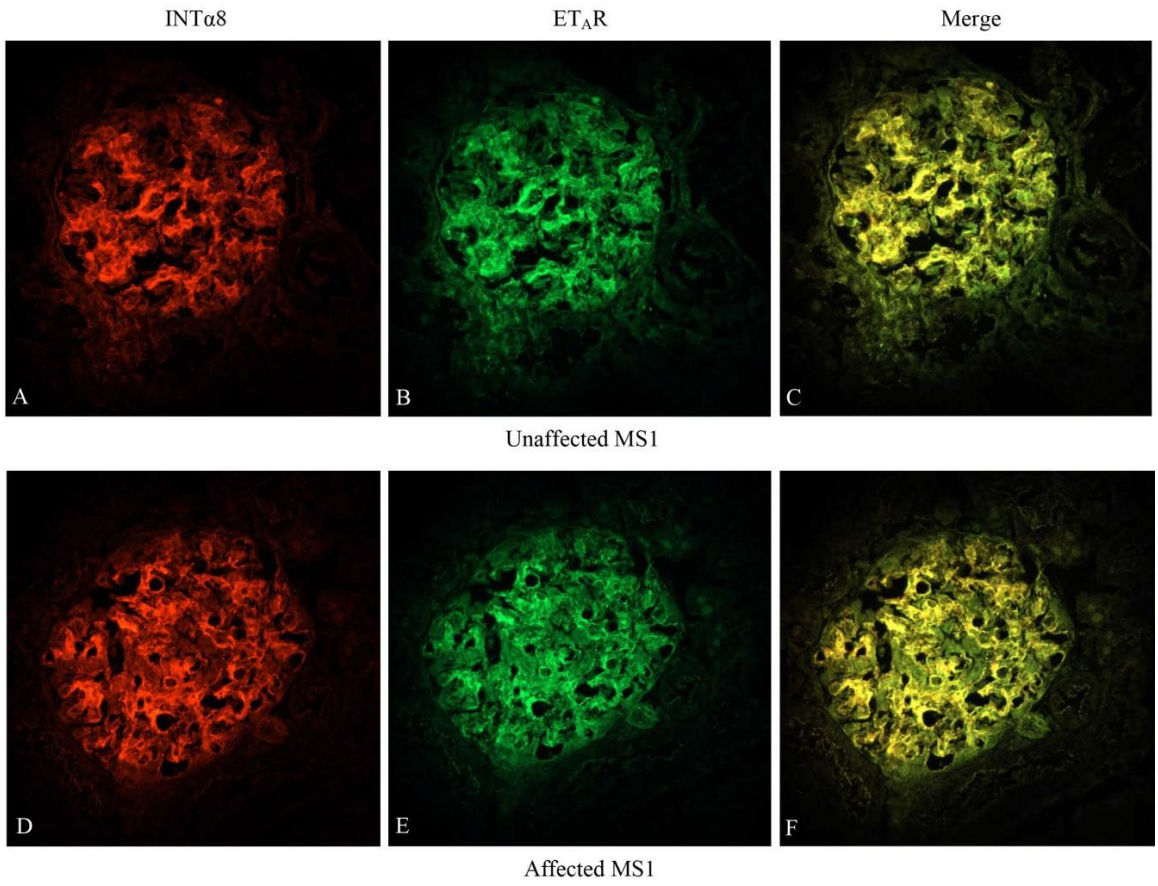

Figure 17 Integrin α8 co-localizes with Endothelin Type A Receptor in canine kidney tissue of both unaffected and affected dogs (A-F). Confocal images provided by Brianna Dufek.

Preliminary Validation of the ET-1 ELISA

Spike-and-recovery and linearity-of-dilution for validating and assessing the accuracy of each ELISA was performed, and performance differed significantly between the two assays.

For kit 1, we observed high variability between sample wells, ranging from 0-141%, including amid those used for establishment of the standard curve. Therefore, calculations could not be performed with high confidence from the results. The cause of the variability is unknown, although technical error has to be considered as a contributing factor.

For kit 2, correlation between the expected and standard curve concentrations and the expected and spiked urine sample concentrations was 0.99659 and 0.99656, respectively. The spike-and-recovery results were within an acceptable range (80-120%, Table 1), indicating that the sample matrix (urine) is not likely causing interference with the assay procedure to measure the analyte (ET-1). However, based on the method used, the results of the linearity-of-dilution at the two highest dilutions were not within the acceptable range (80-120%, Figure 18) indicating that the sample matrix (urine) may affect detectability of the analyte (ET-1) differently at these lower concentrations or that the limit of detection for canine urine was reached.

Table 1 Comparison of expected values for the standard curve and percentage of recovery for spiked urine samples.

Expected Concentration (fmol/mL)	Standard Curve		Spiked Urine		Recovery (%)
	Concentration (avg, fmol/mL)	CV %	Concentration (avg, fmol/mL)	CV %	
10	10.2515	3.4	8.854	26.3	81.934
5	4.5115	15.1	5.3205	3.1	107.858
2.5	2.917	2.9	2.937	12.7	85.105
1.25	1.435	6.1	1.9385	7.6	103.415
0.625	0.651	6.7	1.212	4.6	116.359
0	0	0			

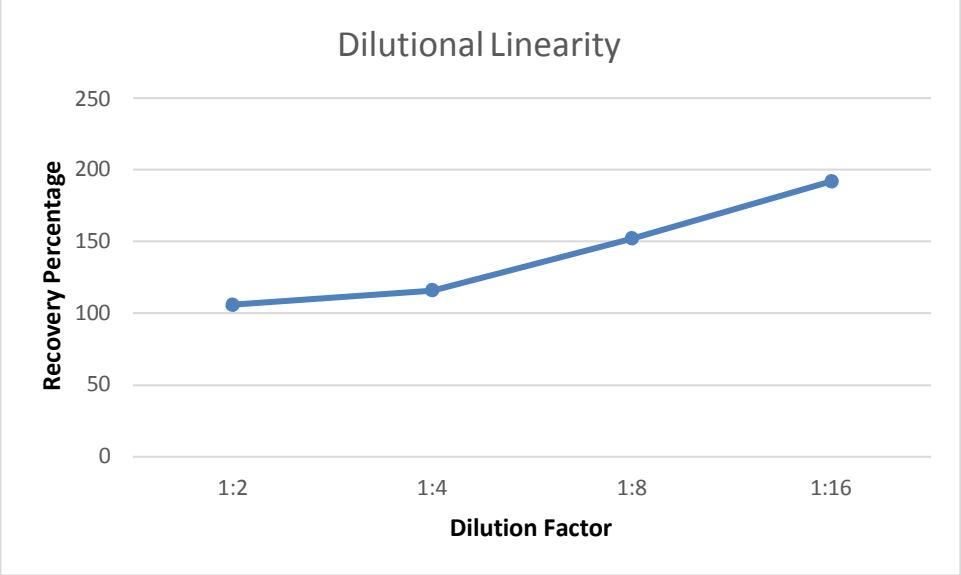

Figure 18 A spiked urine sample was serially diluted and assayed for ET-1. Recovery values ranged between 106-192%; the highest two dilutions were not within acceptable limits.

Detection of ET-1 in urine of unaffected dogs compared to dogs affected with XLHN

Based on both the results of the preliminary validation along with the simplicity of the protocol, kit 2, Endothelin ELISA (1-21), was selected for evaluation of ET-1 levels (fmol/mL) in urine from dogs affected with XLHN and their unaffected littermates. See individual values for unaffected and affected dogs in Tables B-1 and B-2, respectively. At MS1, all of the dogs had low uET-1:uCr ratios (0-1.86) except for one, which had a ratio of 10.7. An exact cause for the discrepancy between these dogs and the others is unknown but possible considerations are addressed below.

In general, there was significant variation between wells in a number of the samples, especially within the unaffected dogs. This may be an indication that the assay is not reliable at lower concentrations of ET-1 (also supported by the dilution-of-linearity findings) and optimization of the assay is needed. Only the values with a coefficient of variation ≤20% were used for statistical analysis. The median and range of uET-1:uCr ratio of unaffected vs. affected dogs were compared at each MS (Table 2). A significant difference between the two groups was detected at MS2.

Table 2 Median and range of uET-1:uCr ratio for unaffected and affected dogs. n=sample number; p-value <0.05.

Milestone	Unaffected Dogs			Affected Dogs			p-value
	n	Median	Range	n	Median	Range	
MS1	3	0	0-10.7	6	0	0-15.81	0.917
MS2	3	0	0	5	2.07	1.21-38.68	0.032
MS3	2	0	0	4	3.165	1.72-11.43	0.100
MS5	4	0	0	5	0	0-10.27	0.556

Discussion

Our objective was to confirm that in canine kidney tissue, glomerular endothelial cells express ET-1 and mesangial cells express ET_AR. We also sought to evaluate the levels of ET-1 in urine collected from both unaffected dogs and dogs affected with CKD caused by XLHN. Our primary goal was to provide supporting evidence for induction of ET-1 as the initiating event resulting in early GBM damage and thus development of CKD in dogs with XLHN, as shown in AS mice.

In this study, we were able to verify that ET-1 is produced in the kidney tissue of both unaffected dogs and dogs with XLHN. Given only partial co-localization with podocytes combined with that fact that endothelial cells are the only other cells in the capillary loop, we can surmise that a significant source of ET-1 is endothelial cells. Additionally, it should be considered that ET-1 may be overlapping or are in the close spatial relationship (i.e. co-existing) with the podocytes but not actually expressed within them. Co-localization quantification analysis would be helpful to further validate this finding in order to assess whether the intensity of staining are actually synchronous as expected if they are in the same complex.[185] This is appropriate given the cellular cross-talk that occurs amongst glomerular cells in both physiologic and pathologic states.[19,22]

Through the connection of multiple integrin pathways, endothelial cells, podocytes, and mesangial cells are able to engage in multidirectional cross-talk, allowing for all three cell types to work together and forming a functional, interdependent unit in which changes in one cell type results in alterations in the others.[19,22] As an example, podocytes produce vascular endothelial cell growth factor (VEGF) that acts on neighboring podocytes and endothelial cells to maintain cell health.[179] It has been shown that loss of VEGF leads to endothelial cell dysfunction and also causes disruption of the podocyte actin cytoskeleton. This results in the development of proteinuria and also promotes the release of ET-1 from podocytes.[186] The tissue used for immunostaining for both affected dogs, were obtained based on the definition of MS1. However, both of the dogs tested negative for microalbuminuria the following week. Therefore, it is possible that the biopsies were collected prior to persistent microalbuminuria and may be representative of the pre-proteinuric stage of disease. This might explain why, at MS1, there was less co-localization of ET-1 within the podocytes, as they are not yet severely damaged enough to be involved in the pathological process. While this does not correlate with the findings of increased co-localization of ET-1 with podocytes in the unaffected dog, it would be more helpful to evaluate expression of ET-1 within endothelial cells to truly make this comparison. Therefore, additional endothelial cell markers for use in canine tissue need to be explored. Additionally, evaluation of kidney tissue from another unaffected dog is needed to verify this pattern of expression. The lack of co-localization within podocytes at MS1 as observed in this study also supports the notion that the podocytes are not the primary source of ET-1 production and secretion early in the development of disease; ET-1 is coming from another source, likely endothelial cells. Then, at MS2 (overt proteinuria), when compared to the unaffected dog, there is a more apparent co-localization of ET-1

with α-actinin-4. This likely reflects an increased production of ET-1 by the podocytes as disease progresses. Using immunofluorescence, we were able to confirm that ET_ARs are expressed by mesangial cells based on the co-localization with the cell marker integrin α8. Given this information, in conjunction with the already established similarities between AS mice and dogs, it is possible that induction of ET-1 from endothelial cells may be an initiating event in canine XLHN. However, additional studies, including confirmation of the cellular source of ET-1 in pre-proteinuric XLHN dogs, need to be conducted to support or refute this hypothesis.

Supporting our second objective, we performed a preliminary validation of a commercially available ELISA kit for the detection of ET-1 in canine urine. One of the greatest concerns when analyzing a biological sample for a specific analyte is accuracy of the method and the potential for unreliable results. Biomarkers play an important role in clinical medicine, particularly in decision-making, so it is imperative that results are reliable.[187] According to recently published guidelines, when validating the use of an ELISA for detection of a potential biomarker, 10 different parameters should be evaluated including: robustness, precision, trueness, uncertainty, limits of quantification, dilutional linearity, parallelism, recovery, selectivity, and sample stability.[187] Of these parameters, spike-and-recovery and linearity-of-dilution experiments are two of the most common and essential methods used for validating and assessing the accuracy of an ELISA, and experiments can be designed to test these simultaneously. These experiments help to assess the ability of the ELISA to measure the true amount of analyte in a sample and reveal unwanted interference problems that may produce inaccurate results.

For this project, two kits were initially evaluated. The Endothelin ELISA (1-21) kit, which is not marketed for use in dogs but is indicated for use with both serum and urine

samples, provided more reliable results than the Dog Canine Endothelin PicoKine™ ELISA Kit. However, the results of the linearity-of-dilution revealed that at concentrations below 1.25 fmol/mL results may not be reliable. While additional validation and assay optimization would be ideal, the manufacturer of this kit has discontinued production.

Identification of biomarkers that can be evaluated in urine for the monitoring and progression of CKD is imperative, and urine is a relatively easy sample to obtain, especially in veterinary patients. Because the time of urine collection, urine concentration, and urine flow rate can all affect the concentration of a biomarker, assays obtained are often normalized to uCr to account for these differences.[188] Thus, urinary biomarker concentrations are frequently reported as a ratio to uCr. To investigate the significance of ET-1 concentrations in urine of unaffected dogs compared to dogs affected with XLHN, uET-1:uCr ratios were calculated. A significant difference was found between the groups at MS2. This is noteworthy given that while UPC is elevated at MS2, decreased glomerular filtration rate and histologic damage are not evident until MS3 in dogs with XLHN.[177]

We hypothesized that ET-1 concentrations would be highest early in the disease, particularly at MS1. However, this was not the case, as there was not a significant difference between unaffected and affected dogs at MS1. One possible explanation for this finding is that ET-1 is considered a low molecular weight (LMW) protein at 2.49 kDa. LMW proteins are freely filtered through the glomerulus and then re-absorb by normally functioning tubules; therefore, ET-1 may be re-absorbed by the tubules before it is excreted and thus measured in the urine. It may not be until there is an appreciable amount of tubular damage, over-abundance of ET-1 for the tubules to reabsorb, or a combination of both, that the ET-1 level in urine becomes significantly increased. Another possible explanation for the lack of difference between the groups at MS1 is that one of the four

unaffected dogs used in this study had a uET-1:uCr ratio of 10.7 at MS1 while the other three dogs had low levels. The significance of the elevated ratio in this one dog is unknown. There were no histologic abnormalities noted on evaluation of the biopsy at this MS, and there were no abnormalities in clinical data that suggested impairment of kidney function. This sample was not determined to be an outlier, and therefore was included in the statistical analysis. Due to the vast discrepancy, a mix-up or mislabeling of the sample should be considered. This may be confirmed by testing the UPC of the sample to confirm that it matches with what would be expected from an unaffected dog. The conjugated antibody uses horseradish-peroxidase (HRP) that causes an enzymatic reaction that causes a change in color from blue to yellow. Therefore, another consideration is that the sample contained a source of peroxidase that generated a color change even though there is actually no ET-1 in the sample. Sources of peroxidase in urine can include hemoglobin, erythrocytes, and leukocytes. Lastly, while the concentrations at MS 1 are low, there could be significant differences between the two groups that could be distinguished if the detection method was optimized. Within many of the samples, the CV% among duplicates was significantly higher than what is considered acceptable (typically $\leq$20%).[187] Coefficient of variation is a measure of precision, so a high value indicates poor performance. While the findings of this study are interesting, it is important to recognize that this is a preliminary study and that optimization of the ELISA along with analysis of additional dogs, and re-evaluation of urine from all the unaffected dogs with detectable ET-1 is required for further evaluation.

In conclusion, we found that in canine kidney tissue, ET-1 is present and is likely expressed by several cellular sources, particularly endothelial cells, at the early stage of disease. We also found that canine mesangial cells express ET_AR and that increased

expression of ET-1 might play an important pathologic role in the progression of the XLHN by binding to ET_ARs on mesangial cells, leading to initiation of disease as observed in AS mice. Furthermore, elevated levels of ET-1 in urine from dogs with XLHN could be used as a supportive biomarker for disease progression. Given its role in early disease development, ET-1 appears to be a good candidate for exploration in other causes of CKD in dogs.

CHAPTER IV

DETERMINATION OF THE URINARY MIRNA PROFILE DURING DISEASE PROGRESSION IN DOGS WITH XLHN

Background and Significance

MicroRNAs (miRNAs) are a class of small non-coding RNAs that bind to complementary target sequences in messenger RNA to serve as posttranscriptional regulators of gene expression, and sequences are highly conserved across species.[109,111] The processing of miRNA is tightly regulated, and miRNAs play a fundamental role in a variety of biological processes, including cell differentiation, apoptosis, cell proliferation, and tissue development.[109,189] Additionally, it has been determined that some miRNAs are expressed at different levels in specific tissues, suggesting organ-specific roles.[190] Studies have shown that miRNAs are vital in a number of processes in the kidney including the regulatory cascade during renal development, maintenance of renal function, and progression of kidney diseases.[189,191] Due to their aberrant expression, the determination of specific miRNA expression profiles for specific diseases has been possible.[114,117] During biogenesis, mature microRNAs are packed into exosomes and microvesicles, which then enter circulation.[192] Additionally, they may be loaded into high-density lipoproteins or bound to AGO2 protein outside of vesicles.[192] As a result, miRNAs are protected from degradation making them extremely stable in extracellular fluid, including serum, body fluids, and urine.[118-120,192] This stability, in conjunction with potential disease specificity and ease of quantification make mature circulating miRNAs good candidates for the use of biomarkers for a number of diseases, including CKD.[118-120]

Given their importance in many cellular processes, identifying alterations in miRNA expression profiles, along with their gene, mRNA and/or resulting protein targets,

can provide insight regarding their involvement in the pathogenesis of disease development. Excitingly, this information may allow for the identification of biomarkers for earlier detection of disease in addition to potential therapeutic targets that could ameliorate renal disease progression. In this study, our primary aim was to evaluate miRNAs in urine at different time points of disease progression in dogs affected with XLHN (as previously described in the introduction) and their unaffected, normal littermates (controls) in order to determine their utility as biomarkers for detection and monitoring of disease progression.

Specific Objectives and Hypothesis

There are two specific objectives of this aim: (1) to determine the miRNA profile in urine at 3 different time points of disease progression using next-generation sequencing and (2) to verify the expression levels of selected target miRNAs in urine using RT-qPCR analysis. Overall, results of these investigations will help determine if urine miRNAs can be used as non-invasive biomarkers for canine CKD. Based on literature reviews and our previously collected preliminary data, our central hypothesis is that specific miRNAs in the urine of dogs with CKD due to XLHN will be altered as compared with normal dogs. By identifying differences in miRNA expression in urine, we can use this information for future studies to gain a better understanding of the pathophysiology contributing to development of CKD in dogs.

Experimental Design and Methods

Samples

Samples utilized for this project are banked samples previously obtained from dogs with CKD that are part of a colony maintained at Texas A&M University, in which the causative mutation of the disease in the affected males is a naturally occurring, 10 base pair

deletion in the gene encoding the α5 chain of type IV collagen.[133] Development and progression of X-linked hereditary nephropathy (XLHN) in these dogs has been previously described.[193] At the time of collection, no treatments were administered to the dogs, and the study protocol was reviewed and approved by the Texas A&M University Institutional Animal Care and Use Committee.

When obtained, blood and mid-stream voided urine were collected for determination of physiologic data, including serum creatinine (sCr) and urine protein: creatinine ratio (UPC) (Vitros 250, Johnson & Johnson Co, Rochester, NY). Glomerular filtration rate (GFR) was also measured as previously described for each dog using either renal scintigraphy[149] or iohexol clearance[178] throughout the advancement of disease. To monitor disease progression, milestones were set and defined by the following criteria: milestone 1 (MS 1)-presence of microalbuminuria for two consecutive weeks, milestone 2 (MS 2)-UPC ≥2 for two consecutive weeks, milestone 3 (MS 3)-sCr ≥1.2 mg/dL, milestone 4 (MS 4)-sCr ≥2.4 mg/dL, and milestone 5 (MS 5)-sCr ≥5 mg/dL or clinical signs of uremia for 2 or more consecutive days (i.e. anorexia, dehydration, vomiting). Testing for microalbuminuria was performed only until milestone 1 was reached using a semi-quantitative test (E.R.D. HealthScreen Canine Urine Test strips, Heska, Loveland, Colorado). Samples were stored at -80°C for a range of four to ten years until evaluation.

RNA Isolation

While dogs were monitored during disease based on the milestones as described above, for this project, we evaluated three general time points during the disease process including: early (T1), middle (T2), and late (T3). To obtain enough samples for RNA isolation, in some cases, urine was pooled from dates two weeks before and after each defined MS1, MS3, and MS5. Due to the quick progressive nature of the disease, urine from MS2 or

MS4 may have been included to generate enough total sample for isolation at each time point. Therefore, T1 may have included pooled urine samples from MS1 and MS2, T2 may have included pooled urine samples from both MS3 and MS4, and T3 may have consisted of pooled urine samples from both MS4 and MS5, although typically only MS5 samples were used. Based on analysis of several kits to maximize RNA yield from urine, performed by another graduate student in the lab, RNA was isolated using the Qiagen exoRNeasy Serum/Plasma Maxi Kit (Qiagen, Hilden, Germany) following the manufacturer's protocol. In short, 3-4 mL of urine was centrifuged four times with XBP and XWP buffer in a spin column to collect RNA material. QIAzol™ Lysis Reagent (Qiagen, Hilden, Germany) was added to the spin column membrane as a cell lysate in order to generate higher yields of total RNA. This was transferred to a 2 mL tube and chloroform was added in order to promote phase separation. The upper aqueous phase, in combination with ethanol, was passed through a spin column using a vacuum manifold. The remaining material was washed using RWT and RPE buffers. As the final step, RNA was eluted using RNase-free water. Altogether, RNA isolation was performed on 27 urine samples from four unaffected and five affected dogs at the three time points.

Next-generation sequencing

Following isolation, an aliquot of RNA from each sample was submitted to the Texas A&M AgriLife Center for Bioinformatics and Genomic Systems Engineering for RNA analysis. Quality control analysis and RNA concentration was determined using the Fragment Analyzer™ (Advanced Analytical Technologies, Inc., Ames, IA). Due to the low sample amount, A2_T2 was not used for library preparation. Library preparation was performed using the NEXTflex® Rapid Directional RNA-Seq preparation kit (Bioo Scientific, Austin, TX) following the manufacturer's instructions with the amendment of

performing 24 PCR cycles in the amplification step due to the low concentration of starting material. Size selection was performed using the PippinHT system (Sage Science Inc., Beverly, MA) with a 3% agarose gel cassette followed by a bead purification step, in which the final library was eluted in 25 uL of the included resuspension buffer. Next-generation sequencing (NGS) was performed using the Illumina® HiSeq 2500 (Illumina, Inc., San Diego, CA) in high output mode per the manufacturer's protocol.

For analysis of the sequencing results, pre-processing was performed using Cutadapt (version 1.9.1) to: (1) remove the 3' adapter, trim the first and the last four bases as in accordance to the BioO NEXTflex manual, (2) filter out reads less than 16 nucleotides, and (3) remove low quality reads (quality score < 30). One sample (C3_T2) was excluded for further evaluation due to low reads.

All further analysis of the sequencing data was performed by Dr. Candice Chu. The FASTX-Toolkit (version 0.0.14) was used to convert the file format from fastq to fasta. Alignment was performed using the default setting in CPSS 2.0 to the canine genome CanFam 3.1 and miRNA annotation miRBase R21. Differential analysis was performed using DESeq2 (version 1.20.0) in R (version 3.5.0). An adjusted p-value (FDR) of 0.05 was set as the cutoff for statistical significance. Additionally, candidate miRNAs for evaluation for use as endogenous controls were determined using NormFinder for R (version 5, released January 5, 2015) to select the most stable miRNAs (based on the lowest stability scores).

Quantitative Real Time-PCR for evaluation of miRNAs in urine

Based on sequencing data, miRNAs that were determined to be the best candidates for endogenous reference miRNAs for normalization, in addition to miRNAs that showed promise for differential expression between unaffected and affected dogs, were selected to

validate their presence in urine by RT-qPCR using pre-designed wet-bench validated Qiagen miRCURY® Locked Nucleic Acid (LNA®) miRNA PCR Assays (see Table B-3 for Assay information) following the manufacturer's protocol. Additionally, a custom-made primer was generated for evaluation of miR-8890. Three primers were designed by the manufactured, and the primer which seemed most appropriate for the mature miRNA sequence of interest was selected.

In short, cDNA was obtained using 2 µL of RNA template followed by RT-qPCR using 3 µL of diluted 1:10 cDNA. For RT-qPCR, a "water only" well and a "no template control" (NTC) were used as negative controls for each miRNA evaluated. To determine the efficiency of each primer in addition to serving as inter-run calibrators, standard curves were generated using a sample from an additional affected dog not used in the above analysis at serial 1:5 dilutions. Test samples were run in triplicate while standards for the standard curve were run in duplicate. Cycling parameters were 95°C for 2 minutes, 45 amplification cycles at 95°C for 10 sec, and 56°C for 60 seconds, followed by melting curve analysis.

Data Analysis, Normalization, and Statistics

Analysis of the qPCR data involved two components: 1) selection of miRNAs to be used as endogenous controls for normalization and 2) analysis of test miRNAs for differential expression in urine of unaffected dogs compared to affected dogs at three time points of disease progression. In both situations, data were analyzed using the Bio-Rad CFX Maestro™ Software (Bio-Rad, Hercules, CA, USA). First, curve analysis was performed for distinct and acceptable amplification curves, melting curves, and melting peaks, and the Tm was verified to be within the known specification for each assay. Cq values were discarded if deviating curves or Tm were observed, the value was above 40, and/or the

difference in values was greater than 1.0 cycle within each triplicate.[194] Cq values up to 40 were considered valid if the amplification curve, melting curve, and melting peak were appropriate.

Eight miRNAs were evaluated for their use as potential endogenous reference miRs: miR-16, miR-28, miR-30e, miR-93, miR-128, miR-151, miR-339, and miR-429 in 15 samples. The urine samples used for this evaluation were from one unaffected dog at the three time points, one clinically normal dog outside of the colony, three dogs affected with XLHN at the three time points, and three dogs outside of the colony diagnosed with glomerular disease whose samples had been submitted to the International Veterinary Renal Pathology Service (IVRPS). In order to account for differences in miRNAs that might be due to differing urine concentrations, data were normalized to urine creatinine (uCr) concentration.[188,195] To do this, all Cq values (after filtered based on the above criteria) were converted into a linear scale assuming amplification efficiency of 100% for every assay using the formula $2^{(40-Cq)}$. The data were normalized to uCr by dividing the linear Cq value by uCr (g/dL). Subsequently, for each miRNA, standard deviation, average, and coefficient of variation (CV %) was calculated, and the two miRNAs with the lowest CV% were selected as endogenous reference miRNAs for use when evaluating the expression of the test miRNAs.

Based on previously performed studies, information in the literature, and potential upstream targets, the miRNAs selected for further evaluation between unaffected and affected dogs were let-7e, miR-21, miR-30d, miR-142, miR-378, miR-489, and miR-8890. The relative normalized expression of the target miRNAs was calculated using the ΔΔCq method using the endogenous reference miRNAs. Normality was determined using the Shapiro-Wilks Normality test, and statistical analysis was performed using a one-way

analysis of variance (ANOVA). The Tukey HSD post hoc test was performed in order to correct for the family-wise error rate.

Results

RNA Isolation

The concentration of RNA isolated from urine was determined using the Fragment Analyzer (Table B-4). The median concentration was 0.675 ng/μL with a range of 0.0005 to 21.1682 ng/μL. However, the extremely low concentrations observed for some samples were suspected to be false readouts. To further evaluate these samples, graphs demonstrating the size distribution of the RNA revealed that, for these low concentration samples, the RNA peak was shifted slightly compared with the peak in the other samples. This resulted in the RNA peak obscuring the 15 nucleotide ladder used to determine the concentration of the sample, explaining the low concentration readout. A trial run of the library preparation was done using several of these samples with low readouts to determine whether they would produce results. Library preparation was successful, supporting that the reported low concentrations were inaccurate.

Sequencing Data Analysis

Table 3 shows the summary statistics for the miRNA-Seq data for urine. Note that one sample was excluded due to a low number of reads. The genome mapping rate indicates the percentage of reads that map to the canine genome. Overall, 87-97% of reads were mapped to the canine genome (*CanFam3.1*, released September 2011). Among the mapped reads, a low percentage consisted of miRNAs. The remainder of RNA mapped to non-coding RNA, unclassified, and/or mRNA.

Table 3 Summary statistics for the urinary miRNA sequencing data. The genome mapping rate indicated the percentage of reads that map to the canine genome.

Group	Sample Name	Input reads	Processed reads	Genome mapping rate (%)	miRNA mapping rate (%)
Unaffected (Control)	C1_T1	7,998,396	7,893,593	94.08	0.16
	C1_T2	10,203,205	10,057,688	94.18	0.526
	C1_T3	8,622,969	8,497,075	94.55	1.38
	C2_T1	4,742,441	4,662,289	95.21	1.08
	C2_T2	12,319,075	12,142,306	95.41	1.24
	C2_T3	1,540,577	1,504,849	95.68	0.98
	C3_T1	12,505,668	12,169,427	95.3	0.04
	C3_T2	5395	Excluded for low reads		
	C3_T3	11,348,652	11,086,124	95.54	0.511
	C4_T1	8,999,878	8,864,200	92.32	0.89
	C4_T2	6,826,261	6,730,101	94.74	0.43
	C4_T3	6,398,646	6,310,325	96.94	2.69
Affected	A1_T1	9,249,077	9,114,112	94.4	0.44
	A1_T2	6,920,635	6,820,074	96.06	3.64
	A1_T3	7,272,755	7,154,881	96.48	21.61
	A2_T1	7,626,156	7,485,897	95.55	0.18
	A2_T3	7,554,966	7,426,368	89.28	16.15
	A3_T1	8,137,231	8,033,580	92.69	0.14
	A3_T2	8,267,806	8,130,580	87.41	17.14
	A3_T3	15,051,150	14,815,866	90.48	20.74
	A4_T1	6,814,251	6,716,691	94.6	0.22
	A4_T2	8,834,616	8,675,267	89.68	26.5
	A4_T3	7,744,132	7,559,283	88.18	17.33
	A5_T1	8,442,981	8,326,067	93.29	0.39
	A5_T2	8,149,111	8,024,844	90.83	21.03
	A5_T3	8,078,216	7,915,609	90.82	19.33

Analysis for differentially expressed miRNAs was performed at each time point comparing unaffected and affected dogs. Principal component analysis (PCA) was performed to assess clustering of samples. PCA is a technique used to emphasize variation and bring out strong patterns in a dataset, in this case, based on miRNA expression patterns. The principal components explain the amount of variation in the data. As noted on the PCA plot, when all samples were evaluated all together, there was a clear distinction in miRNA expression between unaffected and affected dogs, except for affected dogs at T1, which clustered with the unaffected dogs (Figure 19). Principal component 1 (PC1) accounted for 44% of the total variation in miRNA expression while principal component 2 (PC2) accounted for 11% of variation.

Figure 19 PCA plot for all samples irrespective of diseae or time point. The percentage of variance in principal component 1 (PC1) and principal component 2 (PC2) indicate how much variance in miRNA expression is explained by PC1 and PC2. Figure provided by Dr. Candice Chu.

Comparing all affected and unaffected dogs at all time points, there were a total of 39 differentially expressed miRNAs (Figure 20). Within specific time points, there were no differentially expressed miRNAs identified in affected compared to unaffected dogs at T1, while there were 44 and 54 at T2 and T3, respectively. There were 17 differentially expressed miRNAs that were identified in all comparisons between affected dogs and unaffected dogs: cfa-let-7a, cfa-let-7b, cfa-let-7c, cfa-let-7e, cfa-miR-23a, cfa-miR-27a, cfa-miR-30c, cfa-miR-30d, cfa-miR-99b, cfa-miR-142, cfa-miR-155, cfa-miR-181b, cfa-miR-203, cfa-miR-205, cfa-miR-224, cfa-miR-378, and cfa-miR-8858.

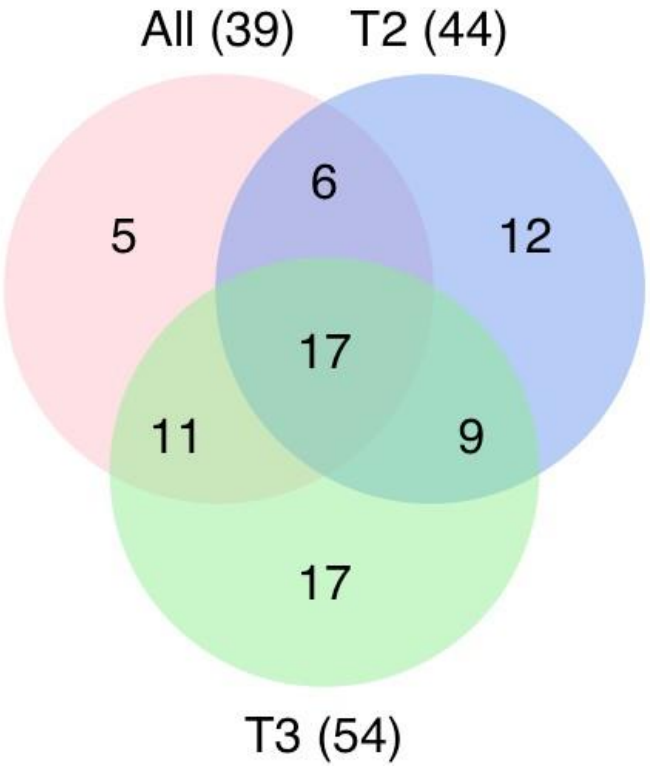

Figure 20 Venn diagram illustrating differentially expressed urinary miRNAs. Comparison is between all affected and unaffected dogs (All) and between affected and unaffected dogs at time point 2 (T2) and 3 (T3). There were no differentially expressed miRNAs at time point 1. 17 miRNAs were identified as differentially expressed in all comparisons between the two groups. The number of total differentially expressed miRNAs is in parentheses. Only miRNAs with an adjusted P-value of < 0.05 were considered differentially expressed. Figured provided by Dr. Candice Chu.

Figure 21 and 22 show the read counts of the top 10 differentially expressed miRNAs in affected compared to unaffected dogs at T2 and T3, respectively.

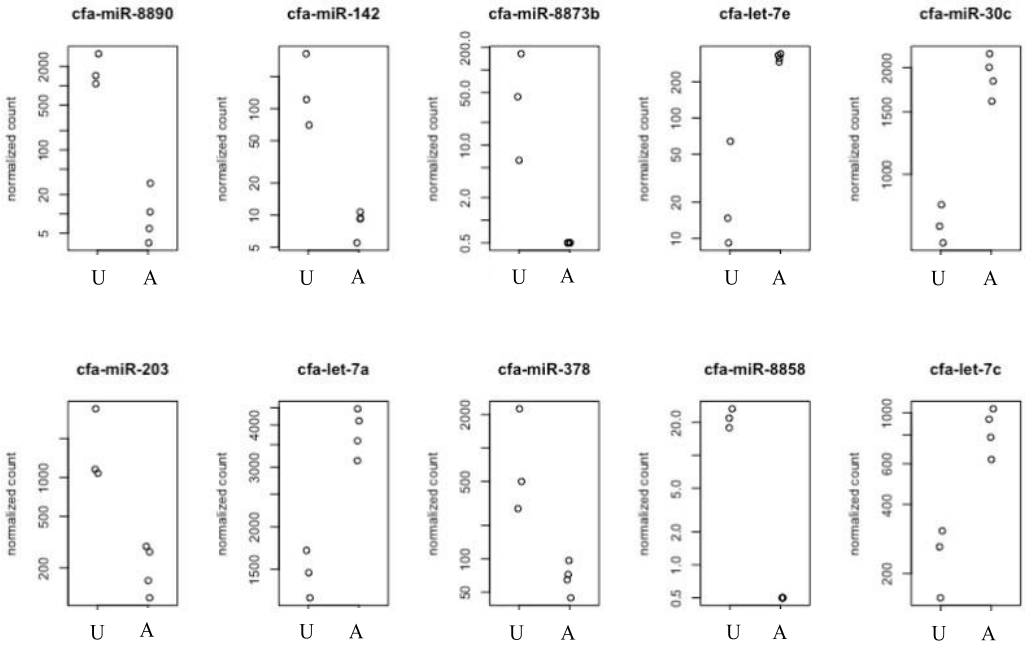

Figure 21 Top 10 differentially expressed urinary miRNAs in affected dogs compared to unaffected dogs at T2. U=unaffected; A=Affected. Figure provided by Dr. Candice Chu.

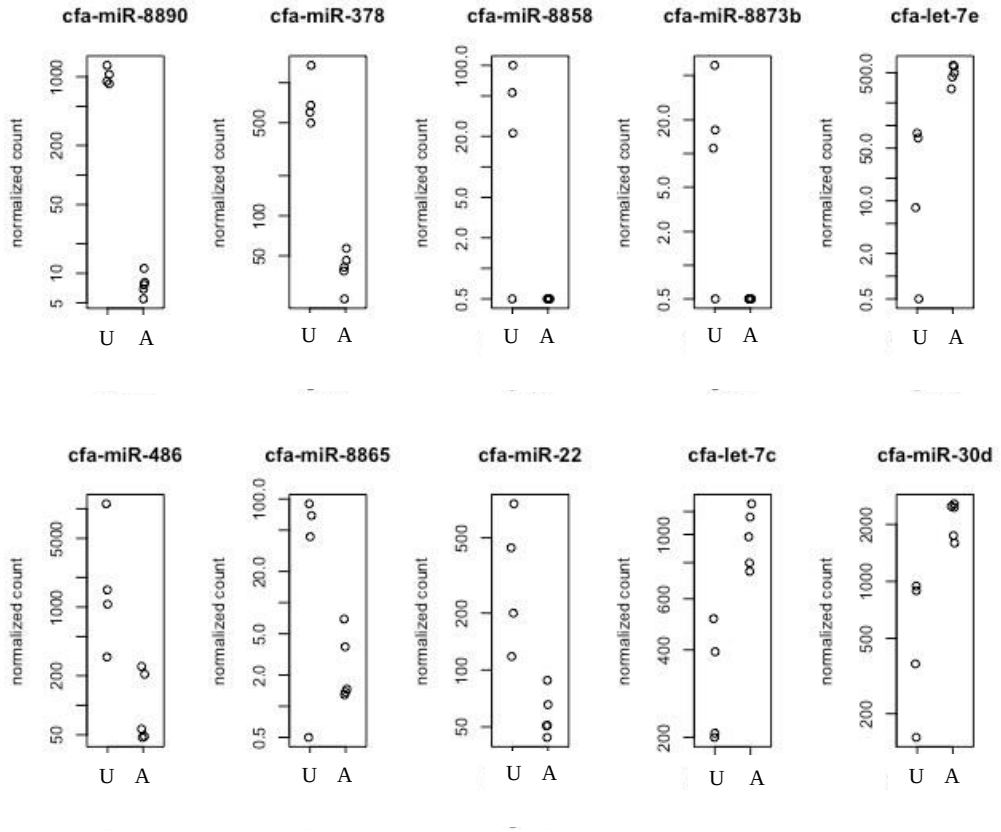

Figure 22 Top 10 differentially expressed urinary miRNAs in affected dogs compared to unaffected dogs at T3. U=unaffected; A=Affected. Figure provided by Dr. Candice Chu.

Selection of endogenous reference urinary miRNAs

As part of the analysis, the sequencing data was used to identify the top 10 reference miRs for use in urine in XLHN dogs using NormFinder for R, which utilizes a mathematical model of measured gene expression values to estimate intra-and intergroup variation within a sample set, which are then combined to form a stability value.[196] The lower the stability value (i.e. variation), the more preferred the miRNA for normalizing purposes (Table 4) as its use will introduce the least systematic error when used for normalization.[196]

Table 4 List of top ten reference urinary miRNAs as determined by sequencing analysis using NormFinder for R.

	GroupDif	GroupSD	Stability
cfa-miR-429	78.81	60.61	32.97
cfa-miR-28	86.79	124.82	48.92
cfa-miR-103	197.81	86.93	90.68
cfa-miR-30e	393.75	84.62	90.76
cfa-miR-148a	311.04	159.16	94.03
cfa-miR-181a	298.3	148.8	102.75
cfa-miR-196b	292.88	157.99	111.18
cfa-miR-16	141.84	341.03	121.92
cfa-miR-128	423.81	200.88	131.35
cfa-miR-140	320.89	235.22	135.55

Additional sequencing data performed on urine obtained from a separate cohort of dogs collected through the IVRPS was performed (unpublished data). In this data, a different set of reference miRNAs was identified, which included miR-93 and miR-151. Samples from three dogs affected with various glomerular diseases and one normal dog from this study, along with the two miRNAs identified as possible reference miRNAs, were also considered in the RT-qPCR validation process in order to explore a broader range of potential reference miRNAs for dogs with CKD.

Two methods were employed for determination of the reference miRNAs to be used in subsequent analyses for endogenous normalization. First, analysis was performed using the "reference gene selection tool" provided in CFX, which categorizes genes based on their stability across all samples in the experiment. In this program, the lower the M score and higher the stability score (defined as [ln (1/AvgM)]), the more suitable a miRNA is for use as a reference miRNA for normalization. The program identified miR-30e as "Ideal" with an average M value of 0.486 and a stability score of 0.722 while miR-16 was categorized as an "Acceptable" reference miRNA, with an average M value of 0.696 and stability score of 0.362.

The second method involved identification of preferential reference miRNAs based on the coefficient of variation percentage (CV %) after normalizing the linear Cq values to uCr. From this method, it was determined that miR-16 and miR-30e were the best endogenous reference miRNAs for normalization out of those evaluated. Both miR-16 and miR-30e were therefore selected for normalization of our following miRNA RT-qPCR experiments, as at least 2 endogenous reference miRNAs should be selected.[194] Table B-5 lists all the results of the RT-qPCR for determination of the endogenous reference miRNAs while Table 5 lists the standard deviation, average, and coefficient of variation (CV) for each miRNAs analyzed.

Table 5 List of standard deviation, average, and coefficient of variation for urinary miRNAs tested for use as an endogenous reference miRNA. The two lowest CV values are highlighted in red.

Target	Standard Deviation	Average	Coefficient of variation %
miR-16	311.10851	494.86691	62.9
miR-28	36.9051	47.411633	77.8
miR-30e	109.1216	158.85971	68.7
miR-93	21.307474	19.466262	109.5
miR-128	0.1952283	0.2611942	75
miR-151	19.786783	17.278941	114.5
miR-339	63.207735	3.4599888	1826.8
miR-429	74.484231	76.908034	96.8

Target miRNA expression in urine during XLHN progression

For the two selected reference miRNAs and all of the target miRNAs, standard curves were generated to determine both the efficiency of the primers and to be used for inter-run calibration. Efficiency (%) of the primers used in this portion of the study is listed in Table 6. For inter-run calibration mean Cq values for each plate, along with the standard deviation, mean, and coefficient of variation for all of the miRNAs are listed in Table B-6.

Table 6 Efficiency of primers (including range) as determined from analysis using generation of standard curves.

Assay	Average Efficiency (%)	Range (%)	Use
let-7e-5p	96.7	93.7-101.9	Test
miR-21-5p	82.4	79.6-86.4	Test
miR-30d	92.6	85.9-95.1	Test
miR-142	88.3	85.2-90.9	Test
miR-378a-5p	86.4	85.6-86.5	Test
miR-486-5p	82.2	75.7-83.2	Test
miR-8890	121.0	N/A	Test
miR-16-5p	84.0	81.6-89.3	Reference
miR-30e-3p	80.0	77.4-81.6	Reference

Figure 23 shows a clustergram that displays data in a hierarchy based on the degree of similarity of expression for different targets and samples. Red indicates upregulation (or higher expression), green indicates downregulation (or lower expression), and black represents no change in expression; the lighter the shade of the color, the greater the

relative expression difference. On the outer edge of the data plot is a dendogram, which indicates the clustering hierarchy. Targets that have similar expression patterns will have adjacent branches. From the clustergram of the data, there are three distinct clusters between the unaffected and affected dogs. The first branch of the cluster contains miR-486 alone. Due to the unreliability of one of the Cq values based on the curve analysis as described in the methods section, one sample (C3_T3) was omitted from analysis. Relative expression of miR-486 generally appeared higher in affected dogs at T1 when compared to T2 and T3 and when compared to unaffected dogs.

The second cluster represents 4 miRNAs, (miR-8890, miR-30d, miR-142, and miR-378) that appear to have an overall lower expression in affected dogs when compared to unaffected control dogs regardless of time point.

The third cluster, comprised of let-7e and miR-21, represent miRNAs that have a relative higher expression in affected dogs when compared to unaffected dogs. Individual normalized expression values for generation of the clustergram are listed in Table B-7.

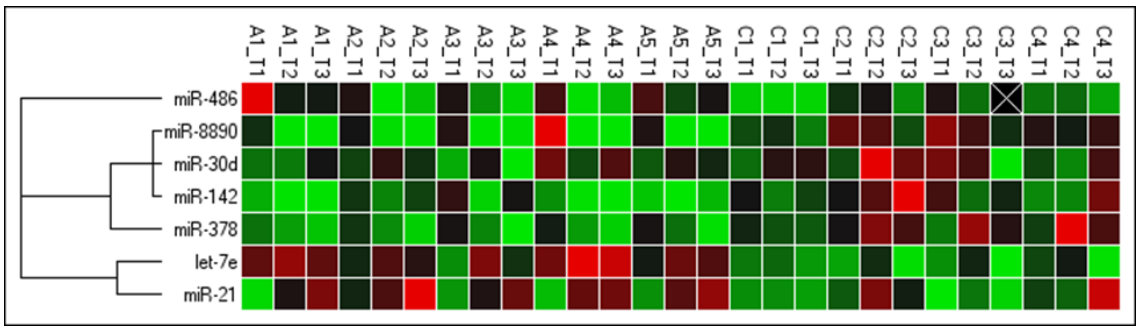

Figure 23 Clustergram displaying data in a hierarchy based on degree of similarity of expression for different urinary miRNA targets.

Next, data were evaluated for each individual miRNA based on dog group (unaffected vs. affected) and time point (T1, T2, and T3). Data was first evaluated based on the change in expression (or fold change) for each urinary miRNA, comparing affected dogs to unaffected dogs at each time point (Table 7).

Table 7 Relative fold change for each urinary miRNA between affected compared to unaffected dogs at each time point. P-value <0.05.

Biological Group	Target	Fold Change	P-Value
Affected vs Unaffected Time point 1	let-7e	1.36	0.06
	miR-142	-2.04	0.23
	miR-21	-1.08	0.81
	miR-30d	-1.10	0.63
	miR-378	1.08	0.61
	miR-486	3.34	0.03
	miR-8890	-1.15	0.77
Affected vs Unaffected Time point 2	let-7e	1.49	0.00
	miR-142	-10.56	0.01
	miR-21	1.51	0.08
	miR-30d	-1.21	0.37
	miR-378	-3.84	0.00
	miR-486	-1.37	0.54
	miR-8890	-113.71	0.00
Affected vs Unaffected Time point 3	let-7e	2.14	0.00
	miR-142	-9.94	0.04
	miR-21	2.14	0.06
	miR-30d	-1.10	0.75
	miR-378	-4.70	0.00
	miR-486	1.28	0.61
	miR-8890	-101.31	0.00

In figures 24-30, box and whisker charts displaying the 25% and 75% quartiles, median, and furthest outliers of the data are presented for each miRNA. In the unaffected dogs, two miRNAs had significant relative differential expression between time points; miR-378 had a statistically significant decreased expression at T1 as compared to T2 while let-7e expression was higher at T2 when compared to T3.

For miR-486, there was a significant difference in fold change in affected dogs compared to unaffected dogs at T1 (Table 7). Additionally, there was significantly higher relative expression in affected dogs at T1 when compared with both T2 and T3 (Figure 24).

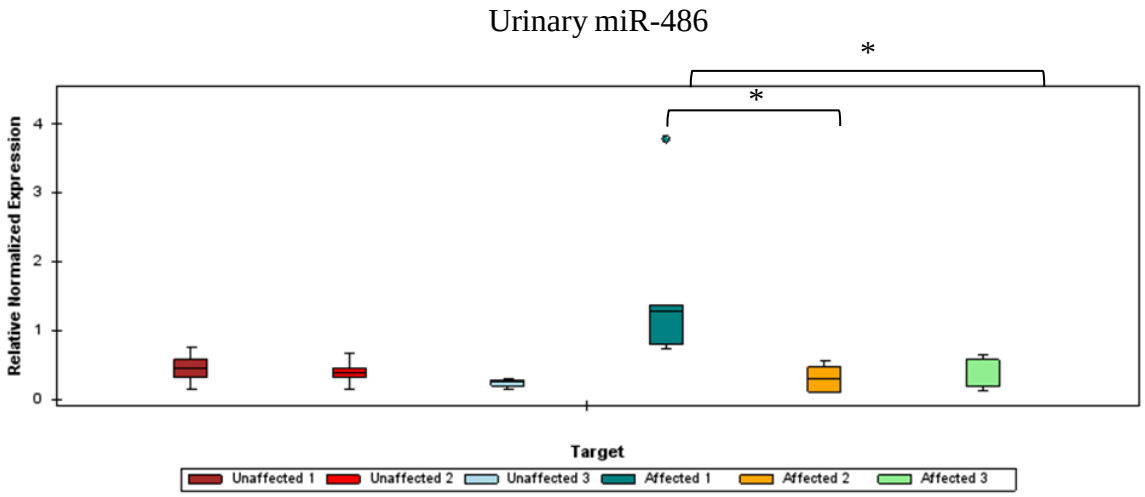

Figure 24 Box and whisker charts displaying the 25% and 75% quartiles, median, and furthest outliers of relative of expression of urinary miR-486 between affected and unaffected dogs at each time point. * indicates P-value < 0.05.

For miR-8890, there was a statistically significant fold change and difference in relative expression between affected vs. unaffected dogs at T2 and T3 but not at T1 suggesting that dogs in the early stage of disease have similar urinary expression of miR-8890 when compared to unaffected dogs (Table 7 and Figure 25). Among the affected dogs, relative expression was significantly higher at T1 when compared to T2 and T3 (Figure 25).

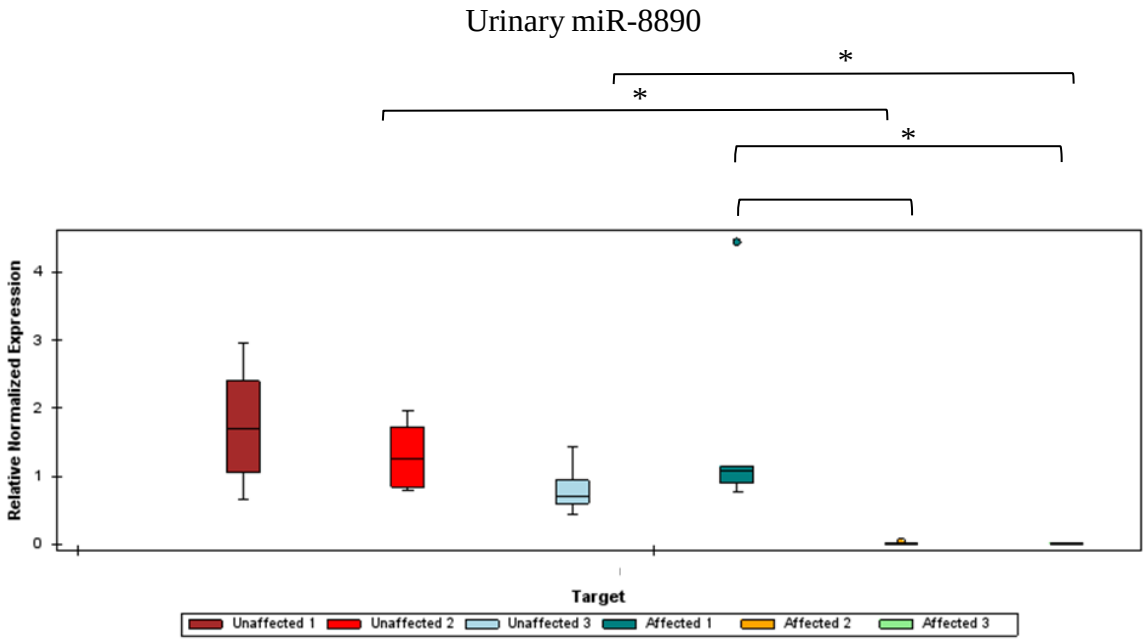

Figure 25 Box and whisker charts displaying the 25% and 75% quartiles, median, and furthest outliers of relative expression of urinary miR-8890 in affected and unaffected dogs at each time point. * indicates P-value < 0.05.

For miR-30d, there was no significant difference between unaffected and affected dogs regardless of time point (Figure 26).

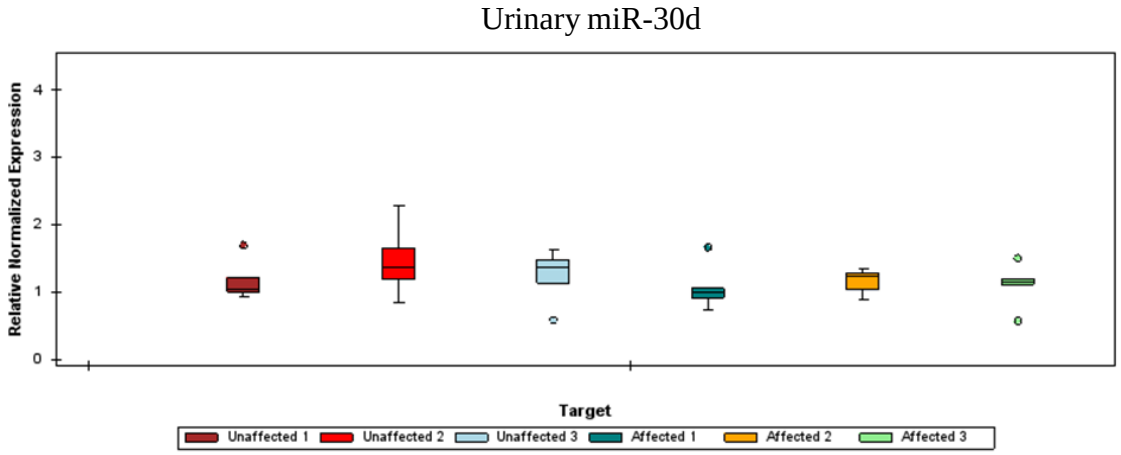

Figure 26 Box and whisker charts displaying the 25% and 75% quartiles, median, and furthest outliers of relative expression of urinary miR-30d in affected and unaffected dogs at each time point. There is no statistical significance between or within the groups, regardless of time point.

For miR-142, affected dogs had significantly lower fold change for miR-142 at T2 and T3 compared with unaffected dogs (Table 7). There was also a significant decreased relative expression in affected dogs at T2 compared to unaffected dogs at T2 (Figure 27).

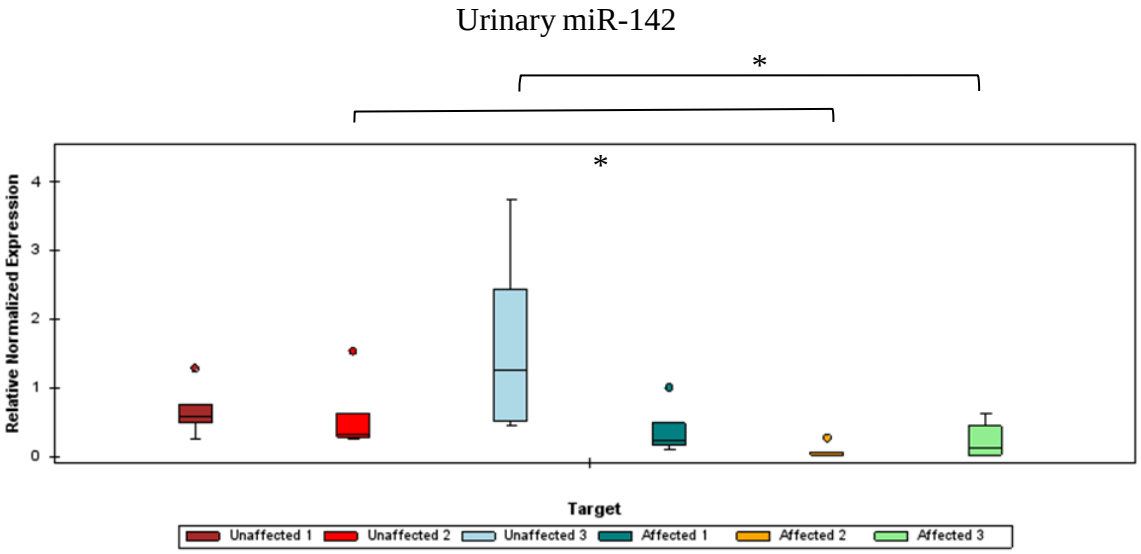

Figure 27 Box and whisker charts displaying the 25% and 75% quartiles, median, and furthest outliers of relative expression of urinary miR-142 in affected and unaffected dogs at each time point. * indicates P-value <0.05.

When comparing affected dogs to unaffected dogs, the fold change of miR-378 was significantly lower at T2 and T3 with similar expression at T1 (Table 7). Relative expression of miR-378 progressively decreased in affected dogs from T1 to T2 and T2 to T3, suggesting a correlation of decreased expression with disease progression (Figure 28).

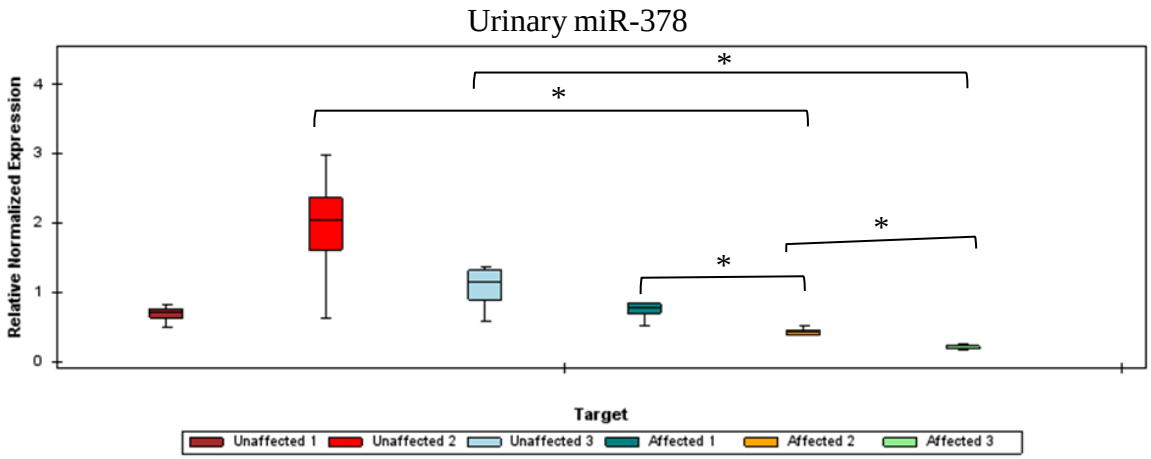

Figure 28 Box and whisker charts displaying the 25% and 75% quartiles, median, and furthest outliers of relative of urinary miR-378 expression in affected and unaffected dogs at each time point. * indicates P-value < 0.05.

Both the fold change and relative expression of let-7e was significantly higher in affected dogs at T2 and T3 when compared to unaffected dogs (Table 7 and Figure 29). There was no difference in expression among affected dogs at any of the time points (Figure 29).

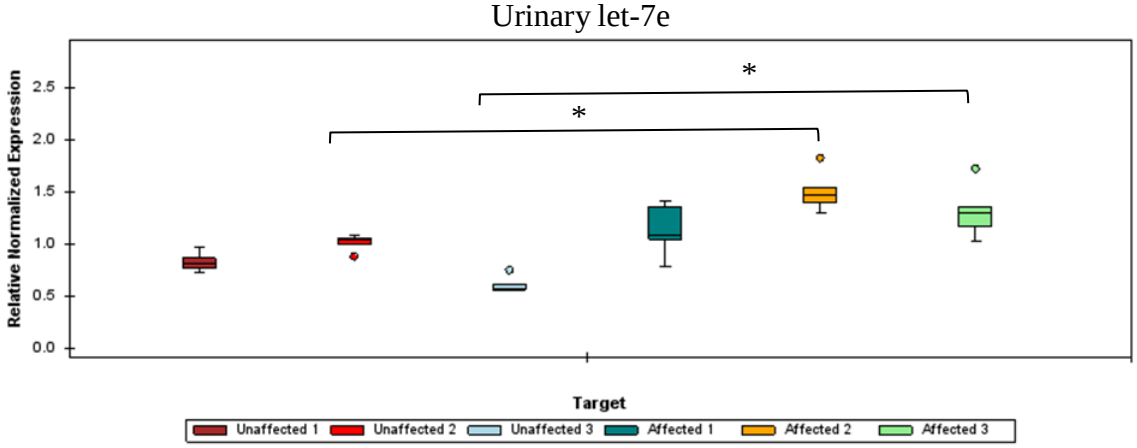

Figure 29 Box and whisker charts displaying the 25% and 75% quartiles, median, and furthest outliers of relative expression of urinary let-7e in affected and unaffected dogs at each time point. * indicates P-value <0.05.

In general, expression of urinary miR-21, a miRNA known to be linked to development of fibrosis, including renal fibrosis, was overall not significantly different between the

unaffected dogs and affected dogs as a whole. Among the affected dogs, expression of miR-21 increased as disease progressed, with significantly lower expression in affected dogs at T1 when compared to T3 (Figure 30).

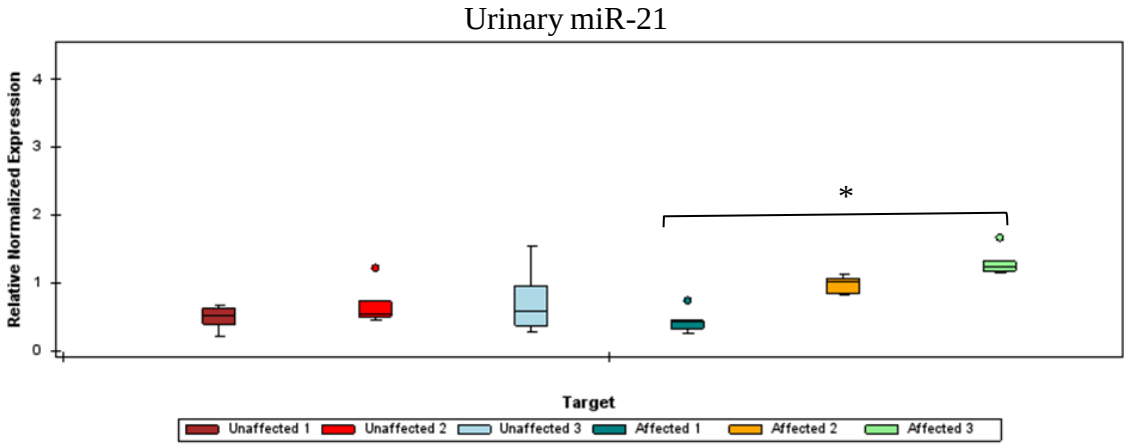

Figure 30 Box and whisker charts displaying the 25% and 75% quartiles, median, and furthest outliers of relative expression of urinary miR-21 in affected and unaffected dogs at each time point**.** * indicates P-value < 0.05.

Discussion

Using urine obtained from unaffected dogs and dogs affected with CKD caused by XLHN, the two primary aims of this study were to: (1) to determine the miRNA profile at 3 different time points of disease progression using next-generation sequencing and (2) to verify the expression levels of selected target miRNAs using RT-qPCR analysis. There were several pertinent observations from this study. First, based on sequencing, we identified a number of miRNAs that were differentially expressed in the urine of affected dogs compared to unaffected dogs as well as within affected dogs during disease progression. To confirm these findings from the sequencing data, several miRNAs were selected for validation using RT-qPCR, a clinically applicable test that could be used to detect any miRNAs that show promise as biomarkers of disease. After normalizing miRNA expression to uCr and evaluating CV, we were able to identify acceptable

miRNAs to be used as endogenous reference miRNAs for normalization and use these to explore differential expression of seven target miRNAs in the urine of dogs affected with XLHN compared to unaffected dogs that served as controls.

In our study, we selected internal reference miRNAs based on their stable expression after accounting for uCr. In our samples, miR-16 and miR-30e were identified as the most stable reference miRNAs out of the 8 evaluated. miR-16 has previously been reported as an endogenous reference miRNA for the normalization of urinary exosome miRNA expression data from CKD patients.[197] Urinary miR-30e has not previously been used as a reference miRNA, and it has been reported as dysregulated in many diseases, including pancreatic ductal adenocarcinoma.[198] This illustrates the importance of validating reference miRNAs within the particular system of interest while remaining aware of the possibility that concurrent diseases might influence their expression.

One of the most interesting findings in our study is the altered expression of urinary miR-8890 in affected dogs. In unaffected dogs and affected dogs at T1, relative expression is similar. However, the expression decreases significantly in affected dogs at both T2 and T3, supporting that miR-8890 may have some contributing role in the pathogenesis of disease progression in dogs with XLHN supporting its use as a potential biomarker for disease. Currently, there is no information in the literature on miR-8890, although it is listed as a canine miRNA in miRBase. There are 207 predicted gene targets for cfa-miR-8890 in miRDB. The top three with a rank score of 100 include: N (alpha)-acetyltransferase 15, NatA auxiliary subunit (*NAA15*), cAMP responsive element binding protein-like 2 (*CREBL2*), and capping protein (actin filament) muscle Z-line, alpha 1(*CAPZA1*). According to information available on NCBI RefSeqGene (www.ncbi.nlm.nih.gov/refseq/rsg/), N-alpha-acetylation, performed by NAA15, is among

the most common post-translational protein modifications in eukaryotic cells and involves the transfer of an acetyl group from acetyl-coenzyme A to the alpha-amino group on a nascent polypeptide, and it is essential for normal cell function. This gene encodes the auxiliary subunit of the N-terminal acetyltransferase A (NatA) complex. The second possible target, *CREBL2*, was discovered during a search to identify genes in a commonly deleted region on human chromosome 12p13 flanked by ETV6 and CDKN1B genes that are frequently associated with hematopoietic malignancies, in addition to breast, non-small-cell lung, and ovarian cancers.[199] CREBL2 shares a 41% identity with CRE-binding protein (CREB) over a 48-base long region that encodes the basic-leucine zipper (bZip) domain of CREB. The bZip domain consists of about 30 amino acids rich in basic residues that are involved in DNA binding, followed by a leucine zipper motif that is involved in protein dimerization. This suggests that CREBL2 encodes a protein with DNA binding capabilities. The occurrence of CREBL2 deletion in malignancy suggests that CREBL2 may act as a tumor suppressor gene. Lastly, *CAPZA1* encodes for the alpha subunit of capping protein (CP). CP is a ~64 kDa heterodimer composed of α and β subunits, which are extensively intertwined and form a mushroom-shaped structure (Figure 31).[200] It is found in nearly all eukaryotic organisms and is a major factor in controlling the behavior and interactions of actin filaments, particularly by restricting actin filament elongation by capping the barbed end of growing actin filaments through electrostatic or hydrophobic interactions.[200,201]

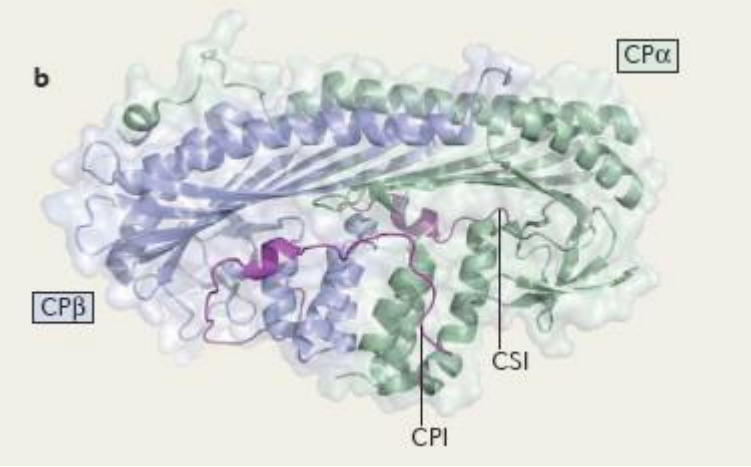

Figure 31 Structure of the heterodimer capping protein. It is composed of a α and β subunit, intertwined in a mushroom-shaped structure.[200]

In the dendritic nucleation model, it has been proposed that the purpose of filament capping is to ensure the network consists of short actin filaments with a high density of branches to provide the mechanical stiffness needed for the efficient generation of force barbed-end growth near the cell membrane.[200] Regulation of CP is important for helping shape the organization and dynamics of cellular actin. While actin is a major component in all cells, when focusing on the kidney, the foot processes of podocytes almost exclusively contain long actin fiber bundles which have a vital role in adhering podocytes (particularly foot processes) to the GBM. In CKD, alterations in the actin filaments result in a morphologic change associated with podocyte injury known as podocyte foot process effacement. Given that miR-8890 may target *CAPZA1*, one may surmise that in later stages of disease, when miR-8890 expression is down-regulated, there may be increased production of CP, which restricts actin filament elongation and may contribute, in some part, to podocyte injury by restricting podocyte repair. Additional studies, such as *in situ* hybridization to localize miR-8890 expression in the kidney and validation of *CAPZA1* as a true target of miR-8890, are needed. Exploring this potential role of miR-8890 may provide additional insight into the pathogenesis of XLHN in dogs.

Another miRNA of particular interest in our study was miR-486, as it may influence genes associated with muscle wasting.[202] A previous study by our group demonstrated decreased expression of miR-486 in the kidney tissue of XLHN dogs at T3 compared with unaffected dogs, and it was also identified as decreased in the urine of azotemic versus non-azotemic dogs with CKD (unpublished observations). In the current study, our results correlated with the tissue in that, based on NGS, urinary miR-486 was significantly lower in affected dogs at T3 when compared to unaffected, age-matched littermates. Additionally, using RT-qPCR urinary miR-486 was statistically significantly higher in affected dogs at T1 when compared to both T2 and T3. Ichii et al. found conflicting results for miR-486, demonstrating an elevated fold change based on sequencing data in the urine of dogs with kidney disease compared to healthy controls (there was no separation of stage of disease), but this finding was not supported by their RT-qPCR results.[203] As mentioned previously, it is not uncommon for discrepancies to exist between two expression profile platforms, which may be one simple explanation for the difference observed in our study. Another possible explanation could be the influence of hematuria. In human erythrocytes, miR-486 has been identified as the most abundant microRNA expressed. In people with IgA nephropathy, where hematuria is a feature, the expression levels of miR-486-5p in microvesicles extracted from urine supernatant were higher in the affected group compared to the control group.[204,205] While hematuria is not a prominent clinical feature in dogs with XLHN (unlike human AS), a small number of RBCs can be observed in the urine sediment in these dogs. As urine becomes more isothenuric, it can cause urinary constituents, including erythrocytes, to lyse and release their contents into the urine. Further investigation into the possible influence of hematuria on urinary miR-486 expression in the unaffected vs affected dogs is needed.

In our study, we found no statistical significance in expression of miR-30d in either unaffected vs affected dogs or during any time points of disease progression based on RT-qPCR. This is in contrast to both our NGS data, which indicate an increase in affected dogs, particularly at T3, and a previous study which employed mouse renal ischemia-reperfusion and streptozotocin (STZ)-induced renal injury as models of acute and chronic kidney injury, respectively.[206] In the mouse model, of all the urinary miRNAs evaluated, urinary miR-30d (in conjunction with miR-10a) was most sensitive for the detection of acute kidney injury. Additionally, using human urine samples, substantial elevations in urinary miR-30d was observed in focal segmental glomerulosclerosis (FSGS) patients when compared to healthy donors. The authors concluded that urinary miR-30d represented a novel, noninvasive, sensitive, specific, and potentially high-throughput method for detecting renal injury.[206] One explanation for these differences could be due to the restricted sample size of the subgroups in our study or due to the different disease types (i.e. XLHN vs FSGS).

For miR-142, a majority of studies looking at differentially expression involving transplanted human kidneys have been performed, and there are conflicting results regarding regulation of miR-142. In one study, miRNA profiles from kidney biopsies have been shown to distinguish patients with acute immunological rejection of the kidney transplant (allograft) from patients with a kidney transplant but no organ rejection. Among the miRNAs that were identified and indicative of acute organ rejection, miR-142-3p and miR-142-5p were identified as being down-regulated.[207] In three reports that studied miRNA changes in both kidney biopsy samples and urine of patients with chronic rejection characterized by interstitial fibrosis and tubular atrophy, miR-142-3p was overly-expressed compared to patients with normal histology.[208] We identified decreased expression in

urinary miR-142 at T2 using both NGS and RT-qPCR and at T3 by RT-qPCR in affected dogs when compared to unaffected, healthy controls, consistent with the study of acute allograft rejection. However, at these time points, the kidney tissue of the dogs should look histologically more similar to that of patients with chronic rejection, characterized by interstitial fibrosis and tubular atrophy, than acute rejection. This illustrates that despite similarities on the histological level in regards to the development of fibrosis, there may be differences in the pathological processes, and general conclusions about miRNA expression in renal disease should be made with caution.

We found significantly decreased expression of urinary miR-378a in affected dogs at both T2 and T3 when compared to unaffected counterparts at the same time points. We also found that miR-378 progressively decreased during progression of disease over the three time points. However, published studies indicate that an increase is more commonly observed with kidney damage. For instance, in rats with cisplatin-induced kidney damage, urinary miR-378 had a 6-fold increase in expression compared to healthy controls.[209] Another study demonstrated that miR-378a-3p was overexpressed in stressed cultured podocytes, in both zebrafish and mice with glomerular dysfunction, and in biopsies from patients with FSGS and membranous nephropathy and that this increase in miR-378 expression was associated with decreased production of the glomerular matrix protein nephronectin.[210] Nephronectin is a podocyte-derived extracellular matrix protein in the glomerular basement membrane and suppression of its expression leads to loss of the integrity of the glomerular filtration barrier and ultimately proteinuria. To our knowledge, the relationship between nephronectin and its association with disease progression in AS has not been explored. It is known that one miRNA is able to regulate many genes, while one gene may be targeted by many miRNAs, thus indicating that the relationships between

miRNAs and their targets are not one-to-one. This further illustrates that while there are similarities in kidney disease, the involvement of a particular miRNA on the molecular level may differ depending on the pathologic process.

Lastly, we found that let-7e and miR-21 were both upregulated in affected dogs with XLHN, although in different ways: let-7e was generally significantly higher throughout the entire disease process while miR-21 appeared to gradually increase as disease progressed. Let-7 (short for Lethal-7) was one of the first discovered miRNAs. The let-7 family, which includes nine slightly different miRNAs, is highly conserved across species and is believed to have a similar function because they all have a common seed region (nucleotides 2-8), which mediates the interaction between the miRNA and its target mRNA.[211] It has been suggested that the let-7 family may have a protective role in renal fibrosis by suppressing TGF-β in renal cells.[211] However, let-7e has been shown to enhance the inflammatory response in vascular endothelial cells by promoting the nuclear translocation of NF-κB and by inhibiting expression of IκBβ (an inhibitor of the NF-κB pathway) by preventing translocation into the nucleus.[212] It is possible that, while thought to have similar roles, each member of the let-7 family may actually have different effects on different cell types even within the same tissue. Additional studies are needed to explore the specific role of let-7e in the development of renal fibrosis. The progressive elevation of miR-21 is supported by findings of its expression in renal tissue obtained from dogs with XLHN compared to unaffected dogs as discussed in the next chapter of this dissertation.

While there are several exciting observations from this study, its limitations cannot be ignored. There are several general factors that should be considered. Since the discovery that miRNAs have unique tissue-specific and disease-specific expression patterns, the

interest in identifying miRNA expression profiles for use as biomarkers for pathogenesis, diagnosis, screening, progression, and therapy has sky-rocketed.[213] However, accurate quantification of miRNA expression profiling is a major challenge for several reasons.[214,215] Mature miRNAs are extremely short (~22 nucleotides) and are low in abundance. Additionally they are heterogeneous in their GC content, resulting in a relatively large range of melting temperatures (Tm), making simultaneous measurement difficult. Mature miRNAs also lack a common sequence feature that would facilitate their selective purification (i.e., the target sequence is present in both the primary and precursor transcript). Additionally, miRNAs within the same family may differ by just a single nucleotide (i.e. Let-7 family) making separation difficult. Several methods have been developed to quantify miRNA expression, such as northern blotting using radiolabeled probes, oligonucleotide microarrays, bead-based flow cytometry, NGS, and qPCR-based detection of mature miRNAs.[213-215] In this study, we utilized two platforms, NGS and RT-qPCR to explore candidate miRNAs for reference normalization and differential expression. NGS provides an unbiased, comprehensive miRNA profile and demonstrates high detection sensitivity, a large dynamic range for detection, and has high accuracy for differential expression analysis. However, it is impractical for routine clinical use at this point in time. Therefore, RT-qPCR is the preferred method for clinical detection, and it is consider by some to be the gold standard for small RNA expression profiling.[213,215,216] One study comparing 12 platforms for miRNA expression profiling noted substantial inter-platform differences when evaluating differential miRNA expression, with an average validation rate for differentially expressed miRNAs of only 54.6% between any two platform combinations.[217] Therefore, it is strongly advised that when trying to identify differences in miRNA expression across comparative samples, observations from

screening studies should be followed by performing a targeted validation study using an alternative platform or technology, in particular, RT-qPCR.[214,217] In our study, we selected 7 total miRNAs that were differentially expressed between unaffected and affected dogs based on NGS. Of those selected for validation by RT-qPCR, there was an overall 81% similarity in findings between the two platforms. This is much higher compared to the findings from the study comparing similarities between two platforms as described above.

While there are a number of factors that will influence the results of an experiment, one of the key factors in quantifying miRNAs is the choice of a proper normalization strategy.[215] In fact, for accurate qPCR results, normalization has been identified as the single most important factor.[218] Normalization is needed to help remove or reduce experimentally induced variation between biological samples in addition to inherent biological variation between samples. Unfortunately, a clear consensus on normalization techniques for urinary miRNAs does not exist. Because concentration levels of urinary microRNAs are so low, RT-qPCR input is typically based on starting volume of the sample rather than amount of RNA present. While various normalization strategies have been proposed, the use of endogenous reference miRNAs is the most widely used method, with at least two endogenous reference miRNAs recommended.[194] It is highly recommended that when selecting reference miRNAs to use for normalization, a pilot study be performed to analyze a set of candidate reference miRNAs (preferentially more than eight, each belonging to a different family) to determine their stability in a selection of samples that is representative of the entire sample set of an individual study (at least 10 independent samples) in which the normalizers will be used.[194,215] Based on these recommendations, we performed a pilot study to identify at least two miRNAs that would serve as reference miRNAs for subsequent studies to identify changes in miRNA expression profiles. One of

the major limitations for this part of the study was the small sample size. Given that banked samples were used, we were unable to select a sample size based on statistical grounds, instead restricted by the number of samples available to us. Additionally, because there were a limited number of samples, the samples used for the pilot study were also used for the second part of the experiment evaluating the miRNAs of interest.

Biomarker concentration can also be influenced by time of collection, urine concentration and urine flow rate, especially in chronic disease, where the ability to concentrate the urine will vary depending on the degree of kidney dysfunction. Traditionally, urinary biomarkers (such as albumin) are normalized to uCr to account for these variations. The assumption for this is that regardless of biomarker production or excretion and urinary flow, uCr excretion is constant within an individual over time and across individuals and that the biomarker will have a linear relationship with uCr excretion across individuals.[219] Therefore it is important to mention that the reliability of this method is under scrutiny, especially in conditions of acute kidney injury.[188,220] Currently, due to the limited number of studies, there is no set recommendation for normalizing the expression of urinary miRNAs for use as biomarkers. Studies evaluating urinary miRNAs for use as biomarkers largely deal with urologic cancer in human medicine, although urinary microRNAs have also been explored in various renal diseases, ovarian and breast cancer, and atopic dermatitis in children, among others.[221-227] In these studies, raw values (including Cq values, fold changes, or relative expression) were typically reported. While a number of studies have normalized miRNA expression levels to other miRNAs as internal controls, few studies have normalized values to uCr. Specifically in veterinary medicine, one study evaluating the expression of urinary exosome-derived microRNAs from dogs

with kidney disease correlated miRNA and uCr, but the miRNA expression levels were not normalized to uCr.[203]

When looking at specific factors, one of the biggest limitations of our study is the small sample size consisting of five affected and four unaffected dogs. Small sample size due to financial constraints and limited patient samples is a common pitfall for miRNA biomarker experiments.[194] This can lead to an underpowered study which can generate both false-positive and false-negative findings because the magnitude of effect size is frequently over-estimated.[194] Outliers can make a huge contribution to the overall effect, creating false-positives, while small sample size leads to large standard errors and wide confidence intervals so that true differences may not reach statistical significance, leading to false-negatives.[194]

In a recent report that reviewed study design and qPCR data analysis guidelines for miRNA biomarker experiments, use of the ΔΔCq method was noted to cause bias in results, in part because these equations ignore the differences in PCR efficiencies between targets and references by assuming 100% efficient PCR assays.[194] The PCR assays contain amplified primers that are supposed to be miRNA specific and optimized with LNA to ensure high sensitivity and specificity even with low levels of miRNAs. Regardless of this guarantee, we performed standard curves for each target miRNA assay on each plate to account for the efficiency of primers in addition to inter-plate variation for each assay and found that a majority of the primers were not at 100% efficiency, and were actually lower than the recommended target range of 90-110%. Regardless of these findings, the ΔΔCq method was used in this study for data analysis and comparison, as the CFX Maestro software is able to automatically input the data and perform calculations based on the standard curves to account for primer efficiency when computing results. Because of this

variation, even with the consideration of primer efficiency built into the calculation, the introduction of bias to the results may still be possible. Troubleshooting should be performed to evaluate for the cause and resolution of the efficiencies outside of the target range.

Another limitation to consider in this study is the variation in starting material, which can introduce bias and contribute to quantification errors. While miRNAs are readily available and extremely stable in bodily fluids, including urine, total concentration of these miRNAs is extremely low, and normal RNA quality control techniques are not feasible. Additionally, not all miRNAs are protected in bodily fluids and may be prone to destruction or contamination, and inhibitors of reverse transcriptase and polymerase enzymes may survive the RNA isolation process.[228] Therefore, an effective and robust isolation method for miRNA extraction is crucial. Unfortunately, there are no set guidelines on the best way to isolate RNA from urine. Prior to this study, analysis of several kits was performed in an attempt to identify the RNA isolation method that would maximize yield. Additionally, supernatant was used for removal of cellular components but contamination from cell remnants is still possible. QIAzol was used in the isolation protocol and while effective, frequent phenol contamination in RNA preparations has proven to be problematic.[229] In the future, the use of a spike-in miRNA for testing key processing steps, including RNA isolation, cDNA synthesis, and RT-qPCR, should be considered to help evaluate for PCR efficiency.

In summary, we were able to 1) to determine the miRNA profile in urine at 3 different time points of disease progression using next-generation sequencing and 2) verify the expression levels of selected target miRNAs in urine using RT-qPCR analysis which involved both identifying the most suitable miRNAs to use as endogenous reference

miRNAs for normalization and determining differential expression of miRNA between unaffected dogs and dogs affected with XLHN and at different time points of disease progression. In this cohort of dogs, urinary miR-16 and miR30e proved to be the most suitable for use as reference miRNAs for endogenous normalization. The most significant differentially expressed miRNAs that appear to be the most promising for use as potential biomarkers and warrant further evaluation and validation include let-7e, miR-21, miR-142, miR-378, miR-486, and miR-8890.

CHAPTER V

ABNORMAL EXPRESSION OF MIR-21 IN KIDNEY TISSUE OF DOGS WITH XLHN[*]

Background and Significance

Small, non-coding RNAs known as microRNAs (miRNAs) play a significant role in a variety of physiologic and disease processes.[114] MicroRNAs act as negative regulators of post-translational gene/protein expression by binding to the 3'-untranslated regions of specific mRNAs, typically resulting in either suppression of protein translation or degradation of the target mRNA.[114] The processing of miRNA is tightly regulated, and miRNAs are expressed in both a tissue-specific and cell type-specific manner. Alterations in miRNA expression profiles in tissue and body fluids have been observed with many diseases, including chronic kidney disease (CKD) in humans and animals[124,189], and dysregulation of miRNAs may contribute to pathogenesis. Due to the important roles of miRNAs in the regulation of gene expression and pathogenesis of different diseases, some miRNAs have been considered as therapeutic targets for a variety of diseases.[230,231]

In dogs, CKD is a common cause of morbidity and mortality.[232] While there are many different causes of CKD in dogs, the mechanisms leading to end-stage renal disease (ESRD) are thought to be similar. One rare, although well-characterized, form of CKD in dogs is X-Linked hereditary nephropathy (XLHN). Affected dogs have abnormal type IV collagen present in their glomerular basement membrane, and affected male dogs demonstrate rapid progression to ESRD, typically by one year of age.[133] This disease is

[*] A majority of the data reported in this chapter is reprinted from Clark SD, Song W, Cianciolo R, Lees G, Nabity M, Liu S. Abnormal Expression of miR-21 in Kidney Tissue of Dogs with X- Linked Hereditary Nephropathy: A Canine Model of Chronic Kidney Disease. *Vet Pathol*.
 DOI: https://doi.org/10.1177/0300985818806050.[233]

equivalent to Alport syndrome (AS) in people, and these dogs serve as a large animal model for investigating the pathogenesis of AS disease development.[143,177,234] Furthermore, these dogs serve as a good model of CKD in general due to their predictable nature, thorough monitoring of disease progression, and potential similarities in pathogenesis leading to ESRD.[108,193]

In CKD, interstitial fibrosis is a characteristic finding with progressive renal injury, regardless of cause.[121,235] The TGF-β1 signaling pathway is a key promoter of CKD progression and fibrosis.[235,236] TGF-β activation exerts pro-fibrotic effects in a number of ways, including recruitment and activation of inflammatory cells, stimulation of extracellular matrix synthesis, proliferation of fibroblasts, and increased tubular epithelial cell apoptosis.[235,237] While several miRNAs have been identified as targets regulated by TGF-β and as important modulators of renal fibrosis, one of particular interest is miR-21.[121-124,235] TGF-β promotes miR-21 production by both increasing transcription of miR-21 through activation of the Smad complex (Smad2/3/4) and by enhancing post-translational processing of pre-miR-21.[121,235] In turn, miR-21 promotes TGF-β expression by inhibiting Smad7, an inhibitor of the TGF-β/Smad2/3 pathway, thereby creating a positive feedback loop.[235] Additionally, miR-21 promotes proliferation and inhibits apoptosis of fibroblasts through alteration of several metabolic pathways.[121,122] Further supporting the role of miR-21 in progression of CKD, miR-21 silencing (using anti-miR-21 oligonucleotides or genetic knockout) ameliorated development of kidney fibrosis in several different murine models of CKD, including a model of AS.[121,238,239] Therefore, further investigation of miR-21 and its function in CKD development is essential.

The role of miRNAs in renal fibrosis, particularly miR-21, has been evaluated extensively in various rodent models of CKD.[123,238-241] To date, there are few studies that

have focused on characterizing miRNA expression profiles in dogs.[242-246] In regards to kidney tissue, miRNA expression profiling has been evaluated in both healthy and diseased dogs. In kidney tissue of healthy dogs, expression profiles were found to differ between the renal cortex and medulla.[246] More recently, miRNA expression profiles generated from both urinary exosomes and kidney tissue collected by laser-microdissection from healthy dogs and dogs with kidney disease were created and compared. In dogs with kidney disease, miR-21a was increased in the tubulointerstitium but not in the glomeruli.[203]

The role of miR-21 in both humans with AS and dogs with XLHN is currently unknown. Therefore, the objective of our study was to evaluate the expression of miR-21 and associated genes in renal tissue collected over the course of disease progression in dogs affected with XLHN. Results obtained can provide further insight into the pathogenesis of progression of CKD in dogs and particularly the role of miR-21 in this process. The results might also be applicable to AS progression in humans.

Specific Objectives and Hypothesis

The role of miR-21 in both people with AS and dogs with XLHN is currently unknown. Therefore, the objective of our study was to evaluate the expression of miR-21 and associated genes in renal tissue collected over the course of disease progression in dogs affected with XLHN. Given the known positive correlation between fibrogenesis and miR-21, we hypothesized that miR-21 would be elevated in kidney tissue of dogs with XLHN as disease progresses.

Experimental Design and Methods

Animals

Dogs were from a colony maintained at Texas A&M University, in which the causative mutation of the disease in the affected males is a naturally occurring, 10 base pair deletion

in the gene encoding the α5 chain of type IV collagen.[133] Development and progression of X-linked hereditary nephropathy (XLHN) in these dogs has been described.[193] No treatments were administered to the dogs used in the study. The study protocol was reviewed and approved by the Texas A&M University Institutional Animal Care and Use Committee.

Sample Collection

Blood and mid-stream voided urine were collected for determination of physiologic data, including serum creatinine (sCr) and urine protein: creatinine ratio (UPC) (Vitros 250, Johnson & Johnson Co, Rochester, NY). Glomerular filtration rate (GFR) was also measured as previously described for each dog using either renal scintigraphy[149] or iohexol clearance[178] throughout the advancement of disease. To monitor disease progression, milestones were set and defined by the following criteria: milestone 1 (MS 1)-presence of microalbuminuria for two consecutive weeks, milestone 2 (MS 2)-UPC ≥2 for two consecutive weeks, milestone 3 (MS 3)-sCr ≥1.2 mg/dL, milestone 4 (MS 4)-sCr ≥2.4 mg/dL, and milestone 5 (MS 5)-sCr ≥5 mg/dL or clinical signs of uremia for 2 or more consecutive days (i.e. anorexia, dehydration, vomiting). Testing for microalbuminuria was performed only until milestone 1 was reached using a semi-quantitative test (E.R.D. HealthScreen Canine Urine Test strips, Heska, Loveland, Colorado).

Ultrasound-guided needle biopsies from alternating kidneys were obtained from both affected dogs and unaffected age-matched littermates to serve as a control at each defined milestone during disease progression as previously described.[149,177,178] Biopsy cores were placed into either formalin or RNAlater (Thermo Fisher Scientific, Waltham, MA). Samples in RNAlater were stored at -80ºC for a range of four to ten years until RNA

isolation. In all, biopsy samples obtained from eleven affected and ten unaffected dogs were evaluated.

When affected dogs reached advanced disease as defined by serum creatinine ≥ 5 mg/dL, or had clinically significant disease (as described above), they were humanely euthanized under anesthesia following biopsy collection. Additional kidney tissue was collected for evaluation at autopsy and was snap frozen in liquid nitrogen and stored at -80°C for a range of four to ten years until RNA isolation. Autopsy samples from a total of 27 affected and five unaffected dogs were evaluated.

Light Microscopy Evaluation

For light microscopy, formalin-fixed, paraffin-embedded biopsies were sectioned at 3 µm and stained with hematoxylin and eosin, Masson's trichrome, and periodic acid-Schiff. Sections were scored for glomerular and tubulointerstitial damage as previously published and as outlined in Table B-8 and B-9, respectively.[149]

Four histopathologic changes were compared to relative miR-21 expression: glomerular damage, tubular damage, chronic inflammation, and interstitial fibrosis. A glomerular damage score was determined for each dog by assessing the overall percentage of abnormal glomeruli which involved any of the following features: segmental sclerosis, global sclerosis, synechia, obsolescence, fetal glomeruli, crescents, Bowman's capsule dilation, and glomerular atrophy. An average tubular damage score was determined using the following features: tubular dilation, loss of brush border, tubular atrophy, tubular epithelial cell degeneration/regeneration, and tubular single cell necrosis. Chronic inflammation, defined as consisting of lymphocytes, plasma cells, and/or macrophages and interstitial fibrosis, defined as increased extracellular collagenous matrix with an increase

in fibroblasts/myofibroblasts where graded on a scale of 0 to 3 depending on distribution or severity, respectively.

RNA Isolation, Reverse Transcription, and Quantitative Polymerase Chain Reaction (RT-qPCR)

All samples were homogenized in RLT Buffer (Qiagen, Valencia, CA) using a Bead Ruptor Mill Homogenizer (Omni International, Kennesaw, GA). Total RNA was isolated using the mirVana™ miRNA Isolation Kit (ThermoFisher Scientific, Waltham, MA) following the manufacturer's protocol. Total RNA concentration was determined using the NanoDrop 2000 UV-Vis Spectrophotometer (ThermoFisher Scientific, Waltham, MA). RNA quality was assessed by the RNA 6000 Nano kit on the Agilent 2100 Bioanalyzer (Agilent, Santa Clara, CA) according to the manufacturer's protocol. Samples with an RNA Integrity Number greater than 7 or that had adequate 28S to 18S peaks on analysis were considered adequate for further evaluation.

The amount of miRNA present in each sample was determined using the specific commercially available TaqMan® microRNA Assay for miR-21 and miR-16, which served as an endogenous control, (ThermoFisher Scientific, Waltham, MA, miR-21 assay ID 000397; miR-16 assay ID 000391) following the manufacturer's protocol. Briefly, reverse transcription was performed using 5 ng of total RNA in a 15 µl reaction volume. Then, 3 µl of the reverse transcription product along with appropriate non-template negative controls were amplified using the TaqMan® microRNA reaction in a total volume of 20 µl.

Genes associated with miR-21 expression or fibrosis development were evaluated using two-step RT-qPCR. Briefly, total RNA was reverse transcribed using RNA to cDNA EcoDry Premix (ClonTech, Mountain View, CA). The reverse transcription product along

with appropriate non-template negative controls were used in the specific commercially available TaqMan® gene expression assays (ThermoFisher Scientific, Waltham, MA) following the manufacturer's protocol with18s serving as an endogenous control gene. The specific TaqMan® assays used for all RT-qPCR reactions are listed below in Table B-10.

Gene expression data was analyzed using the Delta-Delta-Ct (ΔΔCt) method, and expression in affected dogs is shown as a relative fold change compared to age-matched unaffected controls. There were some unaffected dogs for which we did not have the corresponding affected littermate's tissue available for comparison. For those unaffected dogs, data corresponding to that biopsy was distributed into the different milestones in a manner that provided a reasonable number of control dogs to span the age of the affected dogs within each milestone. Data was first normalized to the endogenous control gene (miR-16). Then, the expression level was calculated as a relative fold change compared to the mean fold change of the unaffected control group at each milestone. The mean fold change of the unaffected control group was artificially set as "1".

In situ hybridization

Chromogenic *in situ* hybridization with the Qiagen miRCURY® LNA® miRNA ISH Optimization kit was used to evaluate miR-21 expression on formalin-fixed paraffin-embedded (FFPE) kidney tissue from five dogs with CKD caused by XLHN at early, middle, and late time points of disease. Additionally, three control dogs at corresponding time points were also evaluated. A probe for U6 snRNA, a small nuclear miRNA known to be ubiquitously expressed in tissue, was used as a positive control. Scramble, a probe that does not show homology with any known miRNA sequence and, therefore, does not identify miRNAs in tissue, was used as a negative control.

The procedure was performed following the manufacturer's protocol with minor adjustments made based on optimization and literature recommendations.[247] In short, FFPE kidney tissue cut at 5 µm sections was deparaffinized and then incubated with proteinase K (10 µg/mL) for proteolytic digestion of the tissue to provide access to the miRNAs. Hybridization was performed at 53°C for 60 minutes (see Table 8 for concentrations and dilutions) followed by stringent washing using saline-sodium citrate (SSC) buffer.

Table 8 Probe information used for *in situ* hybridation on FFPE kidney tissue.

Probe	Final probe concentration	Probe volume	Dilution factor	1x miRNA ISH Buffer volume
LNA Scramble-miR probe (25 µM)	40 nM	3.2 µL	1:625	2 mL
LNA miR-21 probe (25 µM)	40 nM	3.2 µl	1:625	2 mL
LNA U6 snRNA (0.5 µM)	2.0 nM	8 µL	1:250	2 mL

For the humidifying chamber, plastic Tupperware boxes lined with sponges soaked in 5X SSC buffer was used to maintain moist conditions. Sheep anti-DIG-AP antibody was used at a dilution of 1:800. Slides were counterstained with Nuclear Fast Red nuclear counterstain. Upon completion, slides were mounted using Eukitt® mounting medium and were then dried overnight and analyzed by light microscopy the next day.

Statistical Analysis

Statistical analysis of the clinical and histopathologic data comparing affected vs. unaffected dogs was performed using JMP 12.0 software. Normality was assessed using a Shapiro-Wilks Goodness of Fit test on the residuals of sCr, UPC, GFR, and the histopathological scores (glomerular damage, average tubular damage, average chronic inflammation, and average fibrosis). As all the data were nonparametric, a Mann-Whitney

test was performed to determine statistical significance between the two groups in each category at each milestone, with significance set at a p-value of <0.05.

Analysis of miR-21 expression with clinical and histological data was performed using GraphPad Prism 6 (GraphPad Software, San Diego, CA). In affected dogs, for comparison of relative miR-21 expression with UPC, sCr, and GFR, Pearson correlation was applied; for comparison of relative miR-21 expression with histopathological scores, Spearman correlation was applied. Correlation coefficients were calculated and presented as "r" value. For comparison of relative RNA expression of miR-21 among each stage of disease in the affected dogs, analysis was performed using SAS 9.1.4 (SAS Institute Inc., NC, USA). We applied the two-way ANOVA model with random effect nested in the dog, using genotype, stage (categorized) and their interaction as covariates; p-value <0.05 post-Bonferroni adjustment was considered statistically significant. For comparison of relative mRNA expression of miR-21-associated genes between affected and unaffected dogs, a Mann-Whitney test was performed using GraphPad Prism 6 (GraphPad Software, San Diego, CA). Statistical significance was defined as p-value <0.05.

Results

Clinical and histopathologic progression of disease in affected dogs

The first clinical indication of disease in the affected dogs in this study was the onset of microalbuminuria, which occurred between 11 to 21 weeks of age (average 14 weeks). This progressively worsened to overt proteinuria followed by rapid advancement to ESRD between 26 to 46 weeks. Table 9 summarizes the clinicopathologic parameters of affected vs. unaffected dogs throughout disease development. The UPC and sCr were significantly elevated in affected compared to unaffected dogs starting at milestone 2 (17 to 25 weeks of age) and milestone 3 (21 to 29 weeks of age), respectively. The GFR was not significantly different between the two groups until milestone 4 (21 to 40 weeks).

Histopathologic scores at each disease milestone in affected vs. unaffected dogs are described in Table 10. Significant lesions for all 4 of histologic categories were not evident in kidney biopsies from affected dogs until milestone 3, when the dogs were mildly azotemic

Table 9 Comparison of clinical parameters (median, range) at each milestone of disease in dogs with X-linked hereditary nephropathy vs. unaffected, age-matched littermates. Statistical significance defined as p-value <0.05. n=sample size; [a]MS 1-presence of microalbuminuria for two consecutive weeks, [b]MS 2-UPC ≥2 for two consecutive weeks, [c]MS 3-sCr ≥1.2 mg/dL, [d]MS 4-sCr ≥2.4 mg/dL, [e]MS 5-sCr ≥5 mg/dL or clinical signs of uremia for 2 or more consecutive days, [f]categorized based on clinical signs rather than sCr value as described in the methods. Reprinted from [233].

Clinical Parameters	Milestone	Affected Dogs		Unaffected Dogs		p-value
		n	*Median (Range)*	*n*	*Median (Range)*	
Urine protein:creatinine	1[a]	8	0.6 (0.5-1.1)	10	0.45 (0.1-0.8)	0.054
	2[b]	11	4.8 (2.5-11.3)	10	0.2 (0.1-0.5)	0.000
	3[c]	11	18.4 (9.9-30.2)	10	0.1 (0-0.5)	0.000
	4[d]	10	19.85 (17.2-25.7)	8	0.1 (0-0.3)	0.000
	5[e]	10	21.2 (10.6-41.1)	6	0.1 (0-0.8)	0.002
Serum creatinine (mg/dL)	1	8	0.4 (0.37-0.6)	10	0.65 (0.4-0.8)	0.073
	2	11	0.54 (0.4-0.8)	10	0.7 (0.4-0.9)	0.561
	3	11	1.3 (1.2-1.9)	10	0.9 (0.6-1.1)	0.000
	4	10	2.5 (2.1-3.9)	8	0.85 (0.8-1.1)	0.000
	5	9	5.3 (3.9[f]-7.7)	6	1 (0.8-1.1)	0.002
Glomerular filtration rate (mL/min/kg)	1	8	4.575 (3.6-6.26)	10	3.23 (2.79-4.8)	0.073
	2	11	4.23 (3.34-5.56)	10	3.67 (2.64-4.55)	0.307
	3	11	2.39 (1.27-3.06)	10	2.99 (2.64-3.75)	0.549
	4	10	1.63 (0.65-2.33)	8	3.22 (2.5-4.47)	0.000
	5	10	0.93 (0.28-1.61)	6	3.44 (2.41-3.93)	0.002

Table 10 Comparison of histological scores (median, range) for various features on light microscopy as observed on evaluation of kidney biopsies taken at each milestone of disease in dogs with X-linked hereditary nephropathy vs. unaffected, age-matched littermates. The glomerular score is the overall percentage of abnormal glomeruli based on segmental sclerosis, global sclerosis, synechia, obsolescence, fetal glomeruli, fibrinous crescents, Bowman's capsule dilation, and atrophy. The tubular damage score was based on the average of scores determined for tubular dilation, loss of brush border, tubular atrophy, tubular epithelial cell degeneration/regeneration, and tubular single cell necrosis. n=sample size. Statistical significance defined as p-value <0.05. Reprinted from [233].

Histologic Findings	**Milestone**	**Affected Dogs**		**Unaffected Dogs**		**p-value**
		n	*Median (Range)*	*n*	*Median (Range)*	
Glomerular Damage Score	1	9	0.16 (0-0.59)	7	0 (0-0.09)	0.2126
	2	4	0.125 (0-0.5)	4	0.16 (0-0.2)	0.6577
	3	9	0.91 (0.55-1)	10	0.1 (0-0.17)	<0.0001
	4	10	0.99 (0.75-1)	8	0.12 (0-0.81)	<0.0001
	5	5	1 (0.86-1)	6	0.12 (0-0..29)	<0.0001
Tubular Damage Score	1	9	0.01 (0-0.05)	7	0.02 (0-0.04)	1.0000
	2	4	0.01 (0-0.05)	4	0.02 (0-0.05)	0.0658
	3	9	1 (0.66-1.81)	10	0.05 (0-0.16)	<0.0001
	4	10	1.19 (0.5-1.75)	8	0.05 (0.04-0.99)	0.0012
	5	5	1.38 (1.32-1.81)	6	0.03 (0-0.12)	0.008
Inflammation Score	1	9	0 (0-0.1)	7	0 (0-0.1)	0.6312
	2	4	0 (0-0.2)	4	0 (0)	0.4295
	3	9	0.96 (0-2.2)	10	0 (0-0.1)	0.0015
	4	10	1.58 (0.8-2)	8	0 (0-1)	<0.0001
	5	5	2 (0.4-2.55)	6	0 (0-0.05)	0.008
Interstitial Fibrosis Score	1	9	0 (0)	7	0 (0)	0.9601
	2	4	0 (0)	4	0 (0)	0.9601
	3	9	1 (0.4-2.7)	10	0 (0-0.4)	0.0004
	4	10	1.45 (0.5-2.45)	8	0.05 (0-2.35)	0.0029
	5	5	3 (2.43-3)	6	0 (0-0.1)	0.008

miR-21 Expression during Disease Progression

Based on measurements performed on RNA isolated from biopsy samples, relative expression of miR-21 did not significantly increase in affected dogs until milestone 3 as compared with unaffected, age-matched control dogs (Figure 32).

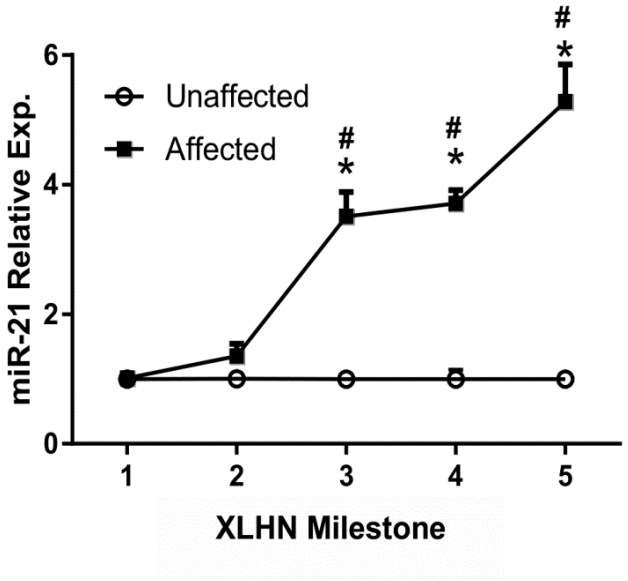

Figure 32 Relative renal miR-21 expression, as determined by RT-qPCR using RNA isolated from kidney biopsies sampled at different milestones during disease progression. The data are presented as the values in dogs affected with X-linked hereditary nephropathy (XLHN) relative to the values in age-matched unaffected dogs. Relative renal miR-21 expression significantly increases from milestone 3 to end stage renal disease (MS 5). Exp.=expression. *****: $p<0.05$ vs. unaffected dogs, and vs. milestone 1 and milestone 2 affected dogs; ******: $p<0.05$ vs. milestone 3 and milestone 4 affected dogs. Figure provided by Dr. Wenping Song. Reprinted from [233].

Graphical representation of individual relative miR-21 expression presented as fold change in unaffected vs. affected dogs at each milestone can be observed in Figure 33. While there was little change in miR-21 expression between milestones 3-4, miR-21 expression significantly increased in the last milestone of disease (MS 5 or ESRD) compared to both MS3 and MS4.

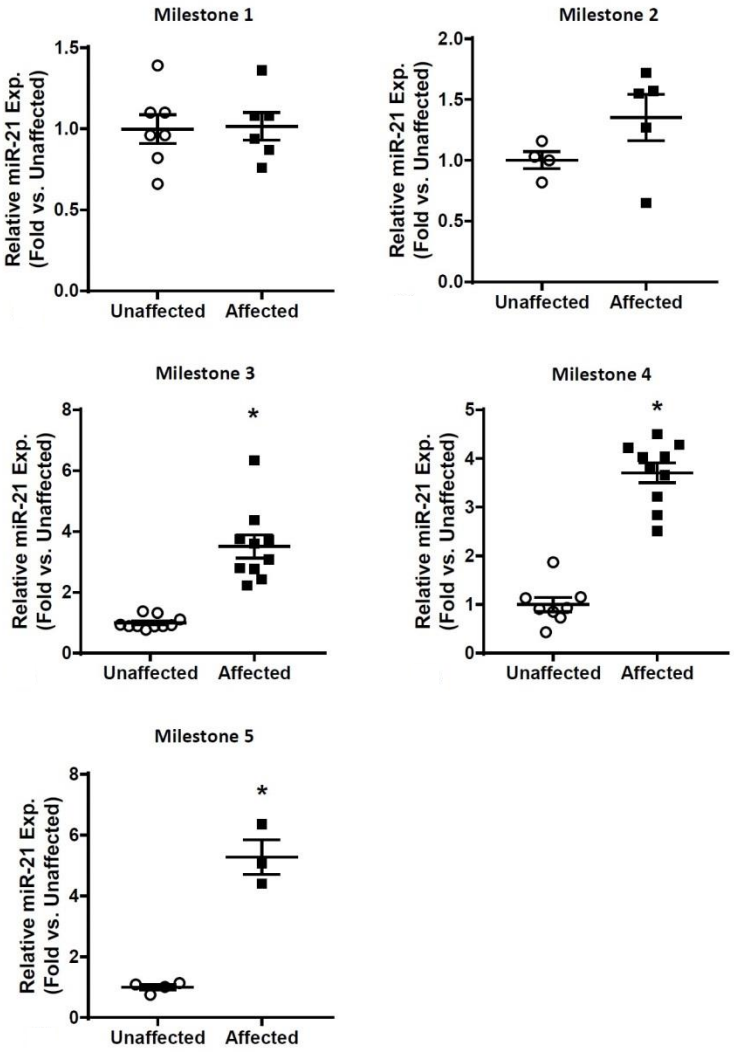

Figure 33 Relative renal miR-21 expression in individual dogs affected with X-linked hereditary nephropathy (XLHN) compared to the values in age-matched unaffected dogs. Determined by RT-qPCR using RNA isolated from kidney biopsies sampled at each milestones during progression of disease. Relative renal miR-21 expression significantly increased from milestone 3 to end stage renal disease (MS 5). Bars represent mean and standard deviation. Exp.=expression. *: $p<0.05$. Figure provided by Dr. Wenping Song. Reprinted from [233].

In affected dogs, alterations in expression of renal miR-21 correlated with clinical markers of kidney function (Figure 34). There was a positive correlation with UPC and sCr ($r=0.798$, $p<0.0001$ and $r=0.737$, $p<0.0001$, respectively) and a negative correlation with GFR ($r=-0.859$, $p<0.0001$).

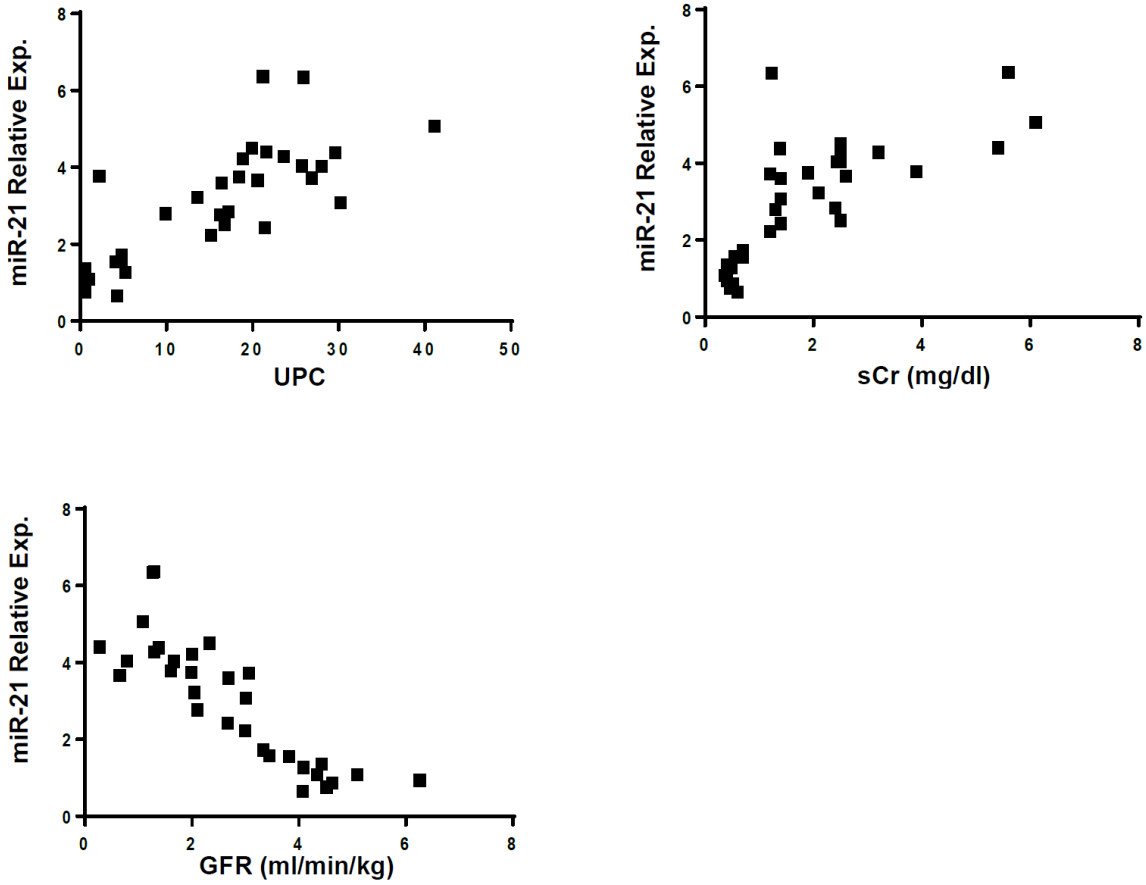

Figure 34 Relative renal miR-21 expression, measured by RT-qPCR using RNA isolated from kidney biopsies correlated to clinical parameters. miR-21 expression positively correlates with urine protein:creatinine ratio (UPC) and serum creatinine concentration (sCr) and negatively correlates with glomerular filtration rate (GFR). The miR-21 relative expression data are presented as the values in dogs affected with X-linked hereditary nephropathy (XLHN) relative to the values in age-matched unaffected dogs. Exp.=expression. $p<0.05$. Figure provided by Dr. Wenping Song. Reprinted from [233].

Additionally, a positive correlation was observed between miR-21 expression and histologic changes indicating that increased miR-21 was associated with more severe pathological damage: glomerular damage ($r=0.6952$, $p<0.0001$), tubular damage ($r=0.799$, $p<0.0001$), chronic inflammation ($r=0.627$, $p=0.0004$), and interstitial fibrosis ($r=0.798$, $p<0.0001$), (Figure 35).

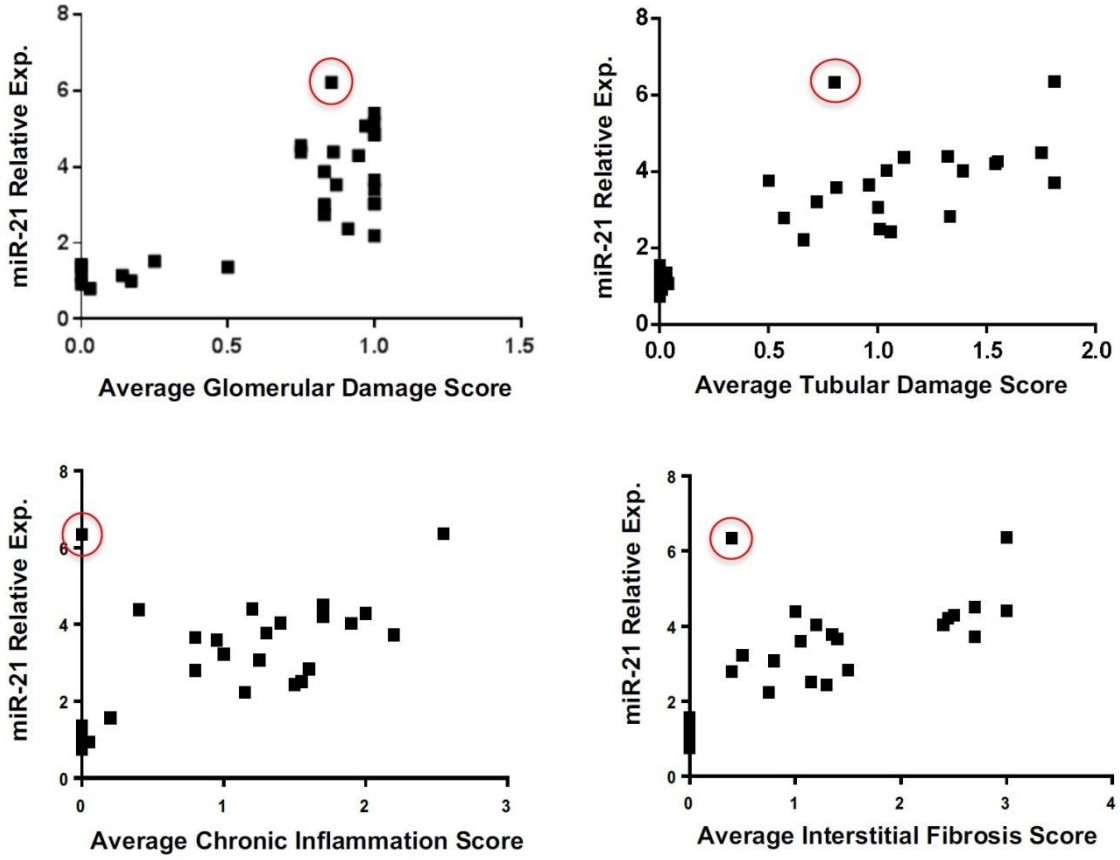

Figure 35 Relative renal miR-21 expression, measured by RT-qPCR using RNA isolated from kidney biopsies correlated to histological findings. miR-21 expression positively correlates with average histopathological scores based on light microscopy, including glomerular damage, tubular damage, chronic inflammation, and interstitial fibrosis. The miR-21 relative expression data are presented as the values in dogs affected with X-linked hereditary nephropathy (XLHN) relative to the values in age-matched unaffected dogs. The circles indicate a sample from an affected male that demonstrated high relative expression of miR-21 but relatively low average histopathological scores. Exp.=expression. $p<0.05$. Figure provided by Dr. Wenping Song. Reprinted from [233].

There was one biopsy sample where high expression of miR-21 (relative expression 6.34 fold) at milestone 3 was present with lower average histological scores (specifically, minimal tubular damage and absence of chronic inflammation, and only mild interstitial fibrosis observed on light microscopy; circled in Figure 35).

To determine if the values from this dog changed the significance of the milestone 3 data in relation to other milestones, his information was removed and the data re-evaluated. While there was a small increase in miR-21 expression between milestone 3 and 4, it was not statistically significant (data not shown). Individual Cq values along with relative miR-21 expression for both the unaffected dogs and the affected dogs at each milestone are shown in Table B-11 and B-12, respectively.

Measurement of miR-21 was also performed on RNA isolated from autopsy samples at ESRD. Autopsy samples have the advantage in that they are larger and therefore more representative of the kidney as a whole compared to biopsy samples. Analysis of the autopsy samples showed a significant, 6-fold increase in miR-21 in dogs at ESRD as compared with tissue from unaffected dogs of similar age (Figure 36). These results support the histology findings based on biopsies, indicating that miR-21 expression is significantly increased in late-stage disease, when fibrosis has been shown to be the most extensive on light microscopy evaluation.[108]

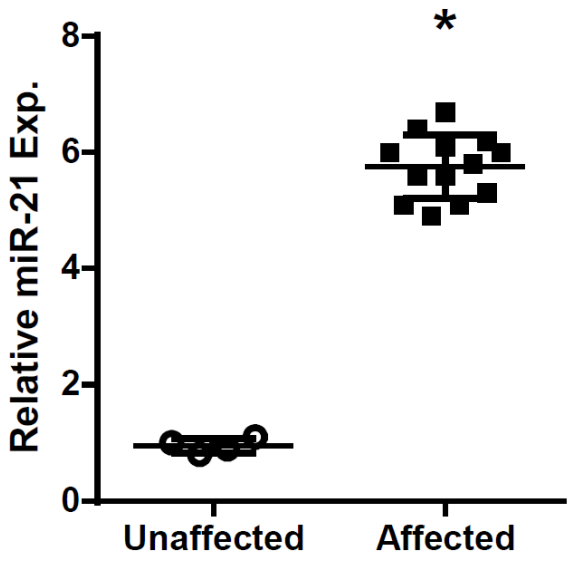

Figure 36 Renal miR-21 expression, measured by RT-qPCR on RNA isolated from tissue obtained at autopsy. miR-21 is significantly increased at end-stage renal disease in dogs affected with X-linked hereditary nephropathy compared with age-matched unaffected dogs. Bars represent mean and standard deviation. Exp.=expression. *$p<0.05$. Figure provided by Dr. Wenping Song. Reprinted from [233].

Dysregulation of genes associated with CKD and miR-21 function

To gain further understanding of the developmental process of renal fibrosis in dogs with XLHN, relative mRNA expression in cortical tissue from the autopsy samples was measured for a number of key genes known to play a pivotal role in the progression of CKD and/or to be involved in the miR-21 pathway of fibrosis development.

Among the twelve genes evaluated, mRNA levels of affected dogs were increased as compared to unaffected dogs for the following genes associated with fibrosis development: collagen 1 alpha 1 (*COL1A1*), transforming growth factor-beta 1 (*TGFB1*) and -beta 2 (TGFB2), transforming growth factor-beta receptor 1 (*TGFBR1*), and S*erpine1* (Figure 37).

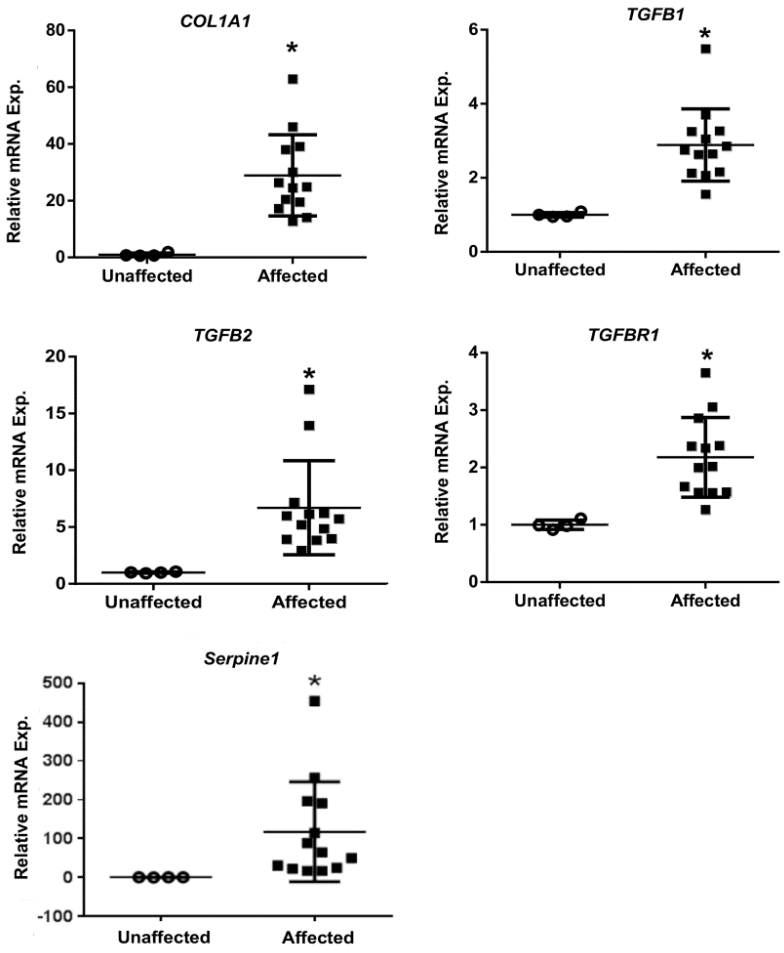

Figure 37 Relative mRNA expression levels of genes associated with fibrosis at end-stage renal disease. Based on RT-qPCR, mRNA expression of collagen 1α1 (COL1A1), transforming growth factor-β1 (TGF-B1) and -β2 (TGF-B2), transforming growth factor beta receptor 1 (TGFBR1), and Serpine1 were increased in renal tissue from dogs affected with X-linked hereditary nephropathy (XLHN) compared to unaffected dogs. Bars represent mean and standard deviation. Exp.=expression. *$p<0.05$. Figure provided by Dr. Wenping Song. Reprinted from [233].

Of those genes, *COL1A1*, a prominent component of the extracellular matrix of fibrotic tissue, had a mean 30-fold increase in affected compared to unaffected dogs. Additionally, Serpine1, the gene that encodes for plasminogen activator inhibitor-1, had a mean 125-fold increase. In contrast, mRNA expression levels of genes related to the regulation of metabolic pathways in the mitochondria were either decreased in affected dogs or had no significant changes including: peroxisome proliferator-activated receptor alpha (*PPARA*), peroxisome proliferator-activated receptor gamma coactivator 1-alpha (*PPARGC1A*), acyl-CoA dehydrogenase (*ACADM*), and carnitine palmitoyltransferase 1A (*CPT1A*) (Figure 38).

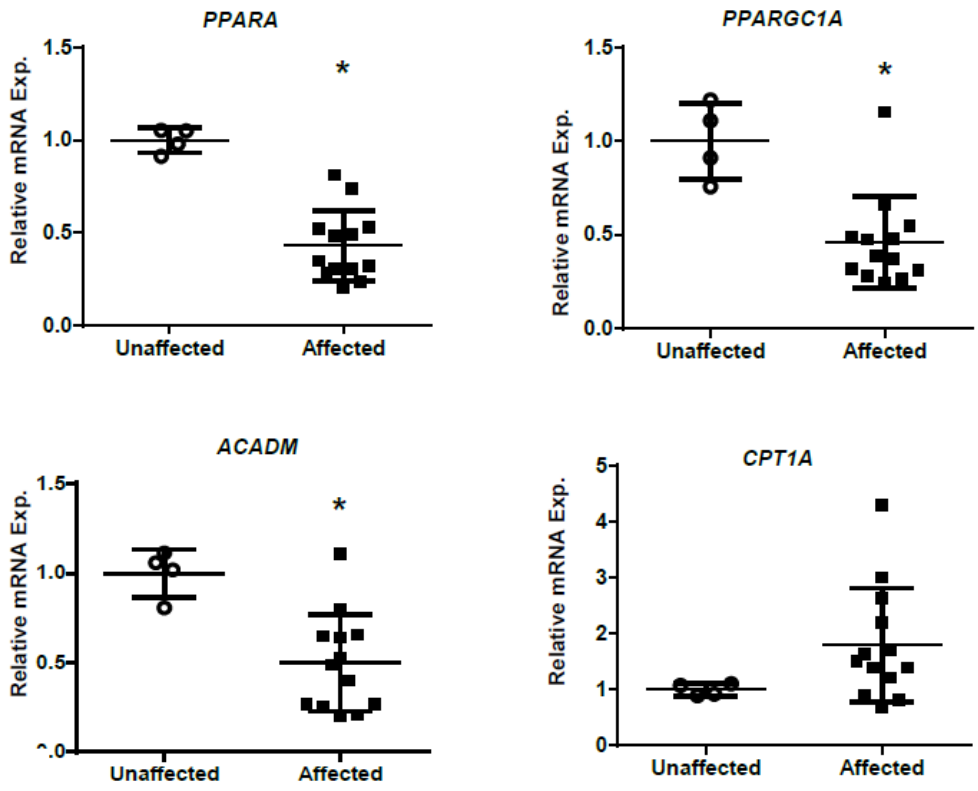

Figure 38 Relative mRNA expression in renal tissue based on RT-qPCR of genes associated with regulation of metabolic pathways in the mitochondria. Gene expression in affected dogs at end stage renal disease is significantly decreased compared to age-matched control dogs, for peroxisome proliferator-activated receptor alpha (PPARA), peroxisome proliferator-activated receptor gamma coactivator 1-alpha (PPARGC1A), and acyl-CoA dehydrogenase (ACADM). Expression of carnitine palmitoyltransferase 1A (CPT1A) was unchanged when compared to unaffected dogs. Bars represent mean and standard deviation. Exp.=expression. *p<0.05. Figure provided by Dr. Wenping Song. Reprinted from [233].

Of the two genes evaluated that encode for antioxidant enzymes, superoxide dismutase 1 (*SOD1*) was significantly decreased while *MPV17* (a mitochondrial inner membrane protein) had no relative change in expression between affected and unaffected dogs (Figure 39).

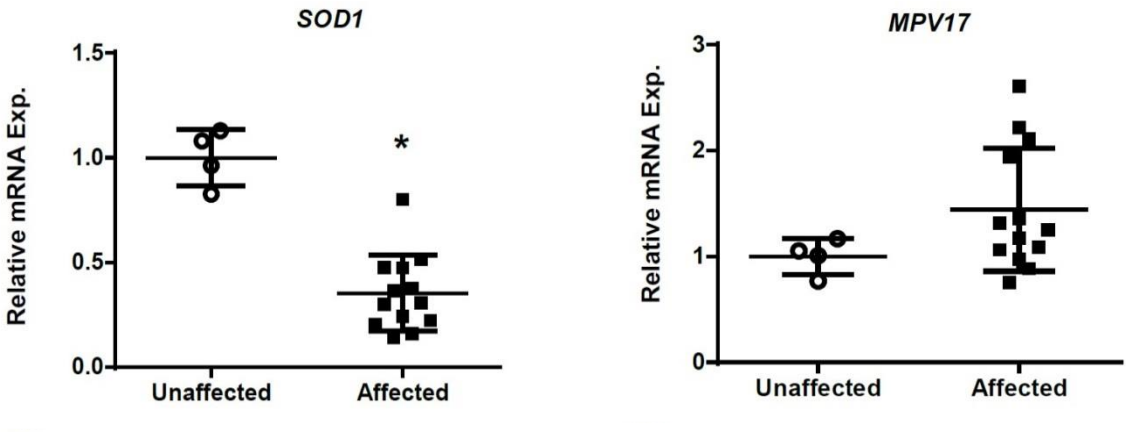

Figures 39 Relative mRNA expression in renal tissue based on RT-qPCR of genes that are responsible for minimizing the generation of reactive oxygen species. Gene expression of superoxide dismutase 1 (SOD1) was significantly decreased while MPV17 (a mitochondrial inner membrane protein) was unchanged, in affected vs. unaffected dogs at end stage renal disease. Bars represent mean and standard deviation. Exp.=expression. *p<0.05. Figure provided by Dr. Wenping Song. Reprinted from [233].

Additionally, relative mRNA expression of epithelial growth factor (*EGF*) was markedly decreased (Figure 40).

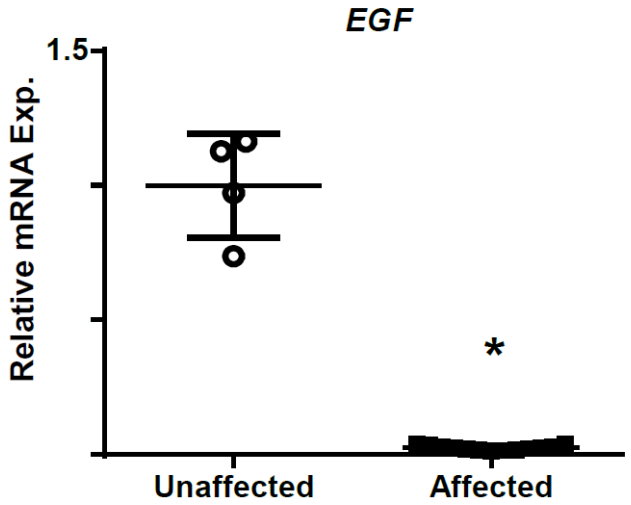

Figure 40 Relative mRNA expression of epithelial growth factor (EGF) at end stage renal disease. EGF was significantly decreased in affected dogs compared to unaffected dogs based on RT-qPCR analysis. Bars represent mean and standard deviation. Exp.=expression. *p<0.05. Figure provided by Dr. Wenping Song. Reprinted from [233].

In situ hybridization of miR-21 in canine kidney tissue

In order to correlate expression of miR-21 in the kidney tissue compared to the RT-qPCR results and to localize expression of miR-21 to specific renal cells, detection using *in situ* hybridization was performed. As expected, Scramble (the negative control) was not detected (Figure 41A). U6 snRNA, used as a positive control, was detected in the nuclei of the cells in the kidney tissue of all the dogs (Figure 41B). For miR-21, unaffected dogs and dogs at MS1 were negative. At MS3, miR-21 expression was frequently evident in the tubules in affected dogs, most often in those morphologically consistent with proximal tubular cells. Expression appeared to be localized predominantly in the cytoplasm of all the cells. At MS5, staining was relatively diffuse, appearing to be present throughout the

tubulointerstitium while glomerular tufts were negative. Subjectively, staining of miR-21 appeared to increase with progression of disease (Figure 42).

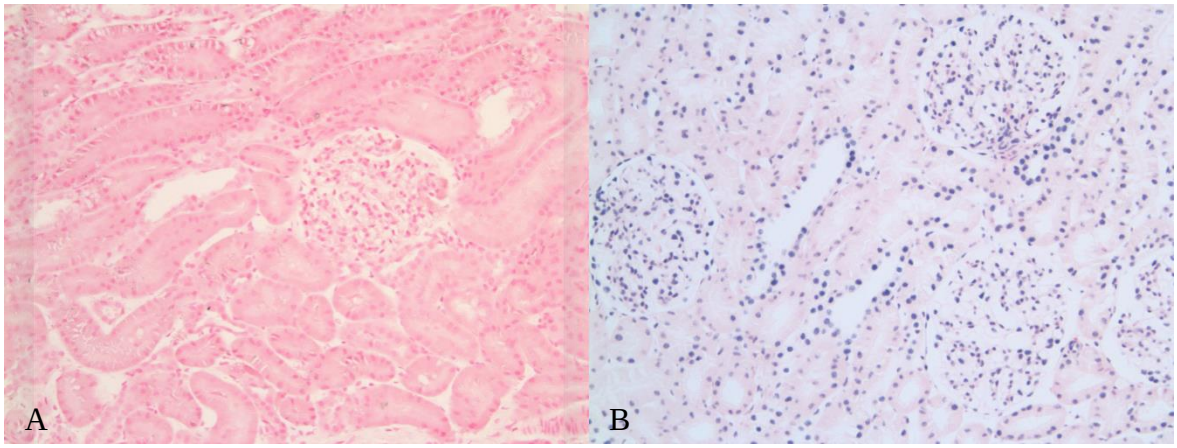

Figure 41 Representative images kidney tissue stained with U6 (positive control) and Scramble (negative control) using *in situ* hybridization. Counterstained with nuclear fast red. Images taken at 20X.

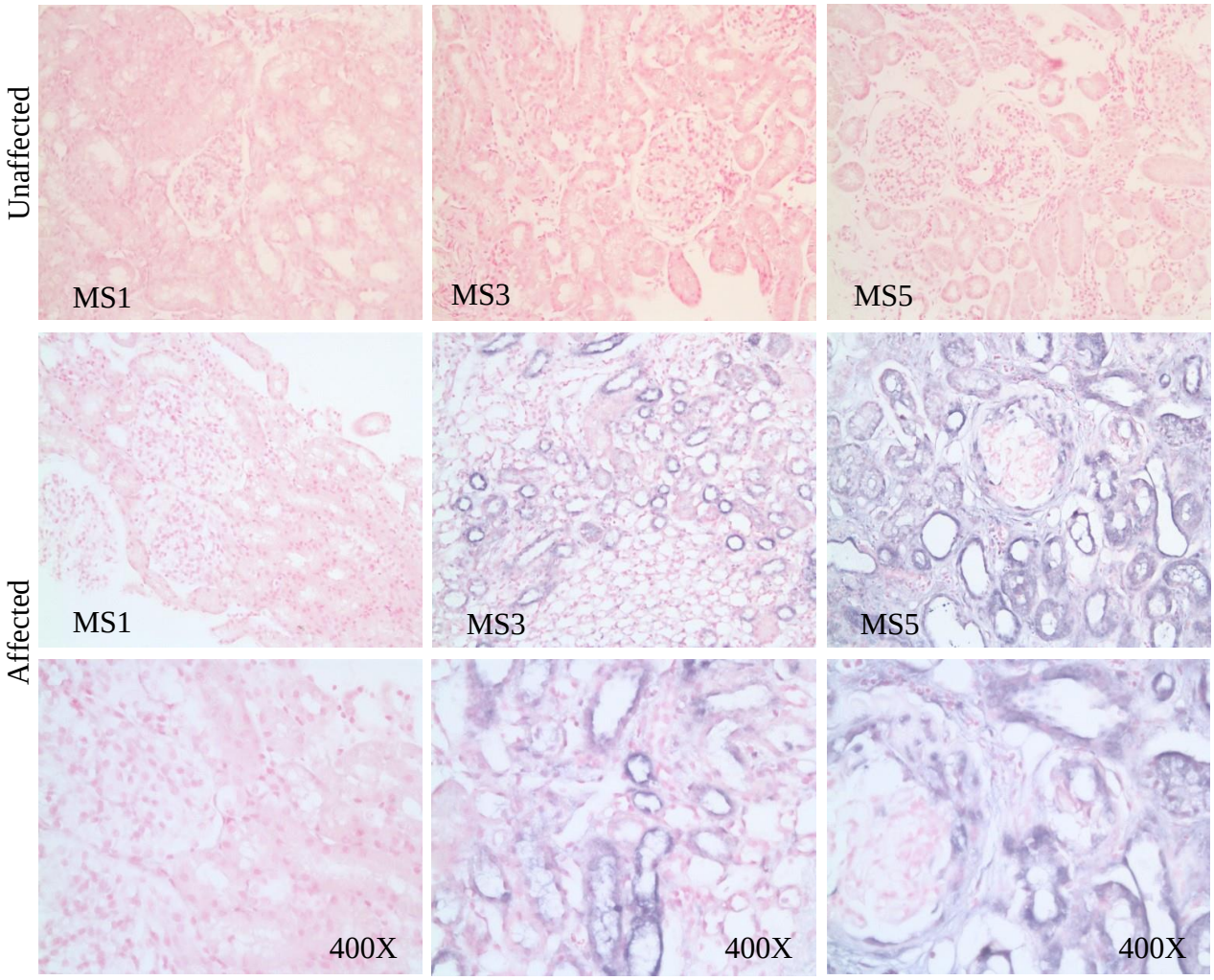

Figure 42 Representative images of kidney tissue collected by renal biopsy from unaffected dogs and dogs affected with XLHN stained by *in situ* hybridization for miR-21. Counterstained with nuclear fast red. Images taken at 200X with inset for affected dog taken at 400X.

Discussion

Our primary objective was to compare the expression of miR-21 in serially collected renal tissue from unaffected dogs to dogs affected with CKD caused by XLHN. Additionally, we sought to explore the association of dysregulated miR-21 expression with clinical and histopathologic changes and with the genes associated with miR-21 function in order to characterize their roles in the development of canine CKD. We found that miR-21 expression correlated with both the clinical parameters of renal function and histological changes, supporting our hypothesis that increased miR-21 expression plays a role in the pathogenesis of CKD. We were also able to characterize changes in relative mRNA expression of a number of genes associated with miR-21 function and/or CKD progression.

Over the course of disease, we determined that a significant increase in miR-21 expression in affected dogs, based on RT-qPCR occurred between milestone 2 and milestone 3, which corresponds with the first clear evidence of decreased GFR (based on sCr) and histologic changes (based on light microscopy). Expression further increased from milestone 4 to milestone 5. Additionally, expression of miR-21 in renal tubular cells using *in situ* hybridization increased with disease progression. These findings support the involvement of miR-21 in the progression of kidney disease, including development of interstitial fibrosis. In affected dogs, the presence of interstitial fibrosis can be detected as early as milestone 1 based on immunofluorescent staining with fibronectin, although the amount of fibrosis is minimal.[177] The lack of increased miR-21 expression in milestone 1 and 2 as compared with unaffected dogs may indicate that either initiation of fibrosis might be directed by other factors, not involving miR-21, or overall expression of miR-21 is not great enough to be detected as a significant difference in expression levels in these kidney tissue samples despite a potential impact on development of fibrosis.

During progression of disease, we expected that miR-21 would show a progressive increase with each milestone. The lack of evident increase between milestone 3 and 4 is partially because one of the affected dogs demonstrated much higher miR-21 expression compared to the other dogs at milestone 3, as presented in the Results. This dog developed more severe clinical signs, including gastrointestinal abnormalities, during the progression of his disease compared with other dogs at a similar sCr. He reached his clinical endpoint based on clinical signs rather than sCr. While the exact cause for these clinical abnormalities were not confirmed, either an additional acute kidney injury or a secondary chronic disease unrelated to the kidneys may have contributed to increased miR-21 expression despite lower interstitial fibrosis and chronic inflammation scores. Alternatively, the samples used for RNA evaluation, while harvested at the same time, are different biopsy cores than those that were used for histologic evaluation. Thus, it is possible to have a discrepancy between the two samples, particularly for patchy changes like tubulointerstitial lesions. When data were re-analyzed excluding this value, there appeared to be a small increase in miR-21 expression in milestone 4 as compared with milestone 3. However, statistical significance remained unchanged, likely in part due to the small number of dogs represented in each group.

The source of miR-21 in kidney tissue might also help to explain, at least in part, some of the lack of statistical difference between relative miR-21 expression between MS 3 and 4. A previous study using unilateral ureteral obstruction (UUO) as a model for inducing renal fibrosis in mice determined that enhanced expression of miR-21 originated primarily from tubular epithelial cells.[123] In the dogs, as disease worsens, functional kidney tissue is replaced by fibrosis, which results in fewer tubular epithelial cells to express miR-21. However, another study also using UUO as a model of fibrosis development in mice,

found that fibroblasts derived from the fibrotic kidney tissue had higher levels of miR-21 expression compared to control fibroblasts.[248] Additionally, TGF-β significantly induced expression of miR-21 in normal kidney fibroblasts.[248] The loss of normal renal tubular cells expressing miR-21 might be offset by increased production of miR-21 by fibroblasts, resulting in similar overall expression between MS3 and 4 in the dogs. Ultimately, there are likely multiple sources and factors that contribute to the production of miR-21 during progression of kidney disease that need to be further explored, and additional studies could be conducted to help gain a more in-depth perspective of the role of miR-21 in the various stages of disease development. For example, evaluation of kidney tissue and miR-21 expression at time points between MS2 and MS3 may help pinpoint a more precise time point of elevation in miR-21 expression, further defining its role in disease development.

The various genes involved in CKD progression and fibrosis have been previously explored in both mice and dogs with various causes of CKD including AS.[108,238,240,249,250] The involvement of TGF-β and its connection with miR-21 in the development of fibrosis is already well established, and elevated *TGFB* mRNA expression in kidney tissue, particularly at early milestones of disease, has previously been identified in dogs with XLHN.[108] TGF-β1 was also identified as the most activated upstream regulator when comparing dogs with rapid vs. slow disease progression.[250] Our study mirrors those findings. COL1α1 is a known component of fibrosis, and is indirectly increased by miR-21 through the TGF-β signaling pathway. Serpine1, the gene that encodes for plasminogen activator inhibitor-1, promotes fibrosis by inhibiting the activities of urokinase, tissue-type plasminogen activator, plasmin, and matrix metalloproteinases.[251] Additionally, plasminogen activator inhibitor-1 expression is induced by TGF-β through activation of the Smad pathway, and it has been shown to be specifically upregulated in the kidney in renal

disease but is essentially undetectable in the normal kidney.[252] Given this relationship, plasminogen activator inhibitor-1 is also indirectly increased by miR-21 through upregulation by the TGF-β signaling pathway. The often markedly increased expression of these genes in affected dogs at ESRD corresponds with collagen accumulation and fibrosis development.

In addition to being a pivotal player in fibrogenesis, miR-21 contributes to the development of disease by dysregulating a number of metabolic pathways in both the mitochondria and peroxisomes of glomerular and tubular epithelial cells. These findings have been demonstrated in mice with diabetic nephropathy, CKD using a doxycycline-inducible transgenic system, and in Alport mice using anti-miR-21 oligonucleotide therapy.[238,253-255] Tubular epithelial cells depend primarily on fatty acid oxidation (FAO) as a source of energy.[255] PPARα and PPARGC1A act together as key transcription factors to regulate expression of enzymes involved in FAO. In addition, PPARα has a number of important downstream effects, including stimulating healthy mitochondrial function, inhibiting NF-κB signaling to promote an anti-inflammatory environment, and inhibiting TGF-β signaling to diminish profibrotic responses.[238,256] *ACADM* is the gene that encodes for medium-chain acyl-CoA dehydrogenase, an enzyme that is also important for FAO. CPT1A is another enzyme that is essential for FAO by connecting carnitine to long-chain fatty acids so that they can cross the inner membrane of mitochondria and be metabolized. It is considered the rate limiting enzyme in FAO. Impaired fatty acid metabolism and detoxification contribute to kidney disease by reprograming tubular epithelial cells into a profibrotic phenotype and causing higher levels of apoptosis, de-differentiation, and increased intracellular lipid accumulation. FAO suppression is controlled through regulation of PPARα and PPARGC1A, which are directly regulated by both TGF-β1 and

miR-21 activity.[238,239,255] We identified decreased gene expression of *PPARA*, *PPARGC1A*, and *ACADM* in affected dogs compared to unaffected dogs, highlighting the potential importance of alterations in cellular metabolism, particularly FAO, in the advancement of kidney fibrosis in dogs with XLHN. Additionally, loss of renal tubular cells during disease progression might also contribute to lower expression of these metabolic-related genes. Further studies are needed to understand the role of FAO in disease progression and fibrosis development in the dog.

Generation of reactive oxygen species (ROS), particularly by kidney epithelial cells, stimulates additional inflammatory responses, which then contributes to further cell damage and fibrosis. In several mouse models of CKD, miR-21 was shown to control generation of ROS in the mitochondria by silencing key antioxidant enzymes, including MPV17 and SOD1.[238,239] Similarly, we found *SOD1* to be significantly decreased in affected dogs compared to unaffected counterparts, and this decreased expression could be contributing to the pathogenesis of disease in affected dogs through ROS-mediated damage. In contrast, *MPV17* did not show significant change between the two groups.

In human kidney tissue, *in situ* hybridization has been used to confirm that synthesis of EGF occurs primarily in the tubular compartments, particularly the thick ascending limb of the loop of Henle and the distal tubules.[257,258] In both acute and chronic kidney disease, EGF has been shown to play a role in regulating cell proliferation and tissue repair response after tubulointerstitial damage.[258-261] Moreover, *EGF* gene expression has been shown to be reduced in CKD.[257,262] Based on the markedly decreased levels of expression of *EGF* at ESRD in affected dogs, our findings support that the reduction of *EGF* reflects damage and loss of renal tubular cells as fibrosis ensues. The dysregulation of the EGFR pathway in mediating renal fibrosis in CKD has already been

established and is in part due to increased expression of TGF-β.[263,264] Given the connection between miR-21 and TGF-β, one can surmise that changes in miR-21 expression may also influence *EGF* expression, however, to the authors' knowledge, a direct correlation has not yet been established.

Our findings are overall concordant with those identified in homogenized kidney from Col4a3$^{-/-}$ Alport mice, whereby expression of miR-21 increased with disease progression.[238] However, in Alport mice, upregulation of miR-21 preceded morphologic changes in tissue on light microscopy, with a 2-fold elevation observed prior to histologic changes.[238] There are several possible reasons for this discrepancy. First, in the dogs, kidney biopsies were collected for evaluation, while in the mice, whole kidney tissue was used. This procedural difference may have resulted in larger variation in both histologic evaluation and miR-21 expression within the canine samples, leading to decreased sensitivity. Second, biopsy samples in the dogs were taken at time points that were based on clinical testing, whereas mice were sampled at predetermined ages in weekly increments up to the point of minor histological changes. Therefore, while the first two kidney biopsies in the dog were taken at the point of mild to moderate dysfunction of the glomerular basement membrane (i.e., microalbuminuria and overt proteinuria), changes resulting in increased miR-21 expression and histologic changes evident by light microscopy appear to have occurred between the onset of overt proteinuria and the onset of azotemia. Certainly, the time frame between milestone 2 and milestone 3 is relatively large (average of 8 weeks), with a vast number of molecular changes occurring between these two times. This may help to explain, at least partially, the marked increase in renal miR-21 from MS2 to MS3. As previously mentioned, evaluation of kidney tissue at time points between MS2 and MS3 could help detect molecular changes that occur prior to substantial

histologic changes in the affected dogs. Lastly, there could be differences in the molecular mechanism of disease occurring in the kidney tissue between the dogs and mice. Therefore, the mechanistic role of miR-21 in the development of fibrosis in canine kidney tissue still needs to be proven.

One prior study evaluated differences in miRNA expression levels based on RT-qPCR between healthy dogs and dogs with kidney disease.[203] In this study, miR-21a was increased in the tubulointerstitium but not the glomeruli, as we observed based on *in situ* hybridization. Also, similar to our study, higher levels correlated with abnormal histopathologic findings. Additionally, urinary exosome-derived miR-21 significantly increased with renal dysfunction. While that study provided insight into miRNA levels in dogs with kidney disease, the dogs were already azotemic with obvious renal lesions identified on light microscopy evaluation of autopsy tissue, and only one time point was evaluated. Additionally, the cause of CKD was not considered, and the dogs used in both groups for the comparison of miR-21 expression varied in age. In our study, the cause of CKD and progression of the disease is known and well characterized by longitudinal sampling done at the level of the individual over the entire course of disease. Therefore, serial evaluation of miR-21 expression from early disease through ESRD was possible, providing a more comprehensive analysis of miR-21 expression during advancement of disease. For instance, this experimental design allowed examination of the temporal relationship between changes in miR-21 expression and development of changes in the kidney during disease progression. In turn, this temporal relationship can help to establish a causal effect between miR-21 expression and progression of disease. This, in addition to the comparison with unaffected age-matched littermates, allows for increased confidence

in corroborating that changes observed in miR-21 expression can be contributed to CKD and not from varying physiological states due to extra-renal disease or age.

This study is relevant to understanding the pathogenesis of AS. The progression of canine XLHN parallels the progression of disease in human AS patients. To our knowledge, this study is the first to demonstrate increased renal miR-21 expression in a model of AS other than mice. Our findings provide more confidence in the pathological role of dysregulated miR-21 expression in Alport syndrome across species.

In both animals and humans, CKD is a prevalent, yet insidious disease. Because of the limitations of traditional diagnostic tools, CKD is often diagnosed only after significant damage to the kidneys has occurred. Moreover, while traditional biomarkers like sCr can provide an estimate of GFR and changes in kidney function during disease progression, evaluation of kidney tissue is the gold standard for determining the extent of renal damage. Irrespective of etiology, renal fibrosis is a key characteristic finding in CKD and has been shown to best correlate with renal function.[232,265] Given the correlation of miR-21 with both clinical markers and pathologic abnormalities, as identified in this study, miR-21 may be a promising biomarker for monitoring disease progression as it relates to fibrosis development. Additionally, because of their stability in bodily fluids, mature circulating miRNAs are good candidates for non-invasive biomarkers as compared to techniques such as renal biopsy.[266,267] Evaluation of miR-21 in serum and urine of dogs with XLHN along with comparison of these values to conventional clinical and histological evidence of disease can provide additional insight regarding the use of miR-21 as a non-invasive biomarker for evaluating progression of CKD and, therefore, should be explored. Furthermore, an understanding of the role of miR-21 in CKD development can provide a basis for the generation of novel therapeutic options. For example, based on observations

in Alport mice, a single-stranded, chemically modified oligonucleotide (RG-012) that binds to and inhibits the function of miR-21 is being developed for treatment of AS in humans.[268]

In conclusion, we found that miR-21 is upregulated in the kidneys of dogs with CKD caused by XLHN. Increased expression of miR-21 might play an important pathologic role in the progression of the XLHN by dysregulating multiple pathways. To gain a better understanding of the role of miR-21 in the pathogenesis of CKD, further evaluation of miR-21 expression in dogs with CKD due to a variety of causes is warranted.

CHAPTER VI CONCLUSION AND FUTURE DIRECTIONS

CKD is a complex disease and a significant cause of illness and death in dogs. While major advancements in veterinary nephrology have been made over the past few decades, there is still much to learn about the disease. The nephron is the essential structural unit of the kidney, and each of the segments are closely linked to create an independent functional unit. Given that CKD commonly originates from dysfunction within the glomerulus, it is reasonable to place emphasis on exploring the molecular mechanisms of disease here. We know that the glomerulus contains unique cells including fenestrated endothelial cells, podocytes, and mesangial cells, that are intimately connected in a complex network involving ligands, integrins, and cytoskeletal components that allow cells to communicate and engage in multidirectional crosstalk. This network functions in an interdependent unit in order to maintain normal homeostasis and filtration under dynamic conditions, such as biomechanical strain that occurs in the kidney. Because of this connection, it is imperative to understand how these cells communicate with one another through this network as modifications in any one cell can initiate a cascade of interactions that generates abnormalities in the other cells and serves as a key component in the pathogenesis of disease. Additionally, changes in normal cellular pathways often lead to aberrant expression of signaling molecules, which are either up-regulated or down-regulated. Due to the rapid, progressive, and well-characterized nature of the disease, dogs with XLHN serve as a good model for the study of CKD development in both veterinary and human medicine. Pathologic evaluation (particularly by the use of renal biopsy) of kidney tissue is considered the gold standard for identifying the type and severity of damage occurring in the kidney. Understanding the pathogenesis of this damage establishes a foundation from which we can explore biomarkers and will allow for the development of minimally

invasive diagnostic tools that can aid in earlier detection and improved monitoring of dogs with CKD. Given that urine is easy to obtain using minimally invasive techniques and is the byproduct of the kidney, it is an attractive diagnostic sample to use for identifying biomarkers of CKD.

In exploring molecular mechanisms of disease development, we were able to provide support that similar initiating events are occurring in canine XLHN as in both Alport mice. The working theory is that the abnormal deposition of laminin 211 activates mesangial filopodia which invade the GBM and lead to destruction of the GBM and disease progression through the activation of an inflammatory cascade. Given the similarities observed in mice and dogs with this disease, it is reasonable to surmise that similar processes are occurring in humans with AS. This data also provides affirmation for the use of the dog as a large animal model of AS in humans.

Expanding on these findings, we were able to establish that ET-1 production occurs in glomerular cells, most likely endothelial cells. In AS mice, under biomechanical strain due to an abnormal composition of the mature GBM, subsequent ET-1 binding to ET_AR on mesangial cells is a likely initiating event in the development of disease. In mice, ET_AR blockage delays Alport glomerular disease initiation and ameliorates the development of interstitial fibrosis, a key characteristic of CKD. Given the production of ET-1 by canine glomerular cells and the presence of ET_AR on mesangial cells, is it possible that a similar initiating process is occurring in dogs with XLHN. To further support this pathway in dogs, additional studies to establish an antibody marker for detection of endothelial cells in canine kidney tissue is needed in order to verify that ET-1 is indeed originating from glomerular endothelial cells. In addition to confirming its expression in canine kidney tissue, we also found that ET-1 levels are increased in urine early in the disease process,

specifically at MS2. This is significant in that, excluding UPC, traditional biomarkers, such as sCr or alterations in GFR, do not provide evidence for alterations in kidney function until later in the disease process, when substantial damage to the kidney has already occurred. Unfortunately, the ELISA used for this project is no longer available. Therefore, validation of additional assays to be used for future measurement of ET-1 levels in urine is needed to observe whether, if after optimizing the detection method and using a larger cohort of dogs, ET-1 may be detectable even sooner than an increased in UPC, thus proving it useful as a marker of XLHN and potentially, AS.

In addition to evaluating the molecular cascade of disease pathogenesis, the discovery of miRNAs has opened a new avenue for understanding the regulatory networks controlling gene expression and protein production in biological processes. Because of their vital role in a number of cellular processes, it is rational to elucidate pathogenesis of disease development through exploration of altered miRNA expression profiles. This may also lead to the discovery of novel therapeutic targets for early disease intervention for dogs with CKD. In this work, we identified endogenous reference miRNAs in urine to use for normalization of expression of miRNAs of interest. We found that let-7e, miR-21, miR-142, miR-378, miR-486, and miR-8890may be involved in disease pathogenesis and are promising biomarkers for either detection of CKD and/or for use to monitor disease development. Next steps should include further validation of the use of these miRNAs in a larger cohort of dogs in addition to correlating their expression with clinical and histological changes to determine their use as non-invasive biomarkers either independently or in a supportive function. Additionally, these microRNAs should be evaluated in dogs with CKD due to other etiologies, with the goal of generating a diagnostic panel of biomarkers for CKD diagnosis and progression.

Regardless of the inciting cause, the development of CKD shares many common histological findings including interstitial fibrosis and inflammation, peritubular capillary loss resulting in tissue hypoxia, and tubular atrophy. These finding worsens with disease progression, as shown in dogs with XLHN through the evaluation of serially obtained kidney biopsies at different milestones of disease development. miR-21 has been associated with fibrosis in a number of organs. We observed that expression of miR-21 had a significant correlation with clinical and histological parameters including UPC, sCr, GFR, glomerular and tubular damage, chronic inflammation, and interstitial fibrosis. We also establish alterations in mRNA expression of a number of proteins known to be associated with development of renal fibrosis either through direct connection to miR-21 or through alterations in important protective mechanisms. Additionally, through the use of *in situ* hybridization, we observed that miR-21 expression in kidney tissue appeared to be most prominent in the renal proximal tubular cells and diffusely increased in expression throughout the tissue as disease worsened. In conjunction with findings of increased expression of miR-21 in the urine of dogs with XLHN as disease progresses, it is reasonable to surmise that monitoring changes in miR-21 expression in urine may be useful as a non-invasive diagnostic tool for monitoring disease progression. Additional studies are needed in a larger sample size of dogs to validate these findings.

The research presented here advances the understanding of some of the mechanisms involved in both the development and progression of CKD in dogs due to XLHN, focusing primarily on the molecular changes associated with disease pathogenesis. Either through signal ligands, such as ET-1, or through regulation of gene and protein expression by the use of miRNAs, these methods of cellular communication and multidirectional crosstalk cause alterations in cell morphology which ultimately leads to the development of CKD. While

additional studies are needed; this material provides a framework in the areas that seem most promising for further exploration involving other etiologies of CKD. Given the clinical challenges with CKD, the establishment of biomarkers for both earlier detection and monitoring of disease is crucial. Furthermore, this information can lead to production of potential therapeutic agents with the goal of improving and extending the overall quality of life of dogs with CKD.

REFERENCES

1. National Kidney F. K/DOQI clinical practice guidelines for chronic kidney disease: evaluation, classification, and stratification. American journal of kidney diseases: the official journal of the National Kidney Foundation 2002; 39:S1-266.

2. Brown S. Introduction from the international renal interest society. Journal of veterinary internal medicine / American College of Veterinary Internal Medicine 2013; 27 Suppl 1:S1.

3. Cianciolo RE, Brown CA, Mohr FC, et al. Pathologic evaluation of canine renal biopsies: methods for identifying features that differentiate immune-mediated glomerulonephritis from other categories of glomerular diseases. Journal of veterinary internal medicine / American College of Veterinary Internal Medicine 2013; 27 Suppl 1:S10-18.

4. Polzin DJ. Chronic kidney disease in small animals. Vet Clin North Am Small Anim Pract 2011; 41:15-30.

5. Braun JP, Lefebvre HP, Watson AD. Creatinine in the dog: a review. Veterinary clinical pathology / American Society for Veterinary Clinical Pathology 2003; 32:162-179.

6. Chapter 1: Definition and classification of CKD. Kidney Int Suppl (2011) 2013; 3:19-62.

7. Subgroup ICGSGST, Brown S, Elliott J, et al. Consensus recommendations for standard therapy of glomerular disease in dogs. Journal of veterinary internal medicine / American College of Veterinary Internal Medicine 2013; 27 Suppl 1:S27-43.

8. Vaden SL. Glomerular disease. Top Companion Anim Med 2011; 26:128-134.

9. Yhee JY, Yu CH, Kim JH, et al. Histopathological retrospective study of canine renal disease in Korea, 2003~2008. J Vet Sci 2010; 11:277-283.

10. Lopez-Novoa JM, Rodriguez-Pena AB, Ortiz A, et al. Etiopathology of chronic tubular, glomerular and renovascular nephropathies: clinical implications. J Transl Med 2011; 9:13.

11. Lees GE. Congenital kidney diseases. Oxford: Blackwell Science Publ; 2011; 568-576.

12. Eisenbrandt DL, Phemister RD. Postnatal development of the canine kidney: quantitative and qualitative morphology. Am J Anat 1979; 154:179-193.

13. Seely JC. A brief review of kidney development, maturation, developmental abnormalities, and drug toxicity: juvenile animal relevancy. J Toxicol Pathol 2017; 30:125- 133.

14. Macdougall DF, Cook T, Steward AP, et al. Canine chronic renal disease: prevalence and types of glomerulonephritis in the dog. Kidney international 1986; 29:1144-1151.

15. Cianciolo RE, Mohr FC, Aresu L, et al. World Small Animal Veterinary Association Renal Pathology Initiative: Classification of Glomerular Diseases in Dogs. Vet Pathol 2016; 53:113-135.

16. Zhuo JL, Li XC. Proximal nephron. Compr Physiol 2013; 3:1079-1123.

17. Cianciolo RE, Benali SL, Aresu L. Aging in the Canine Kidney. Vet Pathol 2016; 53:299-308.

18. Bulger RE, Cronin RE, Dobyan DC. Survey of the morphology of the dog kidney. Anat Rec 1979; 194:41-65.

19. Kitching AR, Hutton HL. The Players: Cells Involved in Glomerular Disease. Clin J Am Soc Nephrol 2016; 11:1664-1674.

20. Friden V, Oveland E, Tenstad O, et al. The glomerular endothelial cell coat is essential for glomerular filtration. Kidney international 2011; 79:1322-1330.

21. Haraldsson B, Nystrom J, Deen WM. Properties of the glomerular barrier and mechanisms of proteinuria. Physiol Rev 2008; 88:451-487.

22. Schlondorff D, Banas B. The mesangial cell revisited: no cell is an island. Journal of the American Society of Nephrology: JASN 2009; 20:1179-1187.

23. Welsh GI, Saleem MA. The podocyte cytoskeleton--key to a functioning glomerulus in health and disease. Nature reviews Nephrology 2011; 8:14-21.

24. Reiser J, Altintas MM. Podocytes. F1000Res 2016; 5.

25. Mathieson PW. The podocyte cytoskeleton in health and in disease. Clin Kidney J 2012; 5:498-501.

26. Garg P. A Review of Podocyte Biology. Am J Nephrol 2018; 47 Suppl 1:3-13.

27. Lennon R, Randles MJ, Humphries MJ. The importance of podocyte adhesion for a healthy glomerulus. Front Endocrinol (Lausanne) 2014; 5:160.

28. Grahammer F, Schell C, Huber TB. The podocyte slit diaphragm--from a thin grey line to a complex signaling hub. Nature reviews Nephrology 2013; 9:587-598.

29. Sachs N, Sonnenberg A. Cell-matrix adhesion of podocytes in physiology and disease. Nature reviews Nephrology 2013; 9:200-210.

30. Giancotti FG, Ruoslahti E. Integrin signaling. Science 1999; 285:1028-1032.

31. Machuca E, Benoit G, Antignac C. Genetics of nephrotic syndrome: connecting molecular genetics to podocyte physiology. Hum Mol Genet 2009; 18:R185-194.

32. Satchell SC, Braet F. Glomerular endothelial cell fenestrations: an integral component of the glomerular filtration barrier. Am J Physiol Renal Physiol 2009; 296:F947-956.

33. Ballermann BJ. Glomerular endothelial cell differentiation. Kidney international 2005; 67:1668-1671.

34. Dane MJ, van den Berg BM, Avramut MC, et al. Glomerular endothelial surface layer acts as a barrier against albumin filtration. The American journal of pathology 2013; 182:1532-1540.

35. Fu J, Lee K, Chuang PY, et al. Glomerular endothelial cell injury and cross talk in diabetic kidney disease. Am J Physiol Renal Physiol 2015; 308:F287-297.

36. Heeringa P, Steenbergen E, van Goor H. A protective role for endothelial nitric oxide synthase in glomerulonephritis. Kidney international 2002; 61:822-825.

37. Zhao HJ, Wang S, Cheng H, et al. Endothelial nitric oxide synthase deficiency produces accelerated nephropathy in diabetic mice. Journal of the American Society of Nephrology: JASN 2006; 17:2664-2669.

38. Sun YB, Qu X, Zhang X, et al. Glomerular endothelial cell injury and damage precedes that of podocytes in adriamycin-induced nephropathy. PloS one 2013; 8:e55027.

39. Vaughan MR, Quaggin SE. How do mesangial and endothelial cells form the glomerular tuft? Journal of the American Society of Nephrology: JASN 2008; 19:24-33.

40. Lowe JS, Anderson PG. Chapter 15 - Urinary System. In: Lowe JS, Anderson PG, eds. Stevens & Lowe's Human Histology (Fourth Edition). Philadelphia: Mosby; 2015:286-318.

41. Miner JH. Renal basement membrane components. Kidney international 1999; 56:2016-2024.

42. Lennon R, Byron A, Humphries JD, et al. Global analysis reveals the complexity of the human glomerular extracellular matrix. Journal of the American Society of Nephrology: JASN 2014; 25:939-951.

43. Marek I, Volkert G, Hilgers KF, et al. Fibrillin-1 and alpha8 integrin are co-expressed in the glomerulus and interact to convey adhesion of mesangial cells. Cell adhesion & migration 2014; 8:389-395.

44. Marek I, Becker R, Fahlbusch FB, et al. Expression of the Alpha8 Integrin Chain Facilitates Phagocytosis by Renal Mesangial Cells. Cell Physiol Biochem 2018; 45:2161- 2173.

45. Kriz W, Elger M, Mundel P, et al. Structure-stabilizing forces in the glomerular tuft. Journal of the American Society of Nephrology: JASN 1995; 5:1731-1739.

46. Scindia YM, Deshmukh US, Bagavant H. Mesangial pathology in glomerular disease: targets for therapeutic intervention. Adv Drug Deliv Rev 2010; 62:1337-1343.

47. Hughes J, Liu Y, Van Damme J, et al. Human glomerular mesangial cell phagocytosis of apoptotic neutrophils: mediation by a novel CD36-independent vitronectin receptor/thrombospondin recognition mechanism that is uncoupled from chemokine secretion. J Immunol 1997; 158:4389-4397.

48. Sakai T, Kriz W. The structural relationship between mesangial cells and basement membrane of the renal glomerulus. Anat Embryol (Berl) 1987; 176:373-386.

49. Suh JH, Miner JH. The glomerular basement membrane as a barrier to albumin. Nature reviews Nephrology 2013; 9:470-477.

50. Cove-Smith A, Hendry BM. The regulation of mesangial cell proliferation. Nephron Exp Nephrol 2008; 108:e74-79.

51. Yasuda T, Kondo S, Homma T, et al. Regulation of extracellular matrix by mechanical stress in rat glomerular mesangial cells. J Clin Invest 1996; 98:1991-2000.

52. Shankland SJ, Smeets B, Pippin JW, et al. The emergence of the glomerular parietal epithelial cell. Nature reviews Nephrology 2014; 10:158-173.

53. Le Hir M, Besse-Eschmann V. A novel mechanism of nephron loss in a murine model of crescentic glomerulonephritis. Kidney international 2003; 63:591-599.

54. Appel D, Kershaw DB, Smeets B, et al. Recruitment of podocytes from glomerular parietal epithelial cells. Journal of the American Society of Nephrology: JASN 2009; 20:333-343.

55. Chang AM, Ohse T, Krofft RD, et al. Albumin-induced apoptosis of glomerular parietal epithelial cells is modulated by extracellular signal-regulated kinase 1/2. Nephrology, dialysis, transplantation: official publication of the European Dialysis and Transplant Association - European Renal Association 2012; 27:1330-1343.

56. Ohse T, Chang AM, Pippin JW, et al. A new function for parietal epithelial cells: a second glomerular barrier. Am J Physiol Renal Physiol 2009; 297:F1566-1574.

57. Miner JH. The glomerular basement membrane. Experimental cell research 2012; 318:973-978.

58. Hynes RO. The extracellular matrix: not just pretty fibrils. Science 2009; 326:1216- 1219.

59. Hynes RO, Naba A. Overview of the matrisome--an inventory of extracellular matrix constituents and functions. Cold Spring Harb Perspect Biol 2012; 4:a004903.

60. Miner JH. Developmental biology of glomerular basement membrane components. Current opinion in nephrology and hypertension 1998; 7:13-19.

61. Pozzi A, Zent R. Integrins in kidney disease. Journal of the American Society of Nephrology: JASN 2013; 24:1034-1039.

62. Kagami S, Kondo S. Beta1-integrins and glomerular injury. J Med Invest 2004; 51:1- 13.

63. Chen X, Moeckel G, Morrow JD, et al. Lack of integrin alpha1beta1 leads to severe glomerulosclerosis after glomerular injury. The American journal of pathology 2004; 165:617-630.

64. Kagami S, Kondo S, Loster K, et al. Alpha1beta1 integrin-mediated collagen matrix remodeling by rat mesangial cells is differentially regulated by transforming growth factor-beta and platelet-derived growth factor-BB. Journal of the American Society of Nephrology: JASN 1999; 10:779-789.

65. Kreidberg JA, Symons JM. Integrins in kidney development, function, and disease. Am J Physiol Renal Physiol 2000; 279:F233-242.

66. McKee KK, Harrison D, Capizzi S, et al. Role of laminin terminal globular domains in basement membrane assembly. The Journal of biological chemistry 2007; 282:21437-21447.

67. Colognato H, Yurchenco PD. Form and function: the laminin family of heterotrimers. Dev Dyn 2000; 218:213-234.

68. Yurchenco PD, O'Rear JJ. Basal lamina assembly. Curr Opin Cell Biol 1994; 6:674- 681.

69. Schymeinsky J, Nedbal S, Miosge N, et al. Gene structure and functional analysis of the mouse nidogen-2 gene: nidogen-2 is not essential for basement membrane formation in mice. Mol Cell Biol 2002; 22:6820-6830.

70. Groffen AJ, Ruegg MA, Dijkman H, et al. Agrin is a major heparan sulfate proteoglycan in the human glomerular basement membrane. The journal of histochemistry and cytochemistry: official journal of the Histochemistry Society 1998; 46:19-27.

71. Bezakova G, Ruegg MA. New insights into the roles of agrin. Nat Rev Mol Cell Biol 2003; 4:295-308.

72. Zeisberg M, Kalluri R. Physiology of the Renal Interstitium. Clin J Am Soc Nephrol 2015; 10:1831-1840.

73. Hodgkins KS, Schnaper HW. Tubulointerstitial injury and the progression of chronic kidney disease. Pediatr Nephrol 2012; 27:901-909.

74. Lemley KV, Kriz W. Anatomy of the renal interstitium. Kidney international 1991; 39:370-381.

75. Lote CJ. Applied physiology: the renal tubule. Current Paediatrics 2001; 11:207-201.

76. Stockham SL, Scott MA. Urinary System. In: Fundamentals of Veterinary Clinical Pathology, Second ed. Ames, Iowa: Blackwell Publishing; 2008:415-494.

77. Brandt LE, Bohn AA, Charles JB, et al. Localization of canine, feline, and mouse renal membrane proteins. Vet Pathol 2012; 49:693-703.

78. Nielsen R, Christensen EI, Birn H. Megalin and cubilin in proximal tubule protein reabsorption: from experimental models to human disease. Kidney international 2016; 89:58-67.

79. Tojo A, Kinugasa S. Mechanisms of glomerular albumin filtration and tubular reabsorption. Int J Nephrol 2012; 2012:481520.

80. Sun J, Hultenby K, Axelsson J, et al. Proximal Tubular Expression Patterns of Megalin and Cubilin in Proteinuric Nephropathies. Kidney Int Rep 2017; 2:721-732.

81. Mount DB. Thick ascending limb of the loop of Henle. Clin J Am Soc Nephrol 2014; 9:1974-1986.

82. Imai M, Taniguchi J, Tabei K. Function of thin loops of Henle. Kidney international 1987; 31:565-579.

83. Tokonami N, Takata T, Beyeler J, et al. Uromodulin is expressed in the distal convoluted tubule, where it is critical for regulation of the sodium chloride cotransporter NCC. Kidney international 2018.

84. Devuyst O, Olinger E, Rampoldi L. Uromodulin: from physiology to rare and complex kidney disorders. Nature reviews Nephrology 2017; 13:525-544.

85. Prajczer S, Heidenreich U, Pfaller W, et al. Evidence for a role of uromodulin in chronic kidney disease progression. Nephrology, dialysis, transplantation: official publication of the European Dialysis and Transplant Association - European Renal Association 2010; 25:1896-1903.

86. Bell PD, Lapointe JY, Peti-Peterdi J. Macula densa cell signaling. Annu Rev Physiol 2003; 65:481-500.

87. Subramanya AR, Ellison DH. Distal convoluted tubule. Clin J Am Soc Nephrol 2014; 9:2147-2163.

88. Lee CT, Ng HY, Lee YT, et al. The role of calbindin-D28k on renal calcium and magnesium handling during treatment with loop and thiazide diuretics. Am J Physiol Renal Physiol 2016; 310:F230-236.

89. Pearce D, Soundararajan R, Trimpert C, et al. Collecting duct principal cell transport processes and their regulation. Clin J Am Soc Nephrol 2015; 10:135-146.

90. Roy A, Al-Bataineh MM, Pastor-Soler NM. Collecting duct intercalated cell function and regulation. Clin J Am Soc Nephrol 2015; 10:305-324.

91. Gabbard W, Milbrandt EB, Kellum JA. NGAL: an emerging tool for predicting severity of AKI is easily detected by a clinical assay. Crit Care 2010; 14:318.

92. Eddy AA, Neilson EG. Chronic kidney disease progression. Journal of the American Society of Nephrology: JASN 2006; 17:2964-2966.

93. Gewin L, Zent R, Pozzi A. Progression of chronic kidney disease: too much cellular talk causes damage. Kidney international 2017; 91:552-560.

94. Cosgrove D, Liu S. Collagen IV diseases: A focus on the glomerular basement membrane in Alport syndrome. Matrix Biol 2017; 57-58:45-54.

95. Savige J. Alport syndrome: its effects on the glomerular filtration barrier and implications for future treatment. J Physiol 2014; 592:4013-4023.

96. Miner JH, Baigent C, Flinter F, et al. The 2014International Workshop on Alport Syndrome. Kidney international 2014; 86:679-684.

97. Kashtan CE. Alport syndrome. An inherited disorder of renal, ocular, and cochlear basement membranes. Medicine 1999; 78:338-360.

98. Pescucci C, Mari F, Longo I, et al. Autosomal-dominant Alport syndrome: natural history of a disease due to COL4A3 or COL4A4 gene. Kidney international 2004; 65:1598- 1603.

99. Fallerini C, Dosa L, Tita R, et al. Unbiased next generation sequencing analysis confirms the existence of autosomal dominant Alport syndrome in a relevant fraction of cases. Clin Genet 2014; 86:252-257.

100. van der Loop FT, Heidet L, Timmer ED, et al. Autosomal dominant Alport syndrome caused by a COL4A3 splice site mutation. Kidney international 2000; 58:1870-1875.

101. Longo I, Porcedda P, Mari F, et al. COL4A3/COL4A4 mutations: from familial hematuria to autosomal-dominant or recessive Alport syndrome. Kidney international 2002; 61:1947-1956.

102. Lees GE, Helman RG, Kashtan CE, et al. New form of X-linked dominant hereditary nephritis in dogs. Am J Vet Res 1999; 60:373-383.

103. Kashtan CE. Animal models of Alport syndrome. Nephrology, dialysis, transplantation: official publication of the European Dialysis and Transplant Association - European Renal Association 2002; 17:1359-1362.

104. Lees GE, Cianciolo RE, Clubb FJ, Jr. Renal biopsy and pathologic evaluation of glomerular disease. Top Companion Anim Med 2011; 26:143-153.

105. Lees GE. Kidney diseases caused by glomerular basement membrane type IV collagen defects in dogs. Journal of veterinary emergency and critical care 2013; 23:184- 193.

106. Khan Z, Pandey M. Role of kidney biomarkers of chronic kidney disease: An update. Saudi J Biol Sci 2014; 21:294-299.

107. Lennon R, Hosawi S. Glomerular cell crosstalk. Current opinion in nephrology and hypertension 2016; 25:187-193.

108. Benali SL, Lees GE, Nabity MB, et al. X-Linked Hereditary Nephropathy in Navasota Dogs: Clinical Pathology, Morphology, and Gene Expression during Disease Progression. Vet Pathol 2016; 53:803-812.

109. Bartel DP. MicroRNAs: genomics, biogenesis, mechanism, and function. Cell 2004; 116:281-297.

110. Sohel M. Extracellular/Circulating MicroRNAs: Release Mechanisms, Functions and Challenges. Achievements in the Life Sciences 2016; 10:175-186.

111. Ichii O, Horino T. MicroRNAs associated with the development of kidney diseases in humans and animals. J Toxicol Pathol 2018; 31:23-34.

112. Winter J, Jung S, Keller S, et al. Many roads to maturity: microRNA biogenesis pathways and their regulation. Nat Cell Biol 2009; 11:228-234.

113. Slezak-Prochazka I, Durmus S, Kroesen BJ, et al. MicroRNAs, macrocontrol: regulation of miRNA processing. RNA 2010; 16:1087-1095.

114. Bhaskaran M, Mohan M. MicroRNAs: history, biogenesis, and their evolving role in animal development and disease. Vet Pathol 2014; 51:759-774.

115. Ha M, Kim VN. Regulation of microRNA biogenesis. Nat Rev Mol Cell Biol 2014; 15:509-524.

116. Wulff BE, Nishikura K. Modulation of microRNA expression and function by ADARs. Curr Top Microbiol Immunol 2012; 353:91-109.

117. Chen X, Ba Y, Ma L, et al. Characterization of microRNAs in serum: a novel class of biomarkers for diagnosis of cancer and other diseases. Cell Res 2008; 18:997-1006.

118. Gilad S, Meiri E, Yogev Y, et al. Serum microRNAs are promising novel biomarkers. PloS one 2008; 3:e3148.

119. Szeto CC, Ching-Ha KB, Ka-Bik L, et al. Micro-RNA expression in the urinary sediment of patients with chronic kidney diseases. Dis Markers 2012; 33:137-144.

120. Alvarez ML, Khosroheidari M, Kanchi Ravi R, et al. Comparison of protein, microRNA, and mRNA yields using different methods of urinary exosome isolation for the discovery of kidney disease biomarkers. Kidney international 2012; 82:1024-1032.

121. Patel V, Noureddine L. MicroRNAs and fibrosis. Current opinion in nephrology and hypertension 2012; 21:410-416.

122. Chung AC, Lan HY. MicroRNAs in renal fibrosis. Front Physiol 2015; 6:50.

123. Zarjou A, Yang S, Abraham E, et al. Identification of a microRNA signature in renal fibrosis: role of miR-21. Am J Physiol Renal Physiol 2011; 301:F793-801.

124. Trionfini P, Benigni A, Remuzzi G. MicroRNAs in kidney physiology and disease. Nature reviews Nephrology 2015; 11:23-33.

125. Neal CS, Michael MZ, Pimlott LK, et al. Circulating microRNA expression is reduced in chronic kidney disease. Nephrology, dialysis, transplantation: official publication of the European Dialysis and Transplant Association - European Renal Association 2011; 26:3794-3802.

126. Poschl E, Schlotzer-Schrehardt U, Brachvogel B, et al. Collagen IV is essential for basement membrane stability but dispensable for initiation of its assembly during early development. Development 2004; 131:1619-1628.

127. Abrahamson DR, Hudson BG, Stroganova L, et al. Cellular origins of type IV collagen networks in developing glomeruli. Journal of the American Society of Nephrology: JASN 2009; 20:1471-1479.

128. Thorner PS. Alport syndrome and thin basement membrane nephropathy. Nephron Clinical practice 2007; 106:c82-88.

129. Noone D, Licht C. An update on the pathomechanisms and future therapies of Alport syndrome. Pediatric Nephrology 2013; 28:1025-1036.

130. Dufek B, Meehan DT, Delimont D, et al. Endothelin A receptor activation on mesangial cells initiates Alport glomerular disease. Kidney international 2016.

131. Hohenester E, Yurchenco PD. Laminins in basement membrane assembly. Cell adhesion & migration 2013; 7:56-63.

132. Rheault MN, Kren SM, Thielen BK, et al. Mouse model of X-linked Alport syndrome. Journal of the American Society of Nephrology: JASN 2004; 15:1466-1474.

133. Cox ML, Lees GE, Kashtan CE, et al. Genetic cause of X-linked Alport syndrome in a family of domestic dogs. Mammalian genome: official journal of the International Mammalian Genome Society 2003; 14:396-403.

134. Cosgrove D, Meehan DT, Grunkemeyer JA, et al. Collagen COL4A3 knockout: a mouse model for autosomal Alport syndrome. Genes & development 1996; 10:2981-2992.

135. Miner JH, Sanes JR. Molecular and functional defects in kidneys of mice lacking collagen alpha 3(IV): implications for Alport syndrome. The Journal of cell biology 1996; 135:1403-1413.

136. Cosgrove D. Glomerular pathology in Alport syndrome: A molecular perspective. Pediatric Nephrology 2012; 27:885-890.

137. Gunwar S, Ballester F, Noelken ME, et al. Glomerular basement membrane. Identification of a novel disulfide-cross-linked network of alpha3, alpha4, and alpha5 chains of type IV collagen and its implications for the pathogenesis of Alport syndrome. The Journal of biological chemistry 1998; 273:8767-8775.

138. Kashtan CE. Alport syndrome and thin basement membrane disease. Curr Diag Pathol 2002; 8:349-360.

139. Kashtan CE, Kim Y, Lees GE, et al. Abnormal glomerular basement membrane laminins in murine, canine, and human Alport syndrome: aberrant laminin alpha2 deposition is species independent. Journal of the American Society of Nephrology: JASN 2001; 12:252-260.

140. Cosgrove D, Rodgers K, Meehan D, et al. Integrin alpha1beta1 and transforming growth factor-beta1 play distinct roles in Alport glomerular pathogenesis and serve as dual targets for metabolic therapy. The American journal of pathology 2000; 157:1649-1659.

141. Zallocchi M, Johnson BM, Meehan DT, et al. alpha1beta1 integrin/Rac1-dependent mesangial invasion of glomerular capillaries in Alport syndrome. The American journal of pathology 2013; 183:1269-1280.

142. Delimont D, Dufek BM, Meehan DT, et al. Laminin alpha2-mediated focal adhesion

kinase activation triggers Alport glomerular pathogenesis. PloS one 2014;9:e99083.

143. Rao VH, Lees GE, Kashtan CE, et al. Increased expression of MMP-2, MMP-9 (type IV collagenases/gelatinases), and MT1-MMP in canine X-linked Alport syndrome (XLAS). Kidney international 2003; 63:1736-1748.

144. Rao VH, Meehan DT, Delimont D, et al. Role for macrophage metalloelastase in glomerular basement membrane damage associated with Alport syndrome. The American journal of pathology 2006; 169:32-46.

145. Zeisberg M, Khurana M, Rao VH, et al. Stage-specific action of matrix metalloproteinases influences progressive hereditary kidney disease. PLoS medicine 2006; 3:e100.

146. Dehoux JP, Gianello P. The importance of large animal models in transplantation. Frontiers in bioscience: a journal and virtual library 2007; 12:4864-4880.

147. Casal M, Haskins M. Large animal models and gene therapy. European journal of human genetics: EJHG 2006; 14:266-272.

148. Nabity MB, Lees GE, Boggess MM, et al. Symmetric Dimethylarginine Assay Validation, Stability, and Evaluation as a Marker for the Early Detection of Chronic Kidney Disease in Dogs. Journal of veterinary internal medicine / American College of Veterinary Internal Medicine 2015; 29:1036-1044.

149. Nabity MB, Lees GE, Cianciolo R, et al. Urinary biomarkers of renal disease in dogs with X-linked hereditary nephropathy. Journal of veterinary internal medicine / American College of Veterinary Internal Medicine 2012; 26:282-293.

150. Hartner A, Schocklmann H, Prols F, et al. Alpha8 integrin in glomerular mesangial cells and in experimental glomerulonephritis. Kidney international 1999; 56:1468-1480.

151. Meehan DT, Delimont D, Cheung L, et al. Biomechanical strain causes maladaptive gene regulation, contributing to Alport glomerular disease. Kidney international 2009; 76:968-976.

152. Dufek B, Meehan D, Delimont D, et al. Endothelin A receptor activation on mesangial cells initiates Alport glomerular disease. Kidney international 2016.

153. Abrahamson DR, Isom K, Roach E, et al. Laminin compensation in collagen alpha3(IV) knockout (Alport) glomeruli contributes to permeability defects. Journal of the American Society of Nephrology: JASN 2007; 18:2465-2472.

154. Sachs N, Claessen N, Aten J, et al. Blood pressure influences end-stage renal disease of Cd151 knockout mice. J Clin Invest 2012; 122:348-358.

155. Savige J, Gregory M, Gross O, et al. Expert guidelines for the management of Alport syndrome and thin basement membrane nephropathy. Journal of the American Society of Nephrology: JASN 2013; 24:364-375.

156. Kashtan CE, Ding J, Gregory M, et al. Clinical practice recommendations for the treatment of Alport syndrome: a statement of the Alport Syndrome Research Collaborative. Pediatr Nephrol 2013; 28:5-11.

157. Shearin AL, Ostrander EA. Leading the way: canine models of genomics and disease. Dis Model Mech 2010; 3:27-34.

158. Coresh J, Selvin E, Stevens LA, et al. Prevalence of chronic kidney disease in the United States. JAMA 2007; 298:2038-2047.

159. Yanagisawa M, Kurihara H, Kimura S, et al. A novel potent vasoconstrictor peptide produced by vascular endothelial cells. Nature 1988; 332:411-415.

160. Firth JD, Ratcliffe PJ. Organ distribution of the three rat endothelin messenger RNAs and the effects of ischemia on renal gene expression. J Clin Invest 1992; 90:1023-1031.

161. Stow LR, Jacobs ME, Wingo CS, et al. Endothelin-1 gene regulation. FASEB J 2011; 25:16-28.

162. Vignon-Zellweger N, Heiden S, Miyauchi T, et al. Endothelin and endothelin receptors in the renal and cardiovascular systems. Life Sci 2012; 91:490-500.

163. Rosano L, Spinella F, Bagnato A. Endothelin 1 in cancer: biological implications and therapeutic opportunities. Nat Rev Cancer 2013; 13:637-651.

164. Inoue A, Yanagisawa M, Kimura S, et al. The human endothelin family: three structurally and pharmacologically distinct isopeptides predicted by three separate genes. Proceedings of the National Academy of Sciences of the United States of America 1989; 86:2863-2867.

165. Yanagisawa M, Masaki T. Molecular biology and biochemistry of the endothelins. Trends Pharmacol Sci 1989; 10:374-378.

166. Russell FD, Coppell AL, Davenport AP. In vitro enzymatic processing of radiolabeled big ET-1 in human kidney. Biochem Pharmacol 1998; 55:697-701.

167. Davenport AP, Hyndman KA, Dhaun N, et al. Endothelin. Pharmacol Rev 2016; 68:357-418.

168. Dhaun N, Pollock DM, Goddard J, et al. Selective and mixed endothelin receptor antagonism in cardiovascular disease. Trends Pharmacol Sci 2007; 28:573-579.

169. Sakurai T, Yanagisawa M, Takuwa Y, et al. Cloning of a cDNA encoding a non-isopeptide-selective subtype of the endothelin receptor. Nature 1990; 348:732-735.

170. Bremnes T, Paasche JD, Mehlum A, et al. Regulation and intracellular trafficking pathways of the endothelin receptors. The Journal of biological chemistry 2000; 275:17596-17604.

171. Kisanuki YY, Emoto N, Ohuchi T, et al. Low blood pressure in endothelial cell-specific endothelin 1 knockout mice. Hypertension 2010; 56:121-128.

172. Abassi ZA, Tate JE, Golomb E, et al. Role of neutral endopeptidase in the metabolism of endothelin. Hypertension 1992; 20:89-95.

173. Grenda R, Wuhl E, Litwin M, et al. Urinary excretion of endothelin-1 (ET-1), transforming growth factor- beta1 (TGF- beta1) and vascular endothelial growth factor (VEGF165) in pediatric chronic kidney diseases: results of the ESCAPE trial. Nephrology, dialysis, transplantation: official publication of the European Dialysis and Transplant Association - European Renal Association 2007; 22:3487-3494.

174. Dhaun N, Lilitkarntakul P, Macintyre IM, et al. Urinary endothelin-1 in chronic kidney disease and as a marker of disease activity in lupus nephritis. Am J Physiol Renal Physiol 2009; 296:F1477-1483.

175. Dhaun N, Webb DJ. The road from AKI to CKD: the role of endothelin. Kidney international 2013; 84:637-638.

176. Ohta K, Hirata Y, Shichiri M, et al. Urinary excretion of endothelin-1 in normal subjects and patients with renal disease. Kidney international 1991; 39:307-311.

177. Clark SD, Nabity MB, Cianciolo RE, et al. X-Linked Alport Dogs Demonstrate Mesangial Filopodial Invasion of the Capillary Tuft as an Early Event in Glomerular Damage. PloS one 2016; 11:e0168343.

178. Kolarcik CL, Luebben SD, Sapp SA, et al. Elastomeric and soft conducting microwires for implantable neural interfaces. Soft matter 2015; 11:4847-4861.

179. De Miguel C, Speed JS, Kasztan M, et al. Endothelin-1 and the kidney: new perspectives and recent findings. Current opinion in nephrology and hypertension 2016; 25:35-41.

180. Pupilli C, Brunori M, Misciglia N, et al. Presence and distribution of endothelin-1 gene expression in human kidney. Am J Physiol 1994; 267:F679-687.

181. Barton M, Sorokin A. Endothelin and the glomerulus in chronic kidney disease. Seminars in nephrology 2015; 35:156-167.

182. Barton M, Tharaux PL. Endothelin and the podocyte. Clin Kidney J 2012; 5:17-27.

183. Herman WH, Emancipator SN, Rhoten RL, et al. Vascular and glomerular expression of endothelin-1 in normal human kidney. Am J Physiol 1998; 275:F8-17.

184. Wendel M, Knels L, Kummer W, et al. Distribution of endothelin receptor subtypes ETA and ETB in the rat kidney. The journal of histochemistry and cytochemistry: official journal of the Histochemistry Society 2006; 54:1193-1203.

185. Jensen E. Technical review: colocalization of antibodies using confocal microscopy. Anat Rec (Hoboken) 2014; 297:183-187.

186. Jin J, Sison K, Li C, et al. Soluble FLT1 binds lipid microdomains in podocytes to control cell morphology and glomerular barrier function. Cell 2012; 151:384-399.

187. Andreasson U, Perret-Liaudet A, van Waalwijk van Doorn LJ, et al. A Practical Guide to Immunoassay Method Validation. Front Neurol 2015; 6:179.

188. Tang KW, Toh QC, Teo BW. Normalization of urinary biomarkers to creatinine for clinical practice and research--when and why. Singapore Med J 2015; 56:7-10.

189. Chandrasekaran K, Karolina DS, Sepramaniam S, et al. Role of microRNAs in kidney homeostasis and disease. Kidney international 2012; 81:617-627.

190. Sun Y, Koo S, White N, et al. Development of a micro-array to detect human and mouse microRNAs and characterization of expression in human organs. Nucleic Acids Res 2004; 32:e188.

191. Li JY, Yong TY, Michael MZ, et al. Review: The role of microRNAs in kidney disease. Nephrology (Carlton, Vic) 2010; 15:599-608.

192. Zhang J, Li S, Li L, et al. Exosome and exosomal microRNA: trafficking, sorting, and function. Genomics Proteomics Bioinformatics 2015; 13:17-24.

193. Lees GE, Helman G, Kashtan CE, et al. New form of X- linked dominant hereditary nephritis in dogs. Am J Vet Res 1999; 60:373-383.

194. de Ronde MWJ, Ruijter JM, Moerland PD, et al. Study Design and qPCR Data Analysis Guidelines for Reliable Circulating miRNA Biomarker Experiments: A Review. Clin Chem 2018; 64:1308-1318.

195. Ortiz A, Sanchez-Nino MD, Sanz AB. The meaning of urinary creatinine concentration. Kidney international 2011; 79:791.

196. Andersen CL, Jensen JL, Orntoft TF. Normalization of real-time quantitative reverse transcription-PCR data: a model-based variance estimation approach to identify genes suited for normalization, applied to bladder and colon cancer data sets. Cancer research 2004; 64:5245-5250.

197. Lange T, Stracke S, Rettig R, et al. Identification of miR-16 as an endogenous reference gene for the normalization of urinary exosomal miRNA expression data from CKD patients. PloS one 2017; 12:e0183435.

198. Debernardi S, Massat NJ, Radon TP, et al. Noninvasive urinary miRNA biomarkers for early detection of pancreatic adenocarcinoma. Am J Cancer Res 2015; 5:3455-3466.

199. Hoornaert I, Marynen P, Baens M. CREBL2, a novel transcript from the chromosome 12 region flanked by ETV6 and CDKN1B. Genomics 1998; 51:154-157.

200. Edwards M, Zwolak A, Schafer DA, et al. Capping protein regulators fine-tune actin assembly dynamics. Nat Rev Mol Cell Biol 2014; 15:677-689.

201. Cooper JA, Sept D. New insights into mechanism and regulation of actin capping protein. Int Rev Cell Mol Biol 2008; 267:183-206.

202. Wang XH. MicroRNA in myogenesis and muscle atrophy. Curr Opin Clin Nutr Metab Care 2013; 16:258-266.

203. Ichii O, Ohta H, Horino T, et al. Urinary exosome-derived microRNAs reflecting the changes of renal function and histopathology in dogs. Sci Rep 2017; 7:40340.

204. Doss JF, Corcoran DL, Jima DD, et al. A comprehensive joint analysis of the long and short RNA transcriptomes of human erythrocytes. BMC Genomics 2015; 16:952.

205. Duan ZY, Cai GY, Li JJ, et al. Urinary Erythrocyte-Derived miRNAs: Emerging Role in IgA Nephropathy. Kidney Blood Press Res 2017; 42:738-748.

206. Wang N, Zhou Y, Jiang L, et al. Urinary microRNA-10a and microRNA-30d serve as novel, sensitive and specific biomarkers for kidney injury. PloS one 2012; 7:e51140.

207. Anglicheau D, Sharma VK, Ding R, et al. MicroRNA expression profiles predictive of human renal allograft status. Proceedings of the National Academy of Sciences of the United States of America 2009; 106:5330-5335.

208. Scian MJ, Maluf DG, David KG, et al. MicroRNA profiles in allograft tissues and paired urines associate with chronic allograft dysfunction with IF/TA. Am J Transplant 2011; 11:2110-2122.

209. Wolenski FS, Shah P, Sano T, et al. Identification of microRNA biomarker candidates in urine and plasma from rats with kidney or liver damage. J Appl Toxicol 2017; 37:278-286.

210. Muller-Deile J, Dannenberg J, Schroder P, et al. Podocytes regulate the glomerular basement membrane protein nephronectin by means of miR-378a-3p in glomerular diseases. Kidney international 2017; 92:836-849.

211. Lv W, Fan F, Wang Y, et al. Therapeutic potential of microRNAs for the treatment of renal fibrosis and CKD. Physiol Genomics 2018; 50:20-34.

212. Lin Z, Ge J, Wang Z, et al. Let-7e modulates the inflammatory response in vascular endothelial cells through ceRNA crosstalk. Sci Rep 2017; 7:42498.

213. Shen Y, Tian F, Chen Z, et al. Amplification-based method for microRNA detection. Biosens Bioelectron 2015; 71:322-331.

214. Benes V, Castoldi M. Expression profiling of microRNA using real-time quantitative PCR, how to use it and what is available. Methods 2010; 50:244-249.

215. D'Haene B, Mestdagh P, Hellemans J, et al. miRNA expression profiling: from reference genes to global mean normalization. Methods Mol Biol 2012; 822:261-272.

216. Tam S, de Borja R, Tsao MS, et al. Robust global microRNA expression profiling using next-generation sequencing technologies. Lab Invest 2014; 94:350-358.

217. Mestdagh P, Hartmann N, Baeriswyl L, et al. Evaluation of quantitative miRNA expression platforms in the microRNA quality control (miRQC) study. Nat Methods 2014; 11:809-815.

218. Derveaux S, Vandesompele J, Hellemans J. How to do successful gene expression analysis using real-time PCR. Methods 2010; 50:227-230.

219. Waikar SS, Sabbisetti VS, Bonventre JV. Normalization of urinary biomarkers to creatinine during changes in glomerular filtration rate. Kidney international 2010; 78:486-494.

220. Goldstein SL. Urinary kidney injury biomarkers and urine creatinine normalization: a false premise or not? Kidney international 2010; 78:433-435.

221. Gasparri ML, Casorelli A, Bardhi E, et al. Beyond circulating microRNA biomarkers: Urinary microRNAs in ovarian and breast cancer. Tumour Biol 2017; 39:1010428317695525.

222. Ding M, Li Y, Wang H, et al. Diagnostic value of urinary microRNAs as non-invasive biomarkers for bladder cancer: a meta-analysis. Int J Clin Exp Med 2015; 8:15432-15440.

223. Lv Y, Qi R, Xu J, et al. Profiling of serum and urinary microRNAs in children with atopic dermatitis. PloS one 2014; 9:e115448.

224. Beltrami C, Clayton A, Phillips AO, et al. Analysis of urinary microRNAs in chronic kidney disease. Biochem Soc Trans 2012; 40:875-879.

225. Janszky N, Susal C. Circulating and urinary microRNAs as possible biomarkers in kidney transplantation. Transplant Rev (Orlando) 2018; 32:110-118.

226. Barutta F, Tricarico M, Corbelli A, et al. Urinary exosomal microRNAs in incipient diabetic nephropathy. PloS one 2013; 8:e73798.

227. Konta T, Ichikawa K, Suzuki K, et al. A microarray analysis of urinary microRNAs in renal diseases. Clin Exp Nephrol 2014; 18:711-717.

228. Brunet-Vega A, Pericay C, Quilez ME, et al. Variability in microRNA recovery from plasma: Comparison of five commercial kits. Anal Biochem 2015; 488:28-35.

229. Zampetaki A, Mayr M. Analytical challenges and technical limitations in assessing circulating miRNAs. Thromb Haemost 2012; 108:592-598.

230. Rupaimoole R, Slack FJ. MicroRNA therapeutics: towards a new era for the management of cancer and other diseases. Nat Rev Drug Discov 2017; 16:203-222.

231. Christopher AF, Kaur RP, Kaur G, et al. MicroRNA therapeutics: Discovering novel targets and developing specific therapy. Perspect Clin Res 2016; 7:68-74.

232. Bartges J, Polzin DJ. Chronic kidney disease In: Bartges J, Polzin DJ, eds. Nephrology and Urology of Small Animals. Hoboken, NJ: Blackwell Publishing Ltd.; 2011:433-471.

233. Clark SD, Song W, Cianciolo R, et al. Abnormal Expression of miR-21 in Kidney Tissue of Dogs With X-Linked Hereditary Nephropathy: A Canine Model of Chronic Kidney Disease. Vet Pathol 2018:300985818806050.

234. Rao VH, Lees GE, Kashtan CE, et al. Dysregulation of renal MMP-3 and MMP-7 in canine X-linked Alport syndrome. Pediatr Nephrol 2005; 20:732-739.

235. Loboda A, Sobczak M, Jozkowicz A, et al. TGF-beta1/Smads and miR-21 in Renal Fibrosis and Inflammation. Mediators Inflamm 2016; 2016:8319283.

236. Bottinger EP. TGF-beta in renal injury and disease. Seminars in nephrology 2007; 27:309-320.

237. Bottinger EP, Bitzer M. TGF-beta signaling in renal disease. Journal of the American Society of Nephrology: JASN 2002; 13:2600-2610.

238. Gomez IG, MacKenna DA, Johnson BG, et al. Anti-microRNA-21 oligonucleotides prevent Alport nephropathy progression by stimulating metabolic pathways. J Clin Invest 2015; 125:141-156.

239. Chau BN, Xin C, Hartner J, et al. MicroRNA-21 promotes fibrosis of the kidney by silencing metabolic pathways. Sci Transl Med 2012; 4:121ra118.

240. Zhong X, Chung AC, Chen HY, et al. miR-21 is a key therapeutic target for renal injury in a mouse model of type 2 diabetes. Diabetologia 2013; 56:663-674.

241. Zhong X, Chung ACK, Chen HY, et al. Smad3-Mediated Upregulation of miR-21 Promotes Renal Fibrosis. Clin J Am Soc Nephrol 2011; 22:1668-1681.

242. Mortarino M, Gioia G, Gelain ME, et al. Identification of suitable endogenous controls and differentially expressed microRNAs in canine fresh-frozen and FFPE lymphoma samples. Leuk Res 2010; 34:1070-1077.

243. Noguchi S, Mori T, Hoshino Y, et al. Comparative study of anti-oncogenic microRNA-145 in canine and human malignant melanoma. J Vet Med Sci 2012; 74:1-8.

244. Boggs RM, Wright ZM, Stickney MJ, et al. MicroRNA expression in canine mammary cancer. Mammalian genome: official journal of the International Mammalian Genome Society 2008; 19:561-569.

245. Gioia G, Mortarino M, Gelain ME, et al. Immunophenotype-related microRNA expression in canine chronic lymphocytic leukemia. Vet Immunol Immunopathol 2011; 142:228-235.

246. Ichii O, Otsuka S, Ohta H, et al. MicroRNA expression profiling of cat and dog kidneys. Res Vet Sci 2014; 96:299-303.

247. Kriegel AJ, Liang M. MicroRNA in situ hybridization for formalin fixed kidney tissues. J Vis Exp 2013.

248. Glowacki F, Savary G, Gnemmi V, et al. Increased circulating miR-21 levels are associated with kidney fibrosis. PloS one 2013; 8:e58014.

249. Denby L, Ramdas V, McBride MW, et al. miR-21 and miR-214 are consistently modulated during renal injury in rodent models. The American journal of pathology 2011; 179:661-672.

250. Chu CP, Hokamp JA, Cianciolo RE, et al. RNA-seq of serial kidney biopsies obtained during progression of chronic kidney disease from dogs with X-linked hereditary nephropathy. Sci Rep 2017; 7:16776.

251. Ghosh AK, Vaughan DE. PAI-1 in tissue fibrosis. J Cell Physiol 2012; 227:493-507.

252. Rerolle JP, Hertig A, Nguyen G, et al. Plasminogen activator inhibitor type 1 is a potential target in renal fibrogenesis. Kidney international 2000; 58:1841-1850.

253. Godel M, Hartleben B, Herbach N, et al. Role of mTOR in podocyte function and diabetic nephropathy in humans and mice. J Clin Invest 2011; 121:2197-2209.

254. Dugan LL, You YH, Ali SS, et al. AMPK dysregulation promotes diabetes-related reduction of superoxide and mitochondrial function. J Clin Invest 2013; 123:4888-4899.

255. Kang HM, Ahn SH, Choi P, et al. Defective fatty acid oxidation in renal tubular epithelial cells has a key role in kidney fibrosis development. Nat Med 2015; 21:37-46.

256. Kulkarni AA, Thatcher TH, Olsen KC, et al. PPAR-gamma ligands repress TGF beta- induced myofibroblast differentiation by targeting the PI3K/Akt pathway: implications for therapy of fibrosis. PloS one 2011; 6:e15909.

257. Ju WJ, Nair V, Smith S, et al. Tissue transcriptome-driven identification of epidermal growth factor as a chronic kidney disease biomarker. Sci Transl Med 2015; 7.

258. Isaka T, Nakayama H, Yokose T, et al. Epidermal Growth Factor Receptor Mutations and Prognosis in Pathologic N1-N2 Pulmonary Adenocarcinoma. Ann Thorac Surg 2016; 102:1821-1828.

259. Torres DD, Rossini M, Manno C, et al. The ratio of epidermal growth factor to monocyte chemotactic peptide-1 in the urine predicts renal prognosis in IgA nephropathy. Kidney international 2008; 73:327-333.

260. Grandaliano G, Gesualdo L, Bartoli F, et al. MCP-1 and EGF renal expression and urine excretion in human congenital obstructive nephropathy. Kidney international 2000; 58:182-192.

261. Humes HD, Cieslinski DA, Coimbra TM, et al. Epidermal Growth-Factor Enhances Renal Tubule Cell Regeneration and Repair and Accelerates the Recovery of Renal-Function in Postischemic Acute Renal-Failure. J Clin Invest 1989; 84:1757-1761.

262. Lindenmeyer MT, Kretzler M, Boucherot A, et al. Interstitial vascular rarefaction and reduced VEGF-A expression in human diabetic nephropathy. Journal of the American Society of Nephrology: JASN 2007; 18:1765-1776.

263. Harskamp LR, Gansevoort RT, van Goor H, et al. The epidermal growth factor receptor pathway in chronic kidney diseases. Nature reviews Nephrology 2016; 12:496- 506.

264. Chen J, Chen JK, Nagai K, et al. EGFR signaling promotes TGF beta-dependent renal fibrosis. Journal of the American Society of Nephrology: JASN 2012; 23:215-224.

265. Efstratiadis G, Divani M, Katsioulis E, et al. Renal fibrosis. Hippokratia 2009; 13:224- 229.

266. Cortez MA, Bueso-Ramos C, Ferdin J, et al. MicroRNAs in body fluids--the mix of hormones and biomarkers. Nat Rev Clin Oncol 2011; 8:467-477.

267. Weber JA, Baxter DH, Zhang S, et al. The microRNA spectrum in 12 body fluids. Clin Chem 2010; 56:1733-1741.

268. Grundy J, Heinlein C, Kersjes K, et al. Treatment with the microRNA-21 inhibitor Rg-012 given with and without Ramipril delays renal impairment progression and prolongs survival when initiated up to chronic kidney disease (CKD) Stage 3 in a mouse model of Alport syndrome. Nephrology, dialysis, transplantation: official publication of the European Dialysis and Transplant Association - European Renal Association 2016; 31:173- 173.

APPENDIX A

ADDITIONAL FIGURES

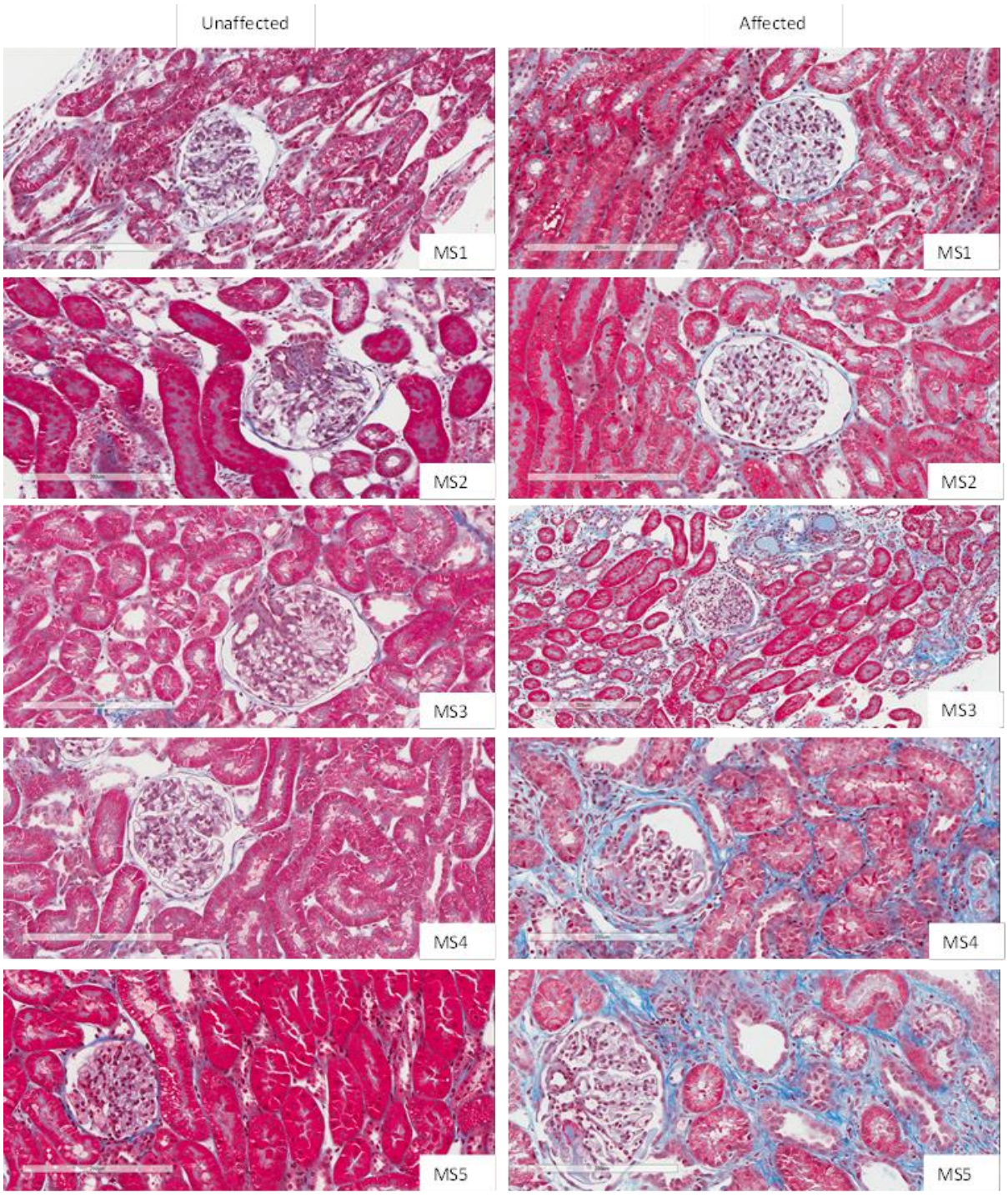

Figure A-1 Representative light microscopy images of serial biopsies taken from both an unaffected dog and an affected dog at each milestone (MS). To evaluate the extent of fibrosis, Masson's Trichrome, which stains collagen, a component of fibrosis blue, is routinely used. Image taken at 200X.

APPENDIX B

ADDITIONAL TABLES

Table B-1 Raw data for unaffected dogs (the "milestone" in the unaffected dog corresponds with the milestone reached by the affected dogs). CV=coefficient of variation, SD=standard deviation, uCr=urine creatinine.

Dog Milestone	ET-1 values						uCr		uET-1:uCr Ratio (converted)
	Well 1	Well 2	Average	CV %	SD	Conversion to pg/mL	mg/dL	(pg/mL)	
Dog 1 MS1	0	0	0	0	0	0	38.6	38600000	0
Dog 1 MS2	0	0	0	0	0	0	142.3	142300000	0
Dog 1 MS3	0	0	0	0	0	0	164.6	164600000	0
Dog 1 MS5	0	0	0	0	0	0	200.5	200500000	0
Dog 2 MS1	0	0	0	0	0	0	40.5	40500000	0
Dog 2 MS2	0	0	0	0	0	0	27.4	27400000	0
Dog 2 MS3	0.183	0.03	0.1065	101.6	0.10819	0.26625	82.7	82700000	0.32
Dog 2 MS5	0	0	0	0	0	0	32	32000000	0
Dog 3 MS1	0.598	0.115	0.3565	95.8	0.34153	0.89125	47.8	47800000	1.86
Dog 3 MS2	0	0	0	0	0	0	59.5	59500000	0
Dog 3 MS3	0.174	0	0.087	141.4	0.12304	0.2175	70.1	70100000	0.31
Dog 3 MS5	0	0	0	0	0	0	125.3	125300000	0
Dog 4 MS1	7.096	4.897	1.55493	16.7	0.25931	3.88731953	36.1	36100000	10.7
Dog 4 MS2	1.472	0	1.04086	135.9	1.41421	2.602152955	58.2	58200000	4.47
Dog 4 MS3	0	0	0	0	0	0	92.1	92100000	0
Dog 4 MS5	0	0	0	0	0	0	51.8	51800000	0

Table B-2 Raw data for affected dogs. CV=coefficient of variation, SD=standard deviation, uCr=urine creatinine.

Dog Milestone	ET-1 values						uCr		uET-1:uCr Ratio (converted)
	Well 1	Well 2	Average	CV %	SD	Conversion to pg/ml	mg/dL	pg/mL	
Dog 5 MS1	0	0	0	0	0	0	36.2	36200000	0
Dog 5 MS2	3.347	0	1.6735	141.4	2.36669	4.18375	63.5	63500000	6.59
Dog 5 MS3	0.673	0.749	0.711	7.6	0.05374	1.7775	53.2	53200000	3.34
Dog 5 MS5	0	1.596	0.798	141.4	1.12854	1.995	28	28000000	7.13
Dog 6 MS1	0	0	0	0	0	0	53	53000000	0
Dog 6 MS2	0	2.046	1.023	141.4	1.44674	2.5575	18.2	18200000	14.05
Dog 6 MS3	0.94	1.03	0.985	6.5	0.06364	2.4625	82.3	82300000	2.99
Dog 6 MS5	0	0	0	0	0	0	84.7	84700000	0
Dog 7MS1	0	0	0	0	0	0	27.1	27100000	0
Dog 7 MS2	2.457	2.866	2.6615	10.9	0.28921	6.65375	17.2	17200000	38.68
Dog 7 MS3	0.276	0.326	0.301	11.7	0.03536	0.7525	43.8	43800000	1.72
Dog 7 MS5	0	0	0	0	0	0	86.7	86700000	0
Dog 8 MS1	0	0	0	0	0	0	36.1	36100000	0
Dog 8 MS2	2.07	3.399	2.7345	34.4	0.93974	6.83625	34.3	34300000	19.93
Dog 8 MS3	0.319	0.188	0.2535	36.5	0.09263	0.63375	33.5	33500000	1.89
Dog 8 MS5	0	0	0	0	0	0	55.1	55100000	0
Dog 9 MS1	0.402	0.443	0.4225	6.9	0.02899	1.05625	54.9	54900000	1.92
Dog 9 MS2	0.279	0.219	0.249	17.0	0.04243	0.6225	22	22000000	2.83
Dog 9 MS3	0.931	1.017	0.974	6.2	0.06081	2.435	21.3	21300000	11.43
Dog 9 MS5	2.354	1.927	2.1405	14.1	0.30193	5.35125	52.1	52100000	10.27

Table B-2 continued

Dog 10 MS1	4.436	4.023	4.2295	6.9	0.29204	10.57375	66.9	66900000	15.81
Dog 10MS2	0.596	0.511	0.5535	10.9	0.0601	1.38375	114.8	114800000	1.21
Dog 10 MS3	1.165	0.838	1.0015	23.1	0.23122	2.50375	16	16000000	15.65
Dog 10 MS5	0.575	0.688	0.6315	12.7	0.0799	1.57875	23.8	23800000	6.63
Dog 11 MS1	1.322	1.329	1.3255	0.4	0.00495	3.31375	41.5	41500000	7.98
Dog 11 MS2	0.448	0.485	0.4665	5.6	0.02616	1.16625	63.5	63500000	1.84
Dog 11 MS3	0.164	0.073	0.1185	54.3	0.06435	0.29625	79.4	79400000	0.37
Dog 11 MS5	1.344	0.893	1.1185	28.5	0.31891	2.79625	26.6	26600000	10.51
Dog 12 MS1	1.072	0.404	0.738	64.0	0.47235	1.845	77.8	77800000	2.37
Dog 12 MS2	0.866	0.773	0.8195	8.0	0.06576	2.04875	98.8	98800000	2.07
Dog 12 MS3	0.907	0.358	0.6325	61.4	0.3882	1.58125	22.4	22400000	7.06
Dog 12 MS5	1.028	0.71	0.869	25.9	0.22486	2.1725	36.2	36200000	6

Table B-3 Qiagen miRCURY LNA miRNA PCR Assays information; pre-designed wet-bench validated assays. * indicates the assay is validated by Qiagen to specifically identify the mature cfa miR sequence.

Product	Cat. no.	Sequence
Reference miRs		
hsa-miR-16-5p miRCURY LNA miRNA PCR Assay*	YP00205702	MIMAT0000069: 5'UAGCAGCACGUAAAUAUUGGCG
hsa-miR-28-3p miRCURY LNA miRNA PCR Assay*	YP00204119	MIMAT0004502: 5'CACUAGAUUGUGAGCUCCUGGA
hsa-miR-30e-3p miRCURY LNA miRNA PCR Assay*	YP00204410	MIMAT0000693: 5'CUUUCAGUCGGAUGUUUACAGC
hsa-miR-93-5p miRCURY LNA miRNA PCR Assay*	YP00204715	MIMAT0000093: 5'CAAAGUGCUGUUCGUGCAGGUAG
hsa-miR-128-3p miRCURY LNA miRNA PCR Assay*	YP00205995	MIMAT0000424: 5'UCACAGUGAACCGGUCUCUUU
hsa-miR-151a-5p miRCURY LNA miRNA PCR Assay*	YP00204007	MIMAT0004697: 5'UCGAGGAGCUCACAGUCUAGU
hsa-miR-339-5p miRCURY LNA miRNA PCR Assay	YP00206007	MIMAT0000764: 5'UCCCUGUCCUCCAGGAGCUCACG
mmu-miR-429-3p miRCURY LNA miRNA PCR Assay*	YP00205068	MIMAT0001537: 5'UAAUACUGUCUGGUAAUGCCGU
Target miRs		
hsa-let-7e-5p miRCURY LNA miRNA PCR Assay*	YP00205711	MIMAT0000066: 5'UGAGGUAGGAGGUUGUAUAGUU
hsa-miR-21-5p miRCURY LNA miRNA PCR Assay*	YP00204230	MIMAT0000076: 5'UAGCUUAUCAGACUGAUGUUGA
cfa-miR-30d miRCURY LNA miRNA PCR Assay*	YP02118689	MIMAT0006616: 5'UGUAAACAUCCCCGACUGGAAGCU
cfa-miR-142 miRCURY LNA miRNA PCR Assay*	YP02102101	MIMAT0006736: 5'CCCAUAAAGUAGAAAGCACUA
hsa-miR-378a-3p miRCURY LNA miRNA PCR Assay*	YP00205946	MIMAT0000732: 5'ACUGGACUUGGAGUCAGAAGGC
hsa-miR-486-5p miRCURY LNA miRNA PCR Assay	YP00204001	MIMAT0002177: 5'UCCUGUACUGAGCUGCCCCGAG
cfa-miR-8890_1 miRCURY LNA miR *Custom* PCR Assay*	YCP0041436	GACTGAGCCACCTASSTACCCCTTA

Table B-4 Total RNA concentration of individual samples as determined by the Fragment Analyzer.

Sample Name	Volume used for isolation (mL)	Fragment Analyzer concentration (ng/µL)
C1_T1	4	0.0019
C1_T2	4	0.0012
C1_T3	4	1.4622
C2_T1	4	0.0005
C2_T2	4	0.0022
C2_T3	3	1.0307
C3_T1	3	0.0019
C3_T2	3	0.005
C3_T3	3	1.8567
C4_T1	4	0.0009
C4_T2	4	0.0059
C4_T3	4	0.005
A1_T1	4	0.3747
A1_T2	4	0.0016
A1_T3	4	1.3413
A2_T1	4	0.4495
A3_T2	4	0.726
A2_T3	3	1.0515
A3_T1	4	1.011
A3_T2	4	8.3016
A3_T3	4	21.1682
A4_T1	3	1.55
A4_T2	3	1.0403
A4_T3	3	0.6239
A5_T1	4	0.001
A5_T2	4	0.7951
A5_T3	4	1.0456

Table B-5 List of Cq values, conversion to linear scale, uCr concentration, and ratio for each dog, in addition to each standard deviation, average, and coefficient of variation (CV) for all of miRNAs tested for use as an endogenous reference miRNA. The two lowest CV values are highlighted in red. C=control; A=affected; T=time point; uCr=urine creatinine concentration.

Target	Sample	Cq	Cq Mean	Cq SD	Linear Cq value	uCr (mg/dL)	Ratio	SD	Average	CV (%)
miR-128	C1_T1	36.05	36.08	0.048	15.498942	40.5	0.3826899	0.1952283	0.2611942	75
miR-128	C1_T1	36.11	36.08	0.048	14.788008	40.5	0.365136			
miR-128	C1_T2	38.38	38.38	0.000	3.067474	82.7	0.0370916			
miR-128	C1_T3	36.01	35.96	0.069	15.882512	46.4	0.3422955			
miR-128	C1_T3	35.91	35.96	0.069	16.99299	46.4	0.3662282			
miR-128	C5	35.71	35.42	0.413	19.584463	357	0.0548584			
miR-128	C5	35.12	35.42	0.413	29.347637	357	0.0822063			
miR-128	A1_T1	37.25	37.25	0.000	6.7055161	53	0.1265192			
miR-128	A1_T2	35.13	35.13	0.000	29.232045	82.3	0.3551889			
miR-128	A1_T3	35.33	35.33	0.000	25.533297	42.1	0.6064916			
miR-128	A2_T1	36.12	36.12	0.000	14.692093	54.9	0.2676155			
miR-128	A2_T3	36.08	36.08	0.000	15.096176	37.3	0.4047232			
miR-128	A4_T1	37.22	36.57	0.913	6.8674253	62.9	0.1091801			
miR-128	A4_T1	35.93	36.57	0.913	16.807369	62.9	0.2672078			
miR-128	A4_T2	35.87	35.87	0.000	17.519234	21.6	0.8110756			
miR-128	A4_T3	37.02	37.02	0.000	7.913022	48.9	0.1618205			
miR-128	A6	36.87	36.68	0.273	8.7340575	150.9	0.0578798			
miR-128	A6	36.49	36.68	0.273	11.413661	150.9	0.0756372			
miR-128	A7	35.37	35.46	0.423	24.778018	117.3	0.2112363			
miR-128	A7	35.92	35.46	0.423	16.883544	117.3	0.1439347			
miR-128	A7	35.09	35.46	0.423	30.036034	117.3	0.2560617			

Table B-5 Continued

Target	Sample	Cq	Cq Mean	Cq SD	Linear Cq value	uCr (mg/dL)	Ratio	SD	Average	CV (%)
miR-151	C1_T1	30.99	30.88	0.158	514.31906	40.5	12.699236	19.786783	17.278941	114.5
miR-151	C1_T1	30.77	30.88	0.158	600.55139	40.5	14.828429			
miR-151	C1_T2	31.22	31.24	0.037	440.74328	82.7	5.329423			
miR-151	C1_T2	31.27	31.24	0.037	424.99719	82.7	5.1390229			
miR-151	C1_T3	30.58	30.58	0.000	686.03831	46.4	14.785309			
miR-151	C5	29.41	29.41	0.000	1544.8824	357	4.3274016			
miR-151	A1_T1	31.03	31.00	0.051	500.44342	53	9.4423286			
miR-151	A1_T1	30.96	31.00	0.051	525.9806	53	9.9241622			
miR-151	A1_T2	29.51	29.61	0.133	1436.0128	82.3	17.448515			
miR-151	A1_T2	29.70	29.61	0.133	1260.8922	82.3	15.320683			
miR-151	A1_T3	29.70	29.70	0.000	1258.0214	42.1	29.881743			
miR-151	A2_T1	31.04	31.03	0.009	498.32627	54.9	9.0769813			
miR-151	A2_T1	31.03	31.03	0.009	502.60759	54.9	9.1549653			
miR-151	A2_T3	30.07	30.07	0.000	974.43225	37.3	26.124189			
miR-151	A4_T1	30.64	30.64	0.000	656.05433	62.9	10.430117			
miR-151	A4_T2	28.91	28.91	0.000	2182.3839	21.6	101.03629			
miR-151	A4_T3	30.54	30.52	0.029	704.95681	48.9	14.416295			
miR-151	A4_T3	30.50	30.52	0.029	724.96761	48.9	14.825513			
miR-151	A6	29.68	29.66	0.039	1274.8272	150.9	8.4481589			
miR-151	A6	29.63	29.66	0.039	1325.1235	150.9	8.7814681			
miR-151	A7	28.98	28.86	0.180	2071.2239	117.3	17.657493			
miR-151	A7	28.73	28.86	0.180	2470.2187	117.3	21.058983			

Table B-5 Continued

Target	Sample	Cq	Cq Mean	Cq SD	Linear Cq value	uCr (mg/dL)	Ratio	SD	Average	CV (%)
miR-16	C1_T1	25.35	25.43	0.109	25715.653	40.5	634.95441	311.10851	494.86691	62.9
miR-16	C1_T1	25.50	25.43	0.109	23106.01	40.5	570.51877			
miR-16	C1_T2	25.79	25.80	0.010	18962.976	82.7	229.29838			
miR-16	C1_T2	25.80	25.80	0.010	18775.964	82.7	227.03705			
miR-16	C1_T3	24.51	24.51	0.000	46105.026	46.4	993.64281			
miR-16	C5	25.20	25.21	0.012	28430.894	357	79.638358			
miR-16	C5	25.22	25.21	0.012	28098.382	357	78.706952			
miR-16	A1_T1	25.46	25.46	0.000	23838.095	53	449.77537			
miR-16	A1_T2	25.36	25.25	0.117	25515.716	82.3	310.033			
miR-16	A1_T2	25.25	25.25	0.117	27538.076	82.3	334.60603			
miR-16	A1_T2	25.13	25.25	0.117	30023.857	82.3	364.80993			
miR-16	A1_T3	25.24	25.14	0.141	27749.058	42.1	659.12252			
miR-16	A1_T3	25.04	25.14	0.141	31851.911	42.1	756.57747			
miR-16	A2_T1	26.16	26.10	0.083	14682.708	54.9	267.44459			
miR-16	A2_T1	26.04	26.10	0.083	15927.052	54.9	290.11023			
miR-16	A2_T3	25.14	25.14	0.000	29696.378	37.3	796.14953			
miR-16	A4_T1	25.45	25.44	0.015	23985.049	62.9	381.32034			
miR-16	A4_T1	25.43	25.44	0.015	24337.11	62.9	386.91749			
miR-16	A4_T2	25.46	25.36	0.133	23844.351	21.6	1103.9051			
miR-16	A4_T2	25.27	25.36	0.133	27160.091	21.6	1257.4116			
miR-16	A4_T3	26.52	26.48	0.053	11437.792	48.9	233.90168			
miR-16	A4_T3	26.44	26.48	0.053	12044.416	48.9	246.30708			
miR-16	A6	24.89	24.76	0.194	35258.497	150.9	233.65472			
miR-16	A6	24.62	24.76	0.194	42627.371	150.9	282.48755			
miR-16	A7	23.69	23.62	0.125	81251.383	117.3	692.68016			

Table B-5 Continued

Target	Sample	Cq	Cq Mean	Cq SD	Linear Cq value	uCr (mg/dL)	Ratio	SD	Average	CV (%)
miR-16	A7	23.69	23.62	0.125	81498.664	117.3	694.78827			
miR-16	A7	23.47	23.62	0.125	94497.725	117.3	805.60721			
miR-28	C1_T1	29.67	29.65	0.032	1285.3923	40.5	31.738081	36.9051	47.411633	77.8
miR-28	C1_T1	29.63	29.65	0.032	1325.9209	40.5	32.738788			
miR-28	C1_T2	29.78	29.67	0.158	1193.708	82.7	14.434195			
miR-28	C1_T2	29.55	29.67	0.158	1394.344	82.7	16.860266			
miR-28	C1_T3	28.12	28.18	0.089	3769.0147	46.4	81.228765			
miR-28	C1_T3	28.25	28.18	0.089	3455.579	46.4	74.473685			
miR-28	A5	26.32	26.30	0.027	13151.553	357	36.839085			
miR-28	A5	26.28	26.30	0.027	13500.817	357	37.817414			
miR-28	A1_T1	30.10	30.22	0.105	952.61155	53	17.973803			
miR-28	A1_T1	30.26	30.22	0.105	853.64058	53	16.106426			
miR-28	A1_T1	30.30	30.22	0.105	829.78852	53	15.656387			
miR-28	A1_T2	28.83	28.82	0.017	2309.1783	82.3	28.05806			
miR-28	A1_T2	28.80	28.82	0.017	2347.0002	82.3	28.51762			
miR-28	A1_T3	28.73	28.73	0.000	2475.0618	42.1	58.790067			
miR-28	A2_T1	29.30	29.36	0.058	1665.64	54.9	30.339526			
miR-28	A2_T1	29.41	29.36	0.058	1541.0854	54.9	28.070772			
miR-28	A2_T1	29.38	29.36	0.058	1574.7949	54.9	28.684789			
miR-28	A2_T3	28.78	28.66	0.107	2383.5354	37.3	63.901752			
miR-28	A2_T3	28.63	28.66	0.107	2639.9225	37.3	70.775403			
miR-28	A2_T3	28.57	28.66	0.107	2754.3514	37.3	73.843202			
miR-28	A4_T1	27.86	27.86	0.000	4508.0662	62.9	71.670368			

Table B-5 Continued

Target	Sample	Cq	Cq Mean	Cq SD	Linear Cq value	uCr (mg/dL)	Ratio	SD	Average	CV (%)
miR-28	A4_T2	28.25	28.20	0.076	3433.3235	21.6	158.95016			
miR-28	A4_T2	28.15	28.20	0.076	3697.4602	21.6	171.17871			
miR-28	A4_T3	29.40	29.34	0.100	1554.8683	48.9	31.796898			
miR-28	A4_T3	29.40	29.34	0.100	1555.0874	48.9	31.801378			
miR-28	A4_T3	29.22	29.34	0.100	1754.1111	48.9	35.871392			
miR-28	A6	28.15	28.14	0.020	3688.387	150.9	24.442591			
miR-28	A6	28.12	28.14	0.020	3762.1031	150.9	24.931101			
miR-28	A7	27.77	27.67	0.091	4801.2864	117.3	40.931683			
miR-28	A7	27.61	27.67	0.091	5359.5934	117.3	45.691333			
miR-28	A7	27.61	27.67	0.091	5354.3823	117.3	45.646908			
miR-30e	C1_T1	27.85	27.79	0.094	4535.8618	40.5	111.99659	109.1216	158.85971	68.7
miR-30e	C1_T1	27.72	27.79	0.094	4975.9876	40.5	122.86389			
miR-30e	C1_T2	27.90	27.90	0.004	4386.5784	82.7	53.04206			
miR-30e	C1_T2	27.90	27.90	0.004	4403.6662	82.7	53.248685			
miR-30e	C1_T3	27.31	27.55	0.331	6598.3098	46.4	142.20495			
miR-30e	C1_T3	27.78	27.55	0.331	4770.5923	46.4	102.81449			
miR-30e	A5	25.98	25.97	0.011	16606.954	357	46.518079			
miR-30e	A5	25.97	25.97	0.011	16781.436	357	47.006823			
miR-30e	A1_T1	27.00	26.95	0.069	8204.9096	53	154.80961			
miR-30e	A1_T1	26.90	26.95	0.069	8778.6384	53	165.63469			
miR-30e	A1_T2	26.14	26.24	0.148	14915.406	82.3	181.23215			
miR-30e	A1_T2	26.34	26.24	0.148	12901.219	82.3	156.75844			
miR-30e	A1_T3	26.48	26.51	0.042	11774.336	42.1	279.67544			

Table B-5 Continued

Target	Sample	Cq	Cq Mean	Cq SD	Linear Cq value	uCr (mg/dL)	Ratio	SD	Average	CV (%)
miR-30e	A1_T3	26.54	26.51	0.042	11294.153	42.1	268.26966			
miR-30e	A2_T1	27.60	27.58	0.035	5389.3827	54.9	98.167263			
miR-30e	A2_T1	27.55	27.58	0.035	5580.0116	54.9	101.63956			
miR-30e	A2_T3	27.35	27.43	0.114	6426.9409	37.3	172.30405			
miR-30e	A2_T3	27.51	27.43	0.114	5748.1685	37.3	154.10639			
miR-30e	A4_T1	26.70	26.74	0.052	10081.384	62.9	160.27638			
miR-30e	A4_T1	26.77	26.74	0.052	9577.2365	62.9	152.26131			
miR-30e	A4_T2	26.71	26.71	0.008	9992.3251	21.6	462.60764			
miR-30e	A4_T2	26.70	26.71	0.008	10073.501	21.6	466.36578			
miR-30e	A4_T3	27.73	27.73	0.000	4943.525	48.9	101.09458			
miR-30e	A6	26.47	26.47	0.000	11847.94	150.9	78.515175			
miR-30e	A7	26.02	26.02	0.000	16196.671	117.3	138.07903			
miR-339	C1_T1	32.31	32.29	0.025	206.17353	40.5	5.0907044	63.207735	3.4599888	1826.8
miR-339	C1_T1	32.28	32.29	0.025	211.21732	40.5	5.2152424			
miR-339	C1_T2	35.50	35.70	0.169	22.570118	82.7	0.2729156			
miR-339	C1_T2	35.82	35.70	0.169	18.167047	82.7	0.2196741			
miR-339	C1_T2	35.77	35.70	0.169	18.73376	82.7	0.2265267			
miR-339	C1_T3	32.47	32.43	0.058	184.45677	46.4	3.9753613			
miR-339	C1_T3	32.39	32.43	0.058	195.28002	46.4	4.2086211			
miR-339	C5	32.26	32.42	0.229	213.90752	357	0.5991807			
miR-339	C5	32.58	32.42	0.229	170.85502	357	0.4785855			
miR-339	A1_T1	32.26	32.33	0.090	213.385	53	4.0261321			
miR-339	A1_T1	32.39	32.33	0.090	195.33724	53	3.6856083			

Table B-5 Continued

Target	Sample	Cq	Cq Mean	Cq SD	Linear Cq value	uCr (mg/dL)	Ratio	SD	Average	CV (%)
miR-339	A1_T2	31.91	31.91	0.000	272.0866	82.3	3.3060341			
miR-339	A1_T3	36.11	36.11	0.000	14.86696	42.1	0.3531344			
miR-339	A2_T1	32.23	32.26	0.031	217.63691	54.9	3.9642425			
miR-339	A2_T1	32.28	32.26	0.031	211.13891	54.9	3.8458817			
miR-339	A2_T3	31.52	31.52	0.000	356.72622	37.3	9.5637056			
miR-339	A4_T1	31.48	31.54	0.058	366.63459	62.9	5.8288487			
miR-339	A4_T1	31.60	31.54	0.058	338.47247	62.9	5.3811204			
miR-339	A4_T1	31.53	31.54	0.058	353.4449	62.9	5.6191558			
miR-339	A4_T2	31.50	31.50	0.000	361.08231	21.6	16.716774			
miR-339	A4_T3	32.87	32.78	0.124	140.24457	48.9	2.867987			
miR-339	A4_T3	32.69	32.78	0.124	158.44143	48.9	3.240111			
miR-339	A6	33.26	33.30	0.075	107.10368	150.9	0.7097659			
miR-339	A6	33.38	33.30	0.075	98.11829	150.9	0.6502206			
miR-339	A6	33.25	33.30	0.075	107.56167	150.9	0.712801			
miR-339	A7	32.15	32.10	0.045	230.86751	117.3	1.9681799			
miR-339	A7	32.07	32.10	0.045	244.09208	117.3	2.0809214			
miR-339	A7	32.07	32.10	0.045	243.07483	117.3	2.0722492			
miR-429	C1_T1	28.62	28.62	0.000	2669.4654	40.5	65.912726	74.484231	76.908034	96.8
miR-429	C1_T2	28.85	28.85	0.000	2268.7918	82.7	27.434			
miR-429	C1_T3	28.69	28.67	0.029	2544.9498	46.4	54.848056			
miR-429	C1_T3	28.65	28.67	0.029	2618.6492	46.4	56.436404			
miR-429	C5	25.69	25.58	0.148	20377.158	357	57.078875			
miR-429	C5	25.48	25.58	0.148	23565.913	357	66.01096			

Table B-5 Continued

Target	Sample	Cq	Cq Mean	Cq SD	Linear Cq value	uCr (mg/dL)	Ratio	SD	Average	CV (%)
miR-429	A1_T1	29.66	29.66	0.000	1293.637	53	24.408245			
miR-429	A1_T2	28.05	27.97	0.112	3945.601	82.3	47.94169			
miR-429	A1_T2	27.89	27.97	0.112	4405.2785	82.3	53.527078			
miR-429	A1_T3	27.57	27.45	0.180	5506.0104	42.1	130.78409			
miR-429	A1_T3	27.32	27.45	0.180	6568.2601	42.1	156.01568			
miR-429	A2_T1	28.69	28.75	0.093	2541.3208	54.9	46.289996			
miR-429	A2_T1	28.82	28.75	0.093	2319.1014	54.9	42.242283			
miR-429	A2_T3	27.50	27.50	0.000	5774.9288	37.3	154.82383			
miR-429	A4_T1	28.49	28.51	0.036	2919.5026	62.9	46.414986			
miR-429	A4_T1	28.54	28.51	0.036	2816.9272	62.9	44.784216			
miR-429	A4_T2	26.91	26.91	0.000	8733.9767	21.6	404.35077			
miR-429	A4_T3	28.32	28.29	0.031	3272.6525	48.9	66.925408			
miR-429	A4_T3	28.28	28.29	0.031	3365.8653	48.9	68.831602			
miR-429	A4_T3	28.26	28.29	0.031	3413.8005	48.9	69.81187			
miR-429	A6	27.29	27.19	0.185	6688.8951	150.9	44.326674			
miR-429	A6	27.31	27.19	0.185	6628.4155	150.9	43.925881			
miR-429	A6	26.98	27.19	0.185	8312.8535	150.9	55.088492			
miR-429	A7	27.26	27.29	0.036	6857.5593	117.3	58.461716			
miR-429	A7	27.33	27.29	0.036	6523.7923	117.3	55.616302			
miR-429	A7	27.29	27.29	0.036	6723.289	117.3	57.317041			
miR-93	C1_T1	30.17	30.16	0.003	912.2774	40.5	22.525368	21.307474	19.466262	109.5
miR-93	C1_T1	30.16	30.16	0.003	914.64902	40.5	22.583926			
miR-93	C1_T2	32.01	32.01	0.000	254.41664	82.7	3.0763801			

Table B-5 Continued

Target	Sample	Cq	Cq Mean	Cq SD	Linear Cq value	uCr (mg/dL)	Ratio	SD	Average	CV (%)
miR-93	C1_T3	29.48	29.49	0.018	1472.3873	46.4	31.732484			
miR-93	C1_T3	29.50	29.49	0.018	1446.4651	46.4	31.173817			
miR-93	A5	29.23	29.33	0.142	1744.3658	357	4.8861787			
miR-93	A5	29.43	29.33	0.142	1518.0305	357	4.2521864			
miR-93	A1_T1	30.80	30.73	0.093	588.82002	53	11.109812			
miR-93	A1_T1	30.67	30.73	0.093	645.00783	53	12.169959			
miR-93	A1_T2	29.75	29.72	0.034	1220.0836	82.3	14.824831			
miR-93	A1_T2	29.70	29.72	0.034	1261.2999	82.3	15.325636			
miR-93	A1_T3	30.10	30.05	0.066	957.18347	42.1	22.735949			
miR-93	A1_T3	30.00	30.05	0.066	1021.0776	42.1	24.253625			
miR-93	A2_T1	31.06	30.92	0.198	492.52252	54.9	8.9712664			
miR-93	A2_T1	30.78	30.92	0.198	598.19363	54.9	10.896059			
miR-93	A2_T3	29.92	29.92	0.004	1081.355	37.3	28.990752			
miR-93	A2_T3	29.93	29.92	0.004	1077.1096	37.3	28.876932			
miR-93	A4_T1	30.15	30.14	0.023	921.87635	62.9	14.656222			
miR-93	A4_T1	30.12	30.14	0.023	942.63201	62.9	14.986201			
miR-93	A4_T2	28.66	28.66	0.000	2591.7412	21.6	119.98802			
miR-93	A4_T3	30.50	30.36	0.115	725.9664	48.9	14.845939			
miR-93	A4_T3	30.29	30.36	0.115	839.7592	48.9	17.17299			
miR-93	A4_T3	30.31	30.36	0.115	826.84009	48.9	16.908795			
miR-93	A6	29.83	29.72	0.100	1154.1005	150.9	7.6481148			
miR-93	A6	29.71	29.72	0.100	1256.0115	150.9	8.3234693			
miR-93	A6	29.63	29.72	0.100	1324.8945	150.9	8.7799502			
miR-93	A7	29.52	29.58	0.084	1426.6079	117.3	12.162045			
miR-93	A7	29.64	29.58	0.084	1313.5764	117.3	11.198435			

Table B-6 Inter-run calibration values including mean Cq value of each standard from each plate along with standard deviation (SD), mean, and coefficient of variation (CV%) of each standard.

let-7e							
		Plate 1	Plate 2	Plate 3	SD	Mean	CV%
	STD1	28.7274	28.4403	28.3224	0.20830739	28.4967	0.730988
	STD2	30.6514	30.8847	31.1873	0.26869576	30.9078	0.869346
	STD3	33.4942	33.3757	33.8947	0.27196921	33.5882	0.809717
	STD4	36.7752	35.5402	35.3942	0.75869427	35.9032	2.113166
	STD5	38.0543	37.5555		0.35270486	37.8049	0.932961
miR-16							
		Plate 1	Plate 2	Plate 3	SD	Mean	CV%
	STD1	26.0291	25.6498	25.5053	0.27052886	25.7280667	1.051493
	STD2	28.1822	28.2255	28.5162	0.18163029	28.3079667	0.641623
	STD3	30.4468	30.3628	30.9752	0.33198803	30.5949333	1.085108
	STD4	33.1283	33.4723	33.511	0.21067075	33.3705333	0.631308
	STD5						
miR-21							
		Plate 1	Plate 2	Plate 3	SD	Mean	CV%
	STD1	24.7498	24.5351	24.5948	0.11081906	24.6265667	0.449998
	STD2	26.9469	27.0601	27.3313	0.19753778	27.1127667	0.728578
	STD3	29.2989	29.5219	29.8176	0.26019774	29.5461333	0.880649
	STD4	32.5064	32.9688	32.4083	0.29933193	32.6278333	0.917413
	STD5						

Table B-6 Continued

miR-30d							
		Plate 1	Plate 2	Plate 3	SD	Mean	CV%
	STD1	27.7521	28.0826	27.5251	0.28034666	27.7866	1.008928
	STD2	30.1057	29.9622	30.3528	0.19757658	30.1402333	0.655524
	STD3	32.3365	32.4054	33.0253	0.37935662	32.5890667	1.164061
	STD4	35.3834	35.2834	34.8118	0.30526849	35.1595333	0.868238
	STD5						
miR-30e							
		Plate 1	Plate 2	Plate 3	SD	Mean	CV%
	STD1	27.4409	27.5962	27.6143	0.09531812	27.5504667	0.345976
	STD2	30.0824	30.029	30.2197	0.09837796	30.1103667	0.326725
	STD3	32.4367	32.366	33.1462	0.43148982	32.6496333	1.321576
	STD4	35.8232	36.1181		0.20852579	35.97065	0.579711
	STD5	38.0777	38.1835		0.0748119	38.1306	0.196199
miR-142							
		Plate 1	Plate 2	Plate 3	SD	Mean	CV%
	STD1	30.3615	30.4497	30.4497	0.05092229	30.4203	0.167396
	STD2	33.0616	33.4732	33.4732	0.23763737	33.336	0.712855
	STD3	36.0454	36.3242	36.3242	0.16096526	36.2312667	0.444272
	STD4	37.6776	38.1298	38.1298	0.26107779	37.9790667	0.687426
	STD5						

Table B-6 Continued

miR-378							
		Plate 1	Plate 2	Plate 3	SD	Mean	CV%
	STD1	27.6866	27.8274	27.4312	0.20084332	27.6484	0.726419
	STD2	29.9566	29.7556	30.1893	0.217043	29.9671667	0.724269
	STD3	32.0772	32.101	33.0599	0.56061795	32.4127	1.729624
	STD4	34.3954	35.287	35.0704	0.46502529	34.9176	1.331779
	STD5	38.1702	38.0012		0.11950105	38.0857	0.313769
miR-486							
		Plate 1	Plate 2	Plate 3	SD	Mean	CV%
	STD1	27.2989	27.367	26.8722	0.26818449	27.1793667	0.986721
	STD2	29.2542	29.3362	29.7247	0.25133858	29.4383667	0.853779
	STD3	31.5384	31.6669	32.5406	0.54532388	31.9153	1.70866
	STD4	35.423	35.4514	35.1288	0.17862016	35.3344	0.505513
	STD5						

Table B-7 Individual normalized expression values for each sample from the clustergram.

Target	Sample Name	Normalized expression
let-7e	A1_T1	0.06444
let-7e	A1_T2	0.07322
let-7e	A1_T3	0.06440
let-7e	A2_T1	0.04960
let-7e	A2_T2	0.06185
let-7e	A2_T3	0.05536
let-7e	A3_T1	0.03700
let-7e	A3_T2	0.06935
let-7e	A3_T3	0.04837
let-7e	A4_T1	0.06713
let-7e	A4_T2	0.08648
let-7e	A4_T3	0.08166
let-7e	A5_T1	0.05124
let-7e	A5_T2	0.06617
let-7e	A5_T3	0.06178
let-7e	C1_T1	0.03957
let-7e	C1_T2	0.04179
let-7e	C1_T3	0.03554
let-7e	C2_T1	0.03417
let-7e	C2_T2	0.04892
let-7e	C2_T3	0.02716
let-7e	C3_T1	0.03681
let-7e	C3_T2	0.04979
let-7e	C3_T3	0.02607
let-7e	C4_T1	0.04589
let-7e	C4_T2	0.05116
let-7e	C4_T3	0.02678
miR-142	A1_T1	0.09588
miR-142	A1_T2	0.01298
miR-142	A1_T3	0.01508
miR-142	A2_T1	0.28858
miR-142	A2_T2	0.16245
miR-142	A2_T3	0.26707
miR-142	A3_T1	0.59638
miR-142	A3_T2	0.03891
miR-142	A3_T3	0.36921
miR-142	A4_T1	0.14478

Table B-7 Continued

Target	Sample Name	Normalized expression
miR-142	A4_T2	0.01658
miR-142	A4_T3	0.01271
miR-142	A5_T1	0.05821
miR-142	A5_T2	0.00743
miR-142	A5_T3	0.08177
miR-142	C1_T1	0.34083
miR-142	C1_T2	0.17324
miR-142	C1_T3	0.26795
miR-142	C2_T1	0.34687
miR-142	C2_T2	0.90784
miR-142	C2_T3	2.20726
miR-142	C3_T1	0.76257
miR-142	C3_T2	0.19934
miR-142	C3_T3	0.31308
miR-142	C4_T1	0.15678
miR-142	C4_T2	0.15915
miR-142	C4_T3	1.18482
miR-21	A1_T1	1.75673
miR-21	A1_T2	5.66718
miR-21	A1_T3	8.37127
miR-21	A2_T1	5.07020
miR-21	A2_T2	6.94038
miR-21	A2_T3	11.35219
miR-21	A3_T1	2.96245
miR-21	A3_T2	5.72387
miR-21	A3_T3	7.76381
miR-21	A4_T1	2.25872
miR-21	A4_T2	7.65863
miR-21	A4_T3	8.00012
miR-21	A5_T1	3.07799
miR-21	A5_T2	7.27605
miR-21	A5_T3	8.98006
miR-21	C1_T1	3.12760
miR-21	C1_T2	3.14735
miR-21	C1_T3	2.80381
miR-21	C2_T1	4.10231
miR-21	C2_T2	8.32439

Table B-7 Continued

Target	Sample Name	Normalized expression
miR-21	C2_T3	5.20183
miR-21	C3_T1	1.47785
miR-21	C3_T2	3.56365
miR-21	C3_T3	1.86354
miR-21	C4_T1	4.57297
miR-21	C4_T2	3.91049
miR-21	C4_T3	10.50585
miR-30d	A1_T1	0.16289
miR-30d	A1_T2	0.15754
miR-30d	A1_T3	0.21281
miR-30d	A2_T1	0.18761
miR-30d	A2_T2	0.23707
miR-30d	A2_T3	0.19666
miR-30d	A3_T1	0.13190
miR-30d	A3_T2	0.21808
miR-30d	A3_T3	0.10161
miR-30d	A4_T1	0.29490
miR-30d	A4_T2	0.18284
miR-30d	A4_T3	0.26603
miR-30d	A5_T1	0.17607
miR-30d	A5_T2	0.22838
miR-30d	A5_T3	0.20223
miR-30d	C1_T1	0.16502
miR-30d	C1_T2	0.23092
miR-30d	C1_T3	0.23379
miR-30d	C2_T1	0.18205
miR-30d	C2_T2	0.40237
miR-30d	C2_T3	0.28809
miR-30d	C3_T1	0.30062
miR-30d	C3_T2	0.25600
miR-30d	C3_T3	0.10335
miR-30d	C4_T1	0.18622
miR-30d	C4_T2	0.15133
miR-30d	C4_T3	0.25373
miR-378	A1_T1	0.54237
miR-378	A1_T2	0.40208
miR-378	A1_T3	0.28314

Table B-7 Continued

Target	Sample Name	Normalized expression
miR-378	A2_T1	0.74024
miR-378	A2_T2	0.46117
miR-378	A2_T3	0.24582
miR-378	A3_T1	0.89789
miR-378	A3_T2	0.48173
miR-378	A3_T3	0.17301
miR-378	A4_T1	0.81463
miR-378	A4_T2	0.40885
miR-378	A4_T3	0.24506
miR-378	A5_T1	0.88769
miR-378	A5_T2	0.55047
miR-378	A5_T3	0.19844
miR-378	C1_T1	0.78966
miR-378	C1_T2	0.65343
miR-378	C1_T3	0.62337
miR-378	C2_T1	0.86602
miR-378	C2_T2	2.04386
miR-378	C2_T3	1.36679
miR-378	C3_T1	0.51882
miR-378	C3_T2	2.26834
miR-378	C3_T3	1.04382
miR-378	C4_T1	0.70939
miR-378	C4_T2	3.13649
miR-378	C4_T3	1.42635
miR-486	A1_T1	0.93561
miR-486	A1_T2	0.14058
miR-486	A1_T3	0.14295
miR-486	A2_T1	0.19726
miR-486	A2_T2	0.02524
miR-486	A2_T3	0.04555
miR-486	A3_T1	0.18131
miR-486	A3_T2	0.07407
miR-486	A3_T3	0.03443
miR-486	A4_T1	0.31498
miR-486	A4_T2	0.02922
miR-486	A4_T3	0.04958
miR-486	A5_T1	0.33876

Table B-7 Continued

Target	Sample Name	Normalized expression
miR-486	A5_T2	0.11788
miR-486	A5_T3	0.16259
miR-486	C1_T1	0.03996
miR-486	C1_T2	0.03541
miR-486	C1_T3	0.03532
miR-486	C2_T1	0.13015
miR-486	C2_T2	0.16574
miR-486	C2_T3	0.07624
miR-486	C3_T1	0.18748
miR-486	C3_T2	0.09210
miR-486	C4_T1	0.09069
miR-486	C4_T2	0.09624
miR-486	C4_T3	0.06354
miR-8890	A1_T1	0.00183
miR-8890	A1_T2	0.00003
miR-8890	A1_T3	0.00002
miR-8890	A2_T1	0.00212
miR-8890	A2_T2	0.00010
miR-8890	A2_T3	0.00005
miR-8890	A3_T1	0.00267
miR-8890	A3_T2	0.00003
miR-8890	A3_T3	0.00007
miR-8890	A4_T1	0.01040
miR-8890	A4_T2	0.00001
miR-8890	A4_T3	0.00002
miR-8890	A5_T1	0.00252
miR-8890	A5_T2	0.00001
miR-8890	A5_T3	0.00000
miR-8890	C1_T1	0.00155
miR-8890	C1_T2	0.00184
miR-8890	C1_T3	0.00103
miR-8890	C2_T1	0.00521
miR-8890	C2_T2	0.00460
miR-8890	C2_T3	0.00152
miR-8890	C3_T1	0.00691
miR-8890	C3_T2	0.00385
miR-8890	C3_T3	0.00183

Table B-7 Continued

Target	Sample Name	Normalized expression
miR-8890	C4_T1	0.00277
miR-8890	C4_T2	0.00201
miR-8890	C4_T3	0.00338

Table B-8 Criteria for identifying glomerular lesions based on evaluation of H&E, PAS, and trichrome biopsy sections. The percentage of abnormal glomeruli within the cortex, which included any of the following features, was used to evaluate the correlation of glomerular damage to miRNA expression.

Lesion	Lesion description
Segmental sclerosis	Increased mesangium (<50% of the tuft) with distortion, compression, or effacement of capillary lumens; non-sclerotic portion within normal limits or abnormal (e.g., glomerular basement membrane (GBM) duplication or wrinkling, podocyte hypertrophy or degeneration
Global sclerosis	Sclerosis (as defined above) which encompasses >50% of the tuft
Synechia	Adhesion of the glomerular tuft to Bowman's capsule
Obsolescence	Effacement of all capillary loops by extracellular matrix
Fetal glomeruli	Immature glomerular tuft with a peripheral ring of podocyte precursor nuclei
Crescents	Fibrin and/or cells within Bowman's space
Bowman's capsule dilation	Dilation of Bowman's capsule such that the diameter of the glomerular tuft is <2/3 the diameter of Bowman's capsule
Atrophy	Acquired diminution of the size of the capillary loops with diminished cellular proliferation

Table B-9 Criteria for scoring lesions in the cortical tubulointerstitium based on evaluation of PAS and H&E biopsy sections. Each lesion was scored (0-3) on 20 different 200x fields. For tubular damage, scores were added together to generate one overall score for statistical analysis.

Lesion (Definition)	Scores for each group of lesions
Tubular Damage *Tubular dilation* Area of the tubular lumen comprised > 1/2 the area of the total tubular profile	0 = feature not present 1 = feature present in scattered tubules (<2 tubules/field) 2 = feature present in many tubules 3 = feature present in most tubules
Brush border Presence of PAS positive brush border on apical surface of tubules	
Tubular atrophy Thickened tubular basement membrane with attenuation of the epithelium	
Tubular epithelial cell degeneration/regeneration Presence of any of the following: cellular swelling, cytoplasmic basophilia, numerous small/few large cytoplasmic vacuoles, closely-crowded, karyomegalic epithelial cells (indicative of regeneration), cytoplasmic protein droplets	
Tubular single cell necrosis Cytoplasmic hypereosinophilia associated with either nuclear pyknosis or karyorrhexis	0 = not present 1 = 1 necrotic cell in 1 tubule / field 2 = 1 necrotic cell in >1 tubule/field 3 = >1 necrotic cell in >1 tubule/field
Interstitial fibrosis Increased extracellular collagenous matrix with increase in fibroblasts/myofibroblasts	0 = not present 1 = fibrosis that does not distort the TI architecture 2 = fibrosis that moderately distorts the TI architecture by widely separating tubules 3 = fibrosis that severely distorts the TI architecture (i.e. replaces tubules)
Chronic interstitial inflammation Lymphocytes, plasma cells and/or macrophages	0 = not present 1 = scattered inflammatory cells 2 = aggregates of inflammatory cells that separate or replace tubules 3 = diffusely distributed inflammatory cells

Table B-10 TaqMan® assays used for RT-qPCR reactions for miR-21-related genes.

Gene Symbol	Gene Name	Assay ID	NCBI Gene Reference
COL1A1	collagen, type I, alpha 1	Cf02623126_m1	NM_001003090.1, AF153062.1, AF197572.1, HM775209.1
SOD1	superoxide dismutase 1, soluble	Cf02624278_m1	NM_001003035.1, AF346417.1
TGFB1	transforming growth factor, beta 1	Cf02741608_m1	NM_001003309.1, L34956.1
TGFB2	transforming growth factor, beta 2	Cf02676763_m1	XM_545713.5, XM_853584.4
TGFBR1	transforming growth factor, beta receptor 1	Cf02687913_m1	XM_014117881.1
CPT1A	carnitine palmitoyltransferase 1A (liver)	Cf02624577_m1	NM_001286860.1, AF482992.1
ACADM	acyl-CoA dehydrogenase, C-4 to C-12 straight chain	Cf02654738_m1	XM_014114896.1
PPARA	peroxisome proliferator-activated receptor alpha	Cf02624289_m1	NM_001003093.1, AF350327.1
PPARGC1A	peroxisome proliferator-activated receptor gamma, coactivator 1 alpha	Cf02631655_m1	XM_846648.4, XM_005618656.2, XM_005618655.2, XM_014112658.1, XM_005618657.2
MPV17	MpV17 mitochondrial inner membrane protein	Cf02660930_m1	XM_005630257.2, XM_014120436.1, XM_014120435.1
EGF	epidermal growth factor	Cf02622114_m1	NM_001003094.1, XM_014109884.1, AB049597.1
SERPINE1	serpin peptidase inhibitor, clade E (nexin, plasminogen activator inhibitor type 1), member 1	Cf02741595_g1	XM_014114124.1, XM_005620896.2, NM_001197095.1, DN399379.1, DN402495.1

Table B-11 Cq values and relative expression of miR-21 obtained from biopsy samples for each unaffected dog at each milestone as measured by RT-qPCR.

Milestone	Unaffected Dog #	Age at biopsy (weeks)	Mean Cq value for miR-21	Mean Cq value for miR-16	Relative fold miR-21 expression
1	1	11	22.23	21.81	1.1
	2	12	22.28	21.66	0.96
	3	12	22.20	21.59	0.96
	6	18	22.12	21.29	0.82
	7	18	22.00	21.57	1.1
	8	14	24.34	23.19	0.66
	9	18	21.79	21.71	1.39
2	4	18	22.15	21.62	1.16
	5	18	22.26	21.56	1.03
	8	18	22.99	21.96	0.82
	10	18	22.00	21.26	1.0
3	1	23	21.90	21.52	0.94
	2	22	21.92	21.46	0.99
	3	21	21.71	21.23	0.88
	4	26	21.84	21.69	1.11
	5	26	22.00	21.54	0.89
	6	28	22.17	21.71	0.89
	7	26	21.96	21.54	0.92
	8	23	22.14	21.48	0.77
	9	26	21.48	21.65	1.38
	10	26	21.64	21.75	1.32
4	1	28	21.71	21.39	0.91
	2	24	22.19	21.78	0.85
	3	28	22.12	21.48	0.73
	6	35	21.60	21.31	0.93
	7	35	21.39	21.41	1.15
	8	32	24.29	22.87	0.43
	9	35	21.51	21.50	1.13
	10	35	20.75	21.48	1.87
5 (ESRD)	1	34	21.86	21.66	1.09
	2	27	21.90	21.69	1.14
	3	36	21.64	21.26	1.01
	8	37	22.26	21.52	0.75

Table B-12 Cq values and relative expression of miR-21 obtained from biopsy samples for each dog affected by X-linked hereditary nephropathy at each milestone as measured by RT-qPCR.

Milestone	Affected Dog #	Age at biopsy (weeks)	Mean Cq value for miR-21	Mean Cq value for miR-16	Relative fold miR-21 expression
1	11	13	21.90	21.45	1.08
	12	18	23.49	22.53	0.76
	13	11	22.13	21.49	0.94
	14	12	21.92	21.48	1.08
	15	12	21.76	21.64	1.36
	19	14	22.96	22.21	0.87
2	11	17	21.84	21.45	1.27
	12	21	21.95	21.86	1.57
	19	18	24.05	22.70	0.65
	20	18	21.29	21.33	1.72
	21	18	21.7	21.59	1.55
3	11	26	18.74	21.12	6.34
	12	29	19.88	21.72	4.38
	13	23	19.97	21.30	3.08
	14	22	19.57	21.13	3.60
	15	21	20.76	21.74	2.43
	16	35	20.49	21.68	2.80
	17	18	20.77	22.37	3.72
	18	28	20.89	21.75	2.23
	20	26	20.37	21.54	2.77
	21	26	19.85	21.47	3.75
4	12	32	19.52	21.36	4.04
	13	28	19.42	21.25	4.03
	14	24	19.35	21.25	4.22
	15	28	19.09	21.07	4.50
	16	40	21.21	22.37	2.51
	17	21	20.35	22.27	4.28
	18	35	20.11	21.44	2.84
	19	32	19.63	21.31	3.66
	20	35	19.48	21.22	3.22
	21	35	20.12	21.62	3.78
5 (ESRD)	14	27	18.70	20.97	6.36
	15	36	19.37	21.32	5.07
	19	37	20.06	21.80	4.40